

Master Thesis

Water Science and Management

Analysis of contribution of the shallow groundwater system to climate adaptations using groundwater modeling

A case study of Stadioneiland in Amsterdam, The Netherlands



Jora Slinger (5774926)
Master student Utrecht University

Prof. Dr. Steven de Jong
Supervisor Utrecht University

s.m.dejong@uu.nl
+31 30 253 4050

Frank Smits MSc.
Supervisor Waternet

frank.smits@waternet.nl
+316 532 714 39

August 2018

TABLE OF CONTENTS

ABSTRACT	5
1 INTRODUCTION.....	6
1.1 Waternet and Amsterdam Rainproof.....	6
1.2 Urban water management	7
1.3 Research area	10
1.3.1 Geological background	10
1.3.2 Current and future climate	11
1.3.3 Local water system	11
1.4 Previous research	13
1.5 Research relevance.....	14
1.6 Research questions.....	15
2 METHODOLOGY	16
2.1 Introduction to MicroFEM.....	16
2.2 Modeling process	17
2.3 Model schematization	18
2.3.1 Spatial dimensions.....	18
2.3.2 Temporal dimensions	19
2.3.3 Finite element network	19
2.3.4 Groundwater recharge	20
2.3.5 Initial head distribution, transmissivity and vertical resistance	20
2.3.6 Drainage.....	20
2.3.7 Leaky sewage.....	21
2.4 Time Series Analysis of groundwater observations	22
2.5 Stationary parameter optimization and calibration.....	23
2.6 Sensitivity analysis.....	24
2.7 Quantification of sewage leakage flux	24
2.8 PEST stationary parameter optimization and calibration	25
2.8.1 Introduction to PEST.....	25
2.8.2 Comparison MicroFEM vs PEST optimization.....	26
2.8.3 Weighting of observations.....	26
2.9 PEST transient parameter optimization and calibration	27
2.9.1 Calculation period.....	27

2.9.2	Storativity	29
2.9.3	Groundwater recharge	29
2.10	Scenarios	29
2.10.1	Scenario I - Climate change	29
2.10.2	Scenario II - Permeable paving	31
2.10.3	Scenario III - DIT sewage and variable drainage depth	32
3	RESULTS CALIBRATION	33
3.1	Pre-optimization fit	33
3.2	Stationary parameter optimization and calibration.....	35
3.3	PEST stationary parameter optimization and calibration	36
3.3.1	Comparison MicroFEM versus PEST optimization.....	36
3.3.2	Weighting of observations.....	37
3.4	PEST transient parameter optimization and calibration	39
3.4.1	Division of canal walls, sewage and drainage parameters.....	39
3.4.2	Revision drainage schematization	41
3.4.3	Incorporation of historical dyke body	43
3.4.4	Construction work Stadionplein	44
3.4.5	Refinements calculation steps and groundwater recharge	45
3.4.6	Reevaluation of weighting factors.....	45
3.5	Final optimization	47
4	RESULTS SCENARIOS.....	50
4.1	Water coverage of foundation poles.....	50
4.2	Scenario I – Climate change	51
4.3	Scenario II - Permeable paving.....	53
4.4	Scenario III - DIT sewage and variable drainage depth	55
5	DISCUSSION	57
5.1	Assumptions in model schematization.....	57
5.2	Measurement of groundwater infiltration.....	58
5.3	Weighting of observations	58
5.4	Model validation.....	58
5.5	Interpretation of optimization results.....	59
5.6	Research relevance.....	59
6	RECOMMENDATIONS	60
6.1	Determination of hydrological parameters.....	60

6.2	Recommendations for improved schematization.....	60
6.3	Recommendations for improved optimization	61
6.4	Recommendations for further research.....	61
7	CONCLUSIONS.....	63
8	ACKNOWLEDGEMENTS.....	65
9	REFERENCES.....	65
10	ANNEXES.....	71
10.1	Quantification of sewage leakage methodology.....	71
10.1.1	Methodology	71
10.1.2	Results.....	72
10.2	Experiment tree evapotranspiration.....	73
10.3	Additional figures	75
10.4	Python code.....	80
10.4.1	Python code for groundwater recharge.....	80
10.4.2	Python code for creating transient pest control file	81
10.4.3	Python code for processing transient hydraulic heads of all nodes.....	85

Front figure *Aerial view of the Olympic Stadium and the surrounding Stadioneiland in Amsterdam, The Netherlands (Olympic Stadium Foundation, 2018).*

ABSTRACT

Climate change models predict an increase in precipitation intensities as well as longer periods of drought during summer for the Netherlands (IPCC, 2014). In urban environments, it is essential to adapt water systems to these changes in climate in order to prevent water nuisance and protect wooden foundation poles. For the Stadionbuurt in Amsterdam, a groundwater model is built in finite element modeling program MicroFEM. Time series analysis is used to pre-process observation data from 2007-2016 on trends, measuring errors and outliers. The transient model is run from 2014 until 2016. The groundwater model is extensively calibrated using both MicroFEM and the automated parameter estimation program PEST for parameter optimization. The maximum average residual is reduced to 0.26 m from 0.46 m initially, with the gross amount of residuals falling below 0.10 m.

In KNMI climate change scenario Wh for the year 2050 (scenario I), the model shows a decrease in lowest calculated groundwater levels up to 0.10 m. Consequently, 64% of wooden foundations would lack water coverage at a certain point during the calculated two years, compared to 49% currently. To prevent these low groundwater levels and the potentially harmful effects on foundations, scenarios are created to analyze the effects of a climate adaptive design. For scenario II, an infiltration experiment is performed and the infiltration capacity of the Drainvoeg permeable paving is determined to be 40mm hour⁻¹ after a lifespan of five years. If constructing this type of permeable paving instead of the current semi-permeable paving, groundwater levels increase to an extent that can be damaging to trees and cellars while not raising the groundwater significantly during drought. In scenario III, DIT-sewage is constructed where currently drainage is located. The sewage has a variable drainage depth of NAP -0.20 m at the end of winter until beginning of summer and NAP -0.40 m during the rest of the year. At locations where foundations is threatened in a scenario of changed climate, this renewed DIT-sewage design can ensure a sufficient water coverage (for example, figure 4.6).

Finally, interpretation of the previously described scenarios leads to answering the main research question of how the shallow groundwater system of the Stadionbuurt can contribute to climate adaptations. The capacity between surface level and groundwater levels indicate possibilities for infiltrating surface water or precipitation. Scenario III shows the shallow groundwater system can contribute to climate adaptations, at least sufficiently for minimizing negative effects of drought. The balance between too high and too low groundwater levels remains delicate and caution has to be taken to the disadvantages of climate adaptations, as shown in scenario II.

The calibrated shallow groundwater model developed in this research for the Stadionbuurt has proved to be useful for climate exploration as well as analyzing the effects, both positive and negative, of possible adaptations. Many more scenarios can be explored by Waternet, for example scenarios of increase in cellars or the expansion of surface waters in the area. In addition, the model can be used to dimension the adaptations.

Increase in drought and extreme precipitation will face challenges not only for Stadioneiland, but for the entire city of Amsterdam. Soil properties and wooden pole foundations are rather specific to Dutch cities, but climate adaptations need to be designed in all urban areas. The technique of calibrating a transient groundwater model for highly urbanized neighbourhoods could be used as a template to design other local models. Furthermore, half of the world's population live in delta regions like the Dutch delta and face similar challenges (VHL, 2018). Water management as modeled in this research might be a source of inspiration for other delta regions.

1 INTRODUCTION

1.1 Waternet and Amsterdam Rainproof

Since 2006, Waternet is the first public water cycle organization of the Netherlands, not only producing drinking water and managing the sewage system, it is also responsible for surface waters, water safety and nautical routes on behalf of the municipality of Amsterdam and water authority Amstel, Gooi and Vecht (Waternet, 2018). This circular approach is unique in the Netherlands and creates a larger innovative capacity within the water cycle (Reedijk, 2012). The service area of Waternet is illustrated in figure 1.1.

Innovative water management is highly necessary with the challenges ahead. Amsterdam is located around sea level and in the delta of the rivers Rhine and Amstel (AHN, 2018). Climate predictions indicate more extreme precipitation combined with drought and sea level is expected to rise, thus challenging the cities spatial design (Van Baaren, 2010). Therefore, Waternet has initiated the *Amsterdam Rainproof* program in 2014, in which organizations, inhabitants, institutes and entrepreneurs work together to create more resilience to extreme precipitation (Amsterdam Rainproof, 2014).



Figure 1.1 Total service area of Waternet with the service area of drinking water in blue, water management and sanitation within the dark blue line and the service area of sewage in grey (Waternet, 2018).

The city of Amsterdam (figure 1.2) is currently designed to withstand a precipitation event of 20 mm hour^{-1} (Van Assenbergh et al., 2016). 'To withstand' means the water system is able to handle the precipitation event without the occurrence of flooding or property damage. During extreme precipitation, temporary storage of water in the street profile is allowed up to the curb. In the 2016 GRPA (*Gemeentelijk Rioleringsplan Amsterdam*), an adjusted, higher norm of 60 mm hour^{-1} is set for the city of Amsterdam by 2020. The GRPA follows the guidelines set out by the national policy of 'retention, storage and drainage' (Commissie Waterbeheer 21^e eeuw, 2000). First, water should be retained locally as much as possible, for

example by green roofs (Pötz & Bleuzé, 2016). Subsequently, it is advised to allow for temporary storage of the water, through infiltration to the groundwater or other forms of storage (Pötz & Bleuzé, 2016). Finally, water will have to be drained out of the system, usually by sewage pipes and pumps (Waternet, 2018).

The current sewage system can process 20 mm hour^{-1} , the additional 40 mm hour^{-1} has to be realized through 'temporary storage' in public and private space (Van Assenbergh et al., 2016). The exact time period of 'temporary' is yet to be defined, but first guidelines taken on by Waternet indicate retention of water for at least 24 hours (Goedbloed, 2018), but preferably more (Smits, 2018).



Figure 1.2 Aerial view of part of the city of Amsterdam, The Netherlands (SERC, 2018).

Waternet is challenged to increase the cities resilience to withstand precipitation events of 60 mm hour^{-1} . This research contributes to Waternet's *Amsterdam Rainproof* program for the neighborhoods of Stadioneiland in analyzing the shallow groundwater system and its possible role in climate adaptations.

1.2 Urban water management

In general, urban water management focuses on precipitation, runoff, drinking water supply, wastewater treatment, surface water and groundwater (Van de Ven, 2011). The urban water balance differs from a global hydrological water balance (figure 1.3). Often, cities are designed to discharge precipitation as quickly as possible to the sewage system (Van Assenbergh et al., 2016). Urban areas have a high percentage of surface area with a relatively low permeability, such as buildings and streets, reducing infiltration of precipitation (Van de Ven, 2011). Besides, cities generally have a low storage capacity for water. As a result, urban environments are vulnerable to changes in climate (KNMI, 2014). Precipitation frequency and

intensity is projected to increase as well as more drought during summer, which puts more pressure on urban water systems (IPCC, 2014).

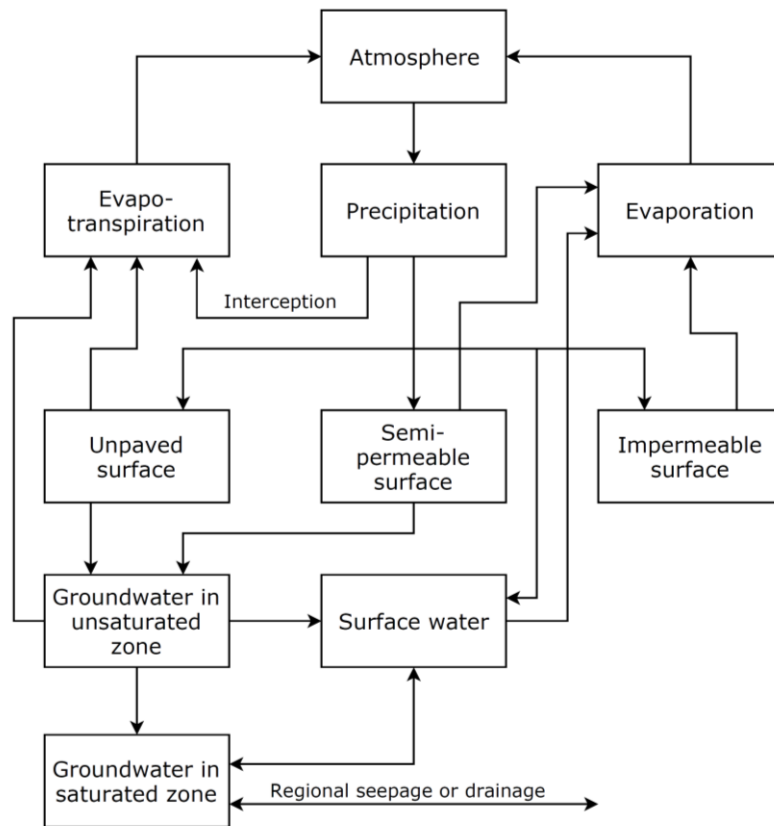


Figure 1.3 Sub-flows water balance in urban water system (Adapted from Van de Ven, 2011).

According to Van Baaren (2010), main factors of Amsterdam's groundwater system are:

- Precipitation and evapo(transpi)ration
- Upwelling and infiltration
- Heterogenic soil profile
- Non permeable barriers
- Drainage through leaky (sewage) pipes

In this research, not the entire city of Amsterdam is analyzed, but the water management of two neighborhoods, the Stadion- and Apollobuurt (figure 1.4).

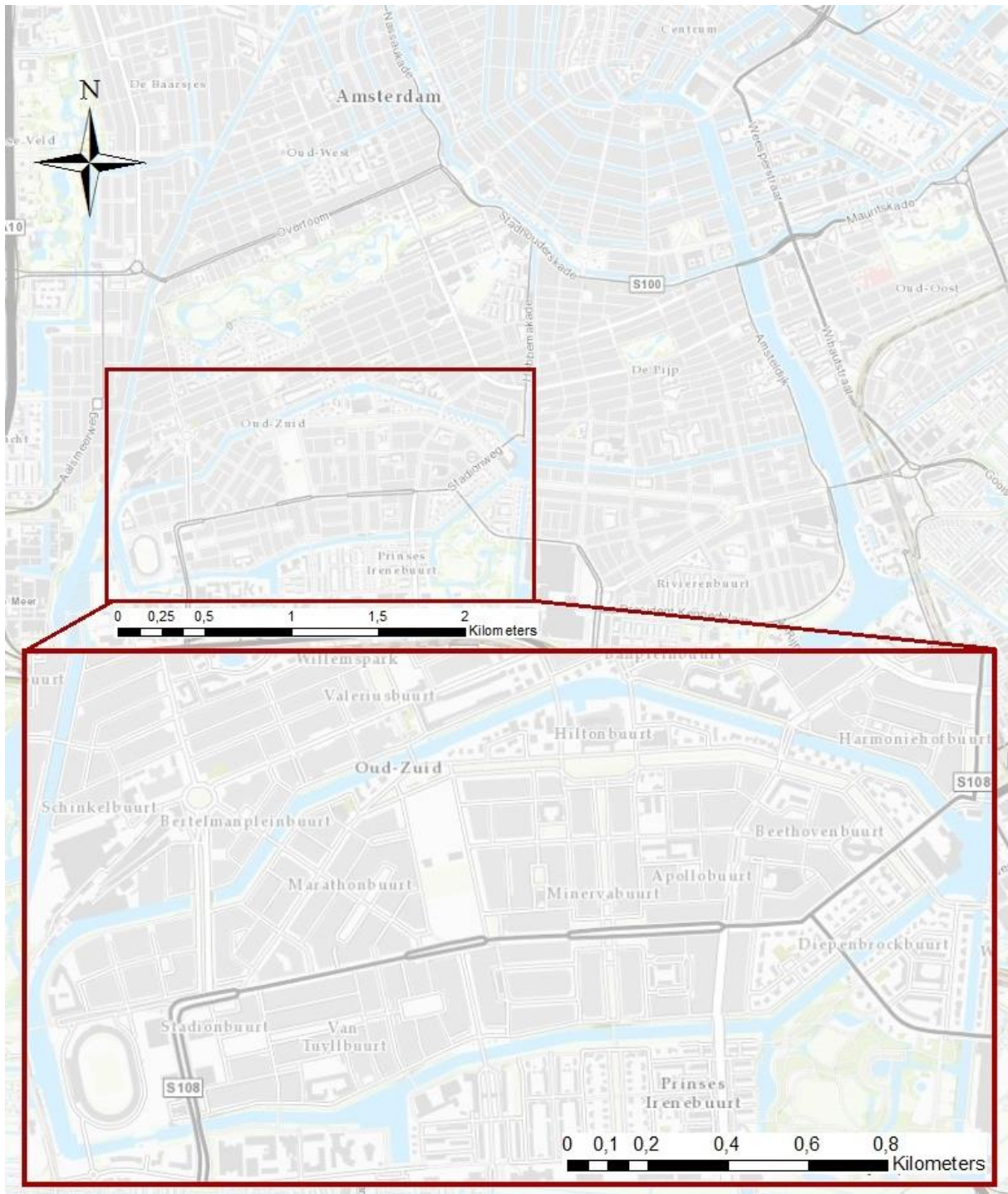


Figure 1.4 Map of the research area Stadioneiland (subset) as located in the city of Amsterdam (Adapted from Waternet database, 2018).

1.3 Research area

The focus of this research is on the Stadionbuurt and Apollobuurt, further referred to as 'Stadioneiland', located in the south of Amsterdam (figure 1.4). The two adjacent areas are surrounded by the Noorder and Zuider Amstelkanaal. The Apollobuurt has a more spacious set-up with wider streets and more garden space, but both neighborhoods are highly urbanized.

1.3.1 Geological background

The geology of the Netherlands is mainly influenced by fluvial, aeolian and glacial factors. A cross section of the first 50 meters of the subsurface is displayed in figure 1.5. Additional cross sections and bore hole depth profiles can be found in annex 10.4 (figure 10A-10C). The main subsurface layers are described subsequently.

The surface level of Stadioneiland was raised during construction in the early 20th century. Due to this raise, the upper subsoil consists of on average 3 to 4 meters of anthropogenic material (TNO, 2018). This material is mostly medium fine sand with a relatively high permeability. The lower boundary of this phreatic aquifer is determined by peat from the Formation of Nieuwkoop. This peat layer with a low permeability was developed during rising groundwater levels in the Holocene (Zagwijn, 1986). The second aquifer in the area is formed by the clayey sand of the Naaldwijk Formation. After the last glacial period, sea levels rose and the Naaldwijk Formation are marine deposits of that period. In between the Naaldwijk Formation and the Pleistocene deposits, a relatively thin layer of peat (the 'Basisveen') can be found (De Mulder & Bosch, 1984). On Stadioneiland, this layer is located at around NAP -12 m and is several tens of centimeters thick.

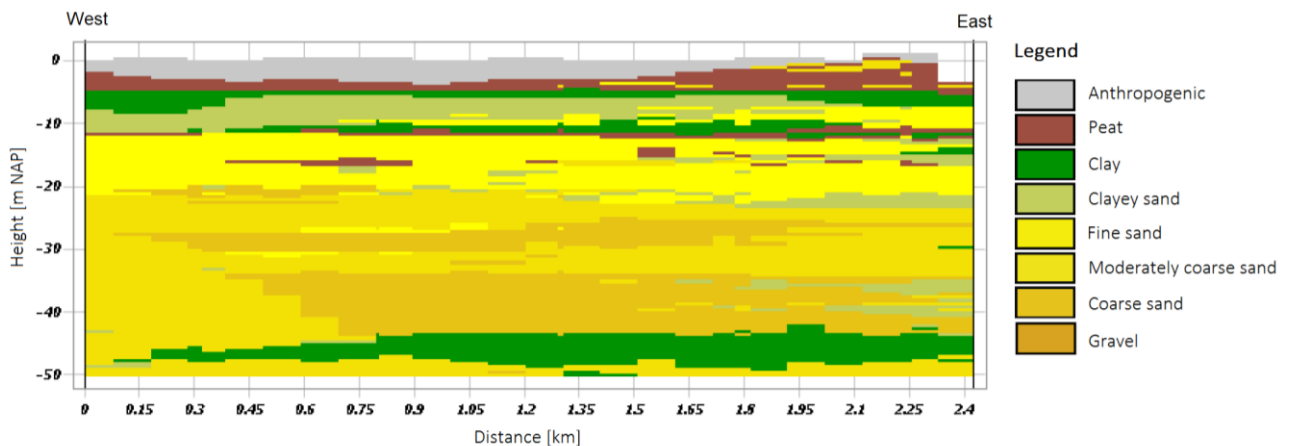


Figure 1.5 Cross section of the top 50 meters of subsurface from west to east of the Stadioneiland (TNO, 2018).

1.3.2 Current and future climate

According to the KNMI (2018a), average temperature of at Schiphol varies around 3 to 4 °C during winter and rises until 18 °C in August. Yearly average temperature in the city of Amsterdam is 10.2 °C (KNMI, 2018a). From 1981-2010, the average yearly precipitation at Schiphol was 838.2 mm, with most precipitation in autumn (figure 1.6).

For the year 2050, Amsterdam's temperatures are predicted to rise, with 40 instead of 20 days above 25 °C per year; 21 instead of 7 nights warmer than 20 °C and heatwaves of higher intensity (KNMI, 2018b). Average yearly precipitation will increase to 975 mm by 2085, with more frequent and more intense extreme precipitation events (KNMI, 2018b).

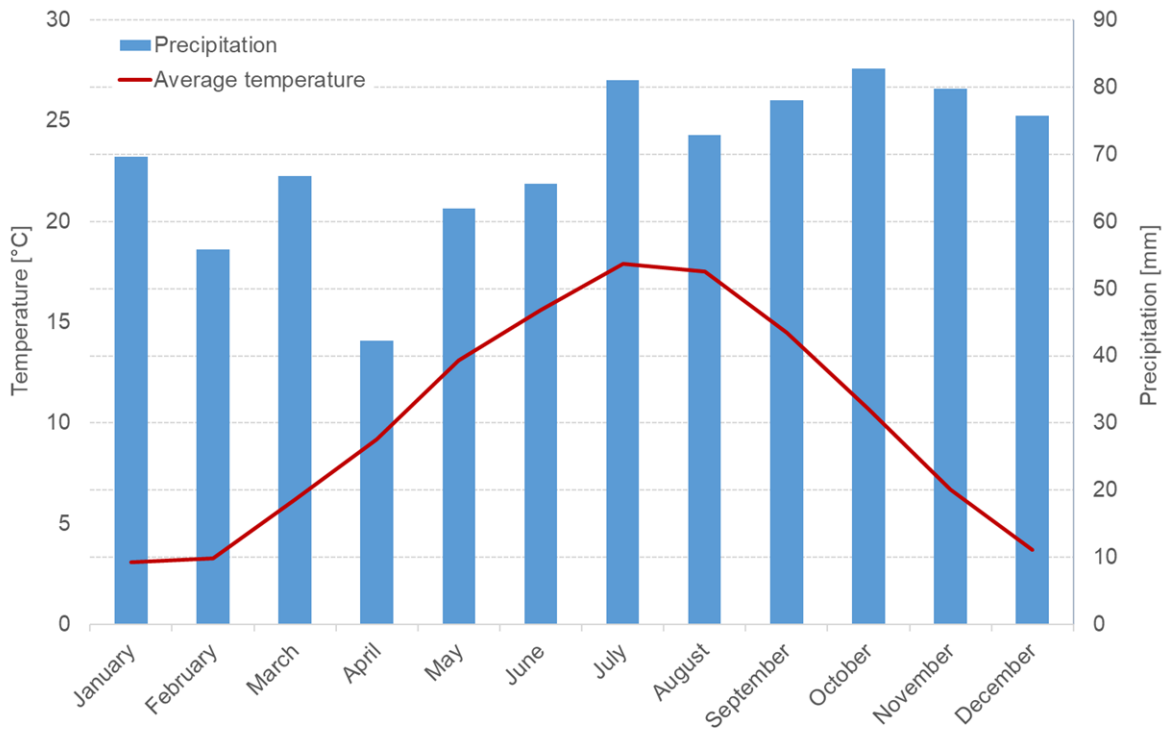


Figure 1.6 Monthly precipitation and average temperature for the Netherlands (Klimaatatlas, 2018).

1.3.3 Local water system

The Noorder and Zuider Amstelkanaal surrounding the research area belong to Amsterdam's main water system where water levels are maintained at NAP -0.40 m (Waternet database, 2018). Stadioneiland is divided into three pumping areas (figure 1.7). The relatively small pumping area 5271 (Olympic Stadium) on the west side of the island has separated dry weather and rainwater sewage. The area south of the Stadionweg has a separated sewage system as well and part of pumping area 5050 Cornelis Doppekkade, also including neighborhoods south of the research area. North of the Stadionweg, both sewage fluxes are combined in the mixed sewage system of 5190 (figure 2.5), which drains most of the west of the city center to pumping station Eerste Weteringsplantsoen. Both in pumping area 5190 and

5050, drainage pipes are located of varying installation date from 1990 until 2013. No drainage is present in pumping area 5271 (figure 1.8).



Figure 1.7 Pumping areas 5271, 5190 and 5050 encompassing the research area. The pumping stations of 5190 and 5050 are located outside the research area (Adapted from Waternet database, 2018).

The height of the groundwater table from a management perspective is a delicate and complicated balance. Ideally, heads are kept at a depth of 0.90 m beneath surface level (Visser, 2009). Though for protection of wooden foundations, a height of 0.40 m of groundwater coverage is needed. Other factors to take into consideration are positioning of cellars or crawls spaces and water availability for trees.

Due to the unstable top layers of the subsurface (section 1.3.1), most housing in Amsterdam is built on long wooden foundation piles reaching into the Pleistocene sand layer (Klaassen, 2008). On Stadioneiland, the top of the foundation wood reaches up to NAP -0.50 m or even NAP -0.30 m for the Olympic Stadium. If foundation wood is not permanently submerged in groundwater, this could result in soft-rot decay and instability of the foundation (Klaassen, 2008).

On Stadioneiland, surface level is around NAP +0.40 m until NAP + 1.10 m and groundwater levels in the period of February 2016 until February 2018 were NAP -0.44 m on average. This indicates the norm of 0.90 m between reference and groundwater level is achieved and infiltration of precipitation is a possibility. More importantly, yearly fluctuations show high groundwater levels in winter and low (up to NAP -0.63 m) in summer. As foundation wood can reach up to NAP -0.50 m, this indicates possible occurrence of increased wooden pole degradation.

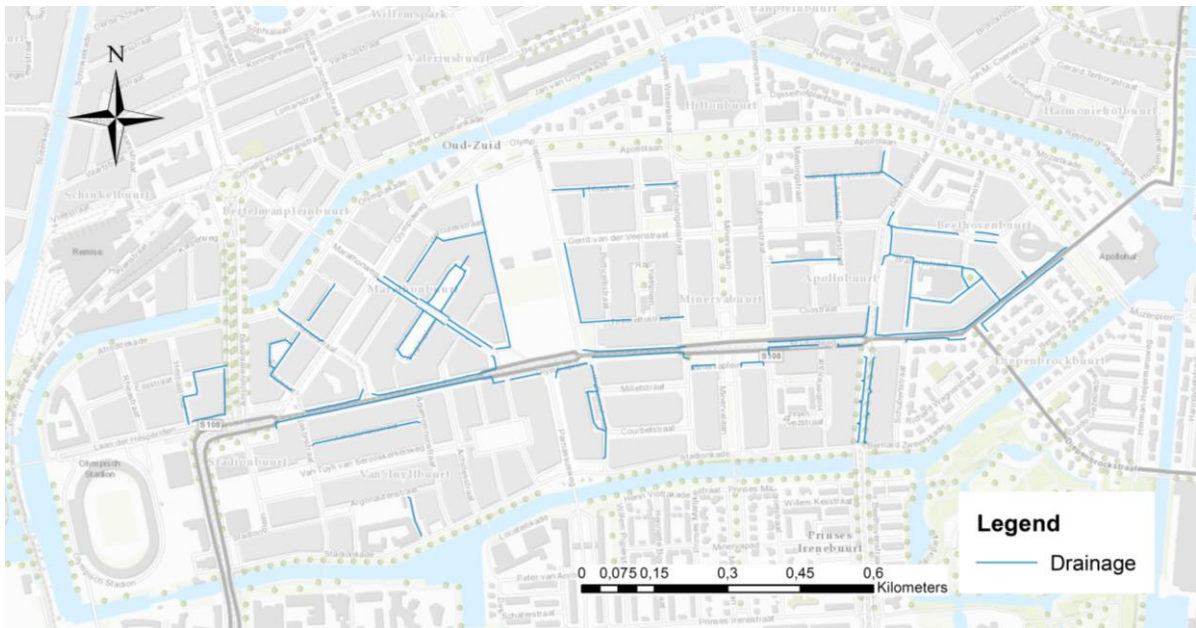


Figure 1.8 Location of drainage sewer in pumping areas 5190 and 5050 according to Waternet registration.

1.4 Previous research

In 2012, the groundwater system of the entire city of Amsterdam is modeled by hydrologist Jos Beemster of Waternet using TRIWACO. The model calculates groundwater levels and fluxes throughout eight model layers of aquifers and aquitards. Calibration was performed manually and iteratively based on data from piezometers since 2008. Only stationary calculations are analyzed with the regional model with the intention to create local detailed models. The neighborhoods of which a detailed model is made will start from the stationary regional model and will be calculated transiently as well. Further information on the regional stationary model can be found in chapter 3 of Beemster (2016). Furthermore, Waternet has performed four field tests in 2016 on an infiltration system in the Argonautenstraat (annex figure 10D).

1.5 Research relevance

In 2017, Waternet has made an analysis of the impact of extreme precipitation on the current water system of the city (figure 1.9). The study shows a rainfall event of 100 mm in one hour may result in water levels up to 20 to 30 cm on the streets in some locations of Stadioneiland. Figure 1.11 also displays the residential reports made to Waternet after the precipitation event of July 28, 2014. During that day, precipitation of 60 to 70 mm fell within 2 hours. Still, this is only half the precipitation intensity of the new norm of 60 mm in one hour of the 2016 GRPA. Furthermore, sewage in some parts of the research area are at the end of their predicted lifespan (Waternet database, 2018). The replacement of these parts of the system are an opportunity for incorporation of climate adaptations. On Stadioneiland, Waternet is considering more infiltration of precipitation to the groundwater as a climate adaptation. Through analysis of the groundwater system and unsaturated zone an advice can be formed on the possibilities and consequences of such adaptations.

The combination of the possible risk (indicated in figure 1.9) and the predicted replacement of the current sewage system, stress the importance and opportunities of the research on Stadioneiland.

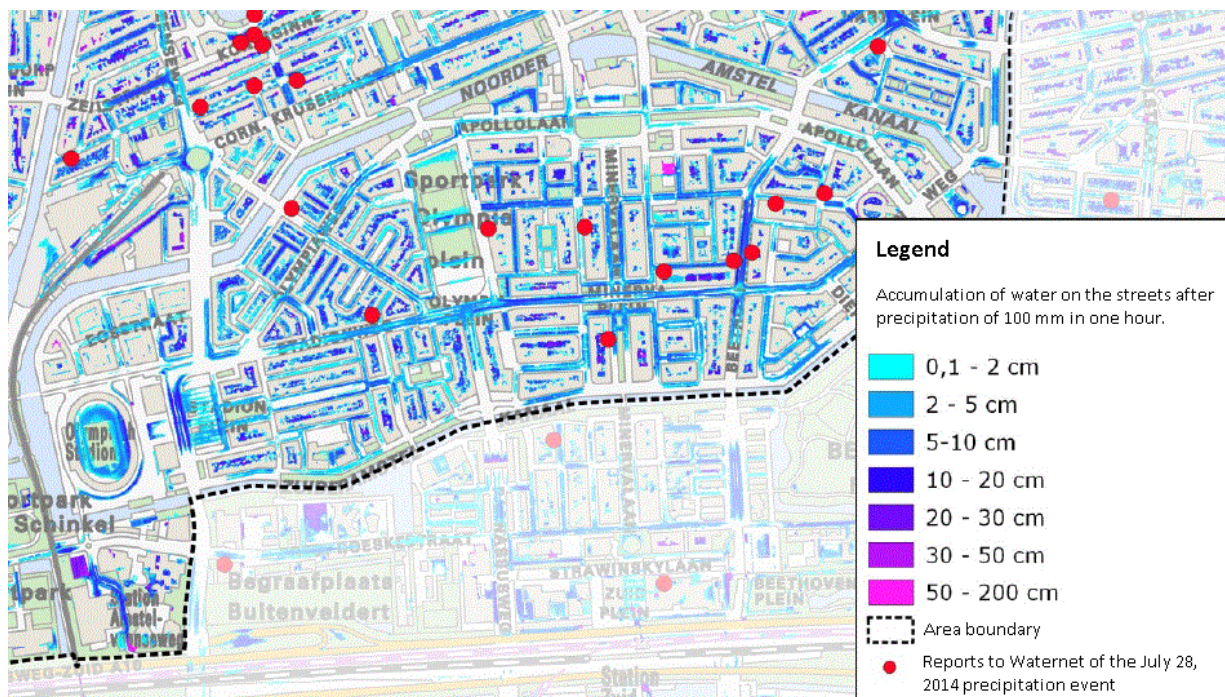


Figure 1.9 Result of a 3Di model simulation of a 100 mm hour⁻¹ precipitation event, lasting for one hour in the South of Amsterdam (Waternet database, 2018).

1.6 Research questions

The main question of the research is: how can the shallow groundwater system contribute to climate adaptations on Stadioneiland, Amsterdam? In order to answer this main question, MicroFEM groundwater modeling will be used as a tool. Through modeling, groundwater characteristics can be simulated. Subsequently, the calibrated model can be used to run possible scenarios of adaptations and analyze the effects on the groundwater system.

Subquestions:

1. Model optimization: What are the values of subsurface properties (e.g. transmissivity, drainage and infiltration resistance) in the research area?
2. Scenario I: What would be the effect of climate change scenario Wh on the groundwater system in its current state?
3. Scenario II:
 - a. What would be the effect on the groundwater system of permeable paving?
 - b. What is the field infiltration capacity of one type of permeable paving, the Drainvoeg?
4. Scenario III:
 - a. What would be the effect of a groundwater system with more DIT-sewers?
 - b. What would be the effect of a variable drainage level?

The methodology used to explore these subquestions is set out in the next chapter.

2 METHODOLOGY

The main research question is best approached using groundwater modeling as a tool. A groundwater model 'provides a quantitative framework for synthesizing field information and for conceptualizing hydrogeological processes' (Anderson & Woessner, 1992). As the subsurface is not easily observable, modeling provides quantitative insights into system dynamics as well impacts of possible adaptations. The research methodology of the modeling process, in which all main factors listed in section 1.2 can be modeled, is described upon in this chapter. After an introduction into the modeling program MicroFEM, this chapter further covers model schematization, sensitivity analysis, stationary and transient parameter optimization and calibration and exploration of climate scenarios.

2.1 Introduction to MicroFEM

For this research, the program MicroFEM is used to build a groundwater model. MicroFEM is a hydrological program for modeling steady-state or transient flow through multiple aquifers (Hemker et al., 2004). MicroFEM uses a finite element method, meaning the model area is divided into small (triangular) elements of which the water balance equation is solved per node on these elements. This method is preferred over finite difference modeling as it allows for more detailed modeling of subsurface and boundary conditions (Janssen & Hemker, 2004). Besides, MicroFEM is more flexible in usage than for example MODFLOW as it enables faster modeling with focus on the area of interest (Nienhuis & Hemker, 2010). In addition, MicroFEM is a suitable program for modeling groundwater of the research area as the sewage system can be represented better in triangular shapes than for example squared elements as used in for example Modflow.

Groundwater flow is assumed to be laminar and of equal density. The governing formulas of groundwater flow used in MicroFEM calculations are based on Darcy's law (Hendriks, 2010):

$$Q = KA \frac{(h_1 - h_2)}{L} \quad (2.1)$$

with Q being volume flux or discharge [$\text{m}^3 \text{d}^{-1}$], hydraulic conductivity K [m d^{-1}], surface area perpendicular to the water flow A [m^2], difference in hydraulic head between two points in h [m] and distance between two points L [m]. If Darcy's Law is written in x,y,z-dimensions with resistance between two groundwater layers given by c [d^{-1}], storage coefficient S [-] and boundary condition of a volume added to or removed from the model I [m^3], equation 2.1 converts into:

$$\frac{\partial}{\partial x} \left(K_x D \frac{\partial h}{\partial x} \right) + \frac{\partial}{\partial y} \left(K_y D \frac{\partial h}{\partial y} \right) + \frac{\partial}{\partial z} \left(K_z D \frac{\partial h}{\partial z} \right) - \frac{h - h'}{c} = S \frac{\partial h}{\partial t} + I_{(x,y,z,t)} \quad (2.2)$$

Equation 2.2 is the basis of all flow calculations performed in MicroFEM (Smits, 2002).

2.2 Modeling process

The model approach used is based on methods described by the NHV: *Nederlandse Hydrologische Vereniging* (1997). The sequence is adjusted for the specific purpose of this research and has a chronology of stationary optimization preceding transient optimization. Generally, the modeling process will follow the steps enlisted below and are described in detail in the corresponding sections:

- 2.3 Model schematization
- 2.4 Time Series Analysis of groundwater observations
- 2.5 Stationary parameter optimization and calibration
- 2.6 Sensitivity analysis
- 2.7 Quantification of sewage leakage flux
- 2.8 PEST stationary parameter optimization and calibration
- 2.9 PEST transient parameter optimization and calibration
- 2.10 Scenarios

Initially, the model is built as a stationary model and parameter values are optimized manually, but mainly through the optimization routine of MicroFEM. Subsequently, the automatic parameter estimation program PEST is used for increased functionality. Then, the model is converted to a transient model whilst using PEST for optimization. The calibrated transient model is used for exploring scenarios of climate adaptations. Fieldwork is done to assist in improving the model schematization (NHV, 1997). Programs such as ArcGIS, Excel and Python are used for data processing, analysis and presentation.

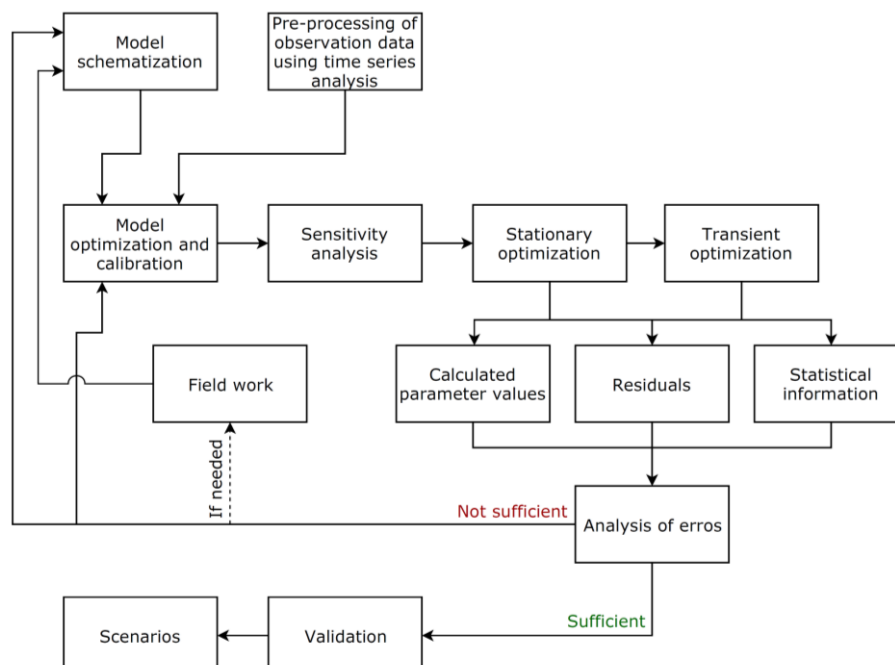


Figure 2.1 Flow diagram of model process with iterative loops in calibration and adjustment in model schematization or optimization after analysis of errors and possible fieldwork.

2.3 Model schematization

2.3.1 Spatial dimensions

The canals Noorder and Zuider Amstelkanaal are maintained at NAP -0,40 m, so Dirichlet (constant head) boundary conditions apply (Hendriks, 2010). Geological analysis shows multiple aquitards are present in the west-side that fade out towards the east (TNO, 2018). Possibly, phreatic heads are influenced by up- or downward seepage through aquifers up to 200 m deep, or eight model layers (figure 2.2). The aquitard below the 8th aquifer, the clayey layer of the Maassluis Formation, will be the lower boundary of the model, located around NAP -210 m (TNO, 2018). To decrease run time, the gross amount of model runs is simplified to three model layers with fixed head conditions in the third aquifer (first sandy unit of the Drenthe Formation), located around NAP -40 m (TNO, 2018). On a regional scale, groundwater fluxes occur as well. The polder Haarlemmermeer, located Southwest of Amsterdam, is maintained at NAP -6.00 m (Hoogheemraadschap van Rijnland, 2018), whereas lake Markermeer is maintained at NAP -0.40 m in winter and NAP -0.20 m in summer (Rijkswaterstaat, 2018). This head difference drives regional groundwater flow to the southwest. Dirichlet boundary conditions are therefore applied to all aquifers.

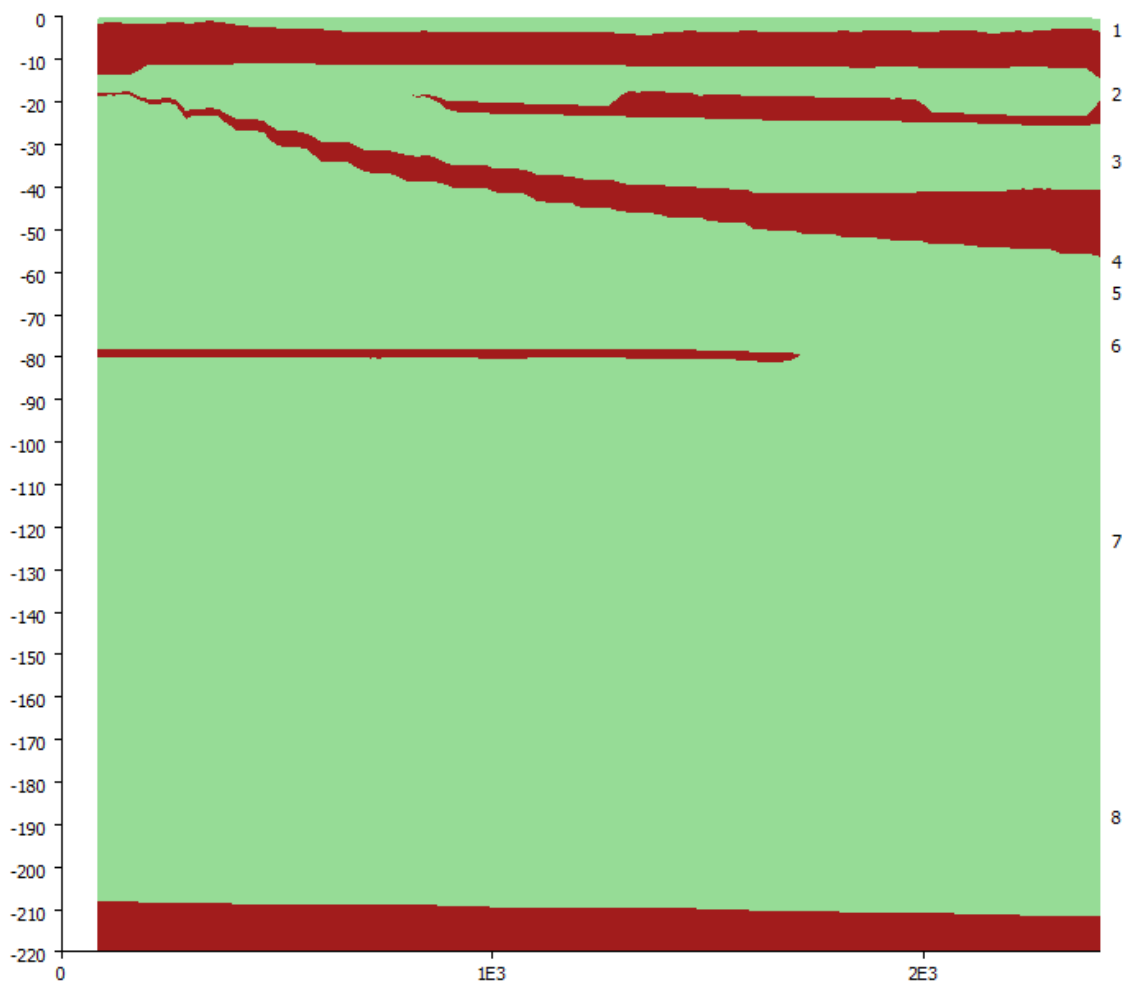


Figure 2.2 Cross-sectional depth from west to east of Stadioneiland, displaying aquifers in green, aquitards in red with depth [m] on the left and model layer number on the right.

2.3.2 Temporal dimensions

Initially, the model will be used for stationary calculations. In stationary schematization, storativity is zero and balanced fluxes are calculated with mean net precipitation as a boundary condition. After stationary calibration, the model is adapted for transient calculations to represent fluctuating groundwater levels, seasonality and other temporal changes. The model calculates heads from July 2014 until January 2017, determined by the available observations as discussed in 2.9.1.

2.3.3 Finite element network

MicroFEM calculates heads based on input parameters for each node of the finite element network. Values are graphically interpolated between the nodes for surface covered maps. On Stadioneiland, Waternet has installed almost hundred piezometers, where heads are measured by hand or using pressure transducers (Waternet database, 2018). The wells will be fixed points to which the finite element network is connected, as here calculated heads will be compared to observed heads. Also line locations of all drainage and sewage are converted to fixed points (section 2.3.6 and 2.3.7). Through trial and error, network spacing is set at 25 m (figure 2.3), which appears to be a workable balance of precision and calculation time.

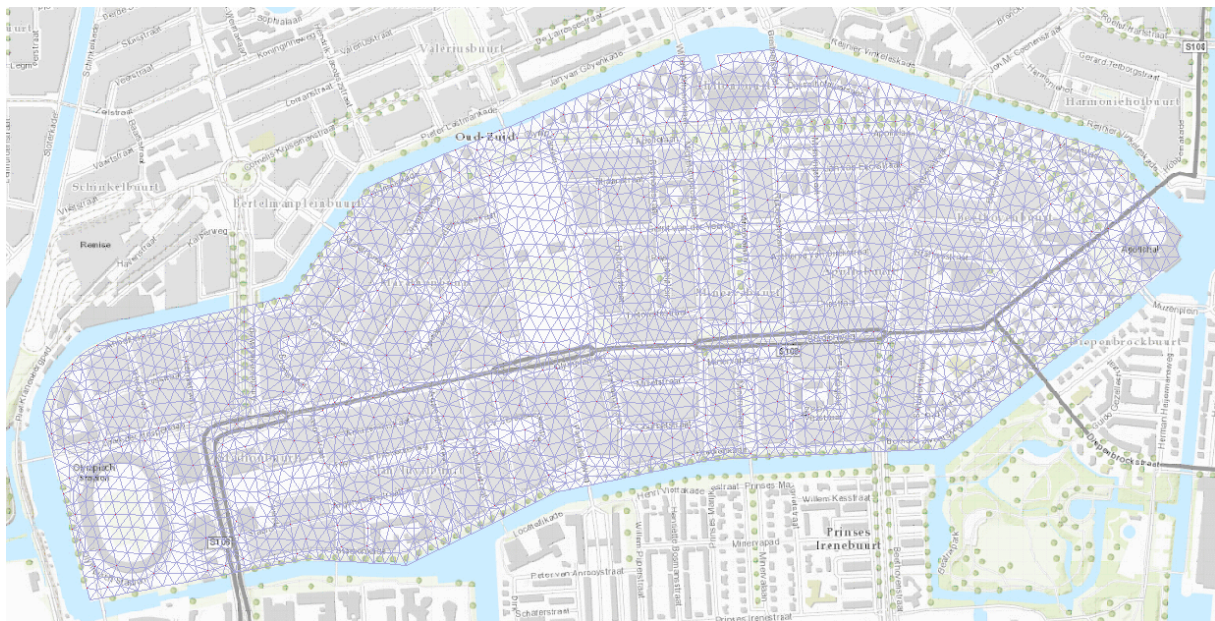


Figure 2.3 *Finite element network based on fixed nodes of piezometers, drainage and sewage with spacing of 25 m.*

2.3.4 Groundwater recharge

As the model does not include an unsaturated zone, the 'precipitation' input parameter is in fact groundwater recharge. Average gross precipitation in the Netherlands is close to 900 mm per year (KNMI, 2018c). The fraction of this precipitation reaching the groundwater is mainly determined by surface type and corresponding infiltration, surface evaporation and storage (Van de Ven, 2011).

On land use maps of Waternet, the surface is categorized in unpaved, permeable or impermeable paving, flat or sloped roofs, or water. In the model, categorization is made into *permeable* (unpaved), *semi-permeable* (permeable paving) and *impermeable* (roofs, impermeable paving and water). It is assumed that all precipitation on impermeable paving, roofs and water does not contribute to the groundwater system. Roofs are connected to rainwater sewage which discharges on surface water. Surface waters are maintained at fixed levels and will barely change in level due to a precipitation event. Precipitation loss on paved surface can be calculated by multiplying gross precipitation with the runoff coefficient. Van de Ven (2011) defines runoff coefficient C as:

$$C = \frac{\text{Total runoff via the sewerage (excluding base flow)}}{\text{Total precipitation on directly connected paved area}} \quad (2.3)$$

According to Kibler (1982), the runoff coefficient for semi-permeable paving (bricks, footpaths) is between 0.70 - 0.85. In other words, 15 to 30% of all precipitation on semi-permeable paving will not be turned into runoff, but can be accounted to one of the loss processes. These losses are not only infiltration, but moisturising loss, depression storage and evaporation as well. Moisturising loss is small compared to other losses that occur (< 1 mm) and depression storage is indicated to be 0.5 – 1.5 mm (Van de Ven, 2011). For parks and non-sloping lawns, the runoff coefficient will be 0.05 - 0.25 (Kibler, 1982).

2.3.5 Initial head distribution, transmissivity and vertical resistance

In MicroFEM, not the hydraulic conductivity K [m day^{-1}] is used for calculations, but the product of K with saturated thickness D [m], resulting in transmissivity T [$\text{m}^2 \text{day}^{-1}$] (Nienhuis & Hemker, 2010). An initial value for transmissivity is estimated by using geological information as described in section 1.3.1 in combination with horizontal permeability as given by Bot (2011) and Hendriks (2010). As mentioned in section 1.4, a regional groundwater model has been developed by Waternet for Amsterdam. On Stadioneiland, no piezometers are in place at lower aquifers than the phreatic aquifer. Therefore, no prior information is available of heads, aquifer transmissivities and vertical resistance of the aquitards below the phreatic aquifer. Therefore, stationary optimized results of the regional model are used as initial values.

2.3.6 Drainage

As described in section 1.3.3, drainage sewage is present in area 5190 and 5050 (figure 1.8). Groundwater drainage can occur at the surface water level the drainage is connected to (principle of communicating vessels). Also, if drainage depth is below surface level, water could theoretically infiltrate to the groundwater system. Therefore, drains are modeled as river

systems (figure 2.4) with a drain level $rh1$ [m], a drainage resistance $rc1$ [d] and infiltration resistance $ri1$ [d]. The drainage flux q_{out} [$m^3 d^{-1}$] is calculated as (Smits & Hemker, 2004):

$$\text{if } h1 > rh1: \quad q_{out} = a \frac{(h1 - rh1)}{rc1} \quad (2.4)$$

$$\text{if } h1 < rh1: \quad q_{in} = a \frac{(rh1 - h1)}{ri1} \quad (2.5)$$

$Rh1$ is equal to surface water level of NAP -0.40 m. For all drainage, resistances $rc1$ and $ri1$ are 100 days initially. The resistances might vary according to age, depth, width and degree of clogging which makes it a typical value to calibrate on.

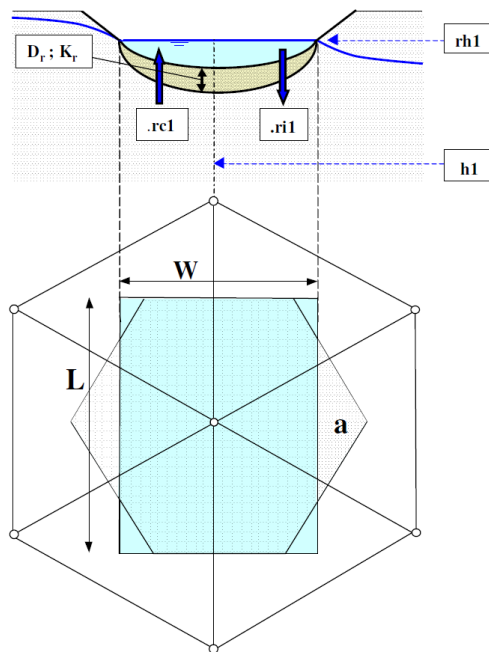


Figure 2.4 Infiltration and drainage with a river system at a node with nodal area a in MicroFEM (Smits & Hemker, 2004).

2.3.7 Leaky sewage

Fluxes transported by mixed or dry weather sewage system or drained by rainwater sewage are considered out of the scope of the model. These fluxes usually do not influence the groundwater system. However, if a sewer is damaged, it can act as a drain (International Association of Hydrological Sciences, 1990; Beemster, 2016). Therefore, it is important to assess the state of the sewage (figure 2.5). Sewage inspection reports of Waternet are consulted and sewers in a poor state modeled as drainage pipes. Whilst maneuvering through the sewage system, live video recordings are made on which the state of the sewage can be checked. Inspection criteria are e.g. sewer displacements, blockages, cracks and growth of tree roots. All factors contributing to groundwater infiltration are categorized under 'waterproofness'. There are four stages of waterproofness: 1) Intervention, 2) Warning 3) No warning 4) Not checked. In MicroFEM, those strings marked 'Intervention' are incorporated as

river systems. The drainage and infiltration resistance values of these leaky parts of the sewer are estimated initial values and calibrated upon.

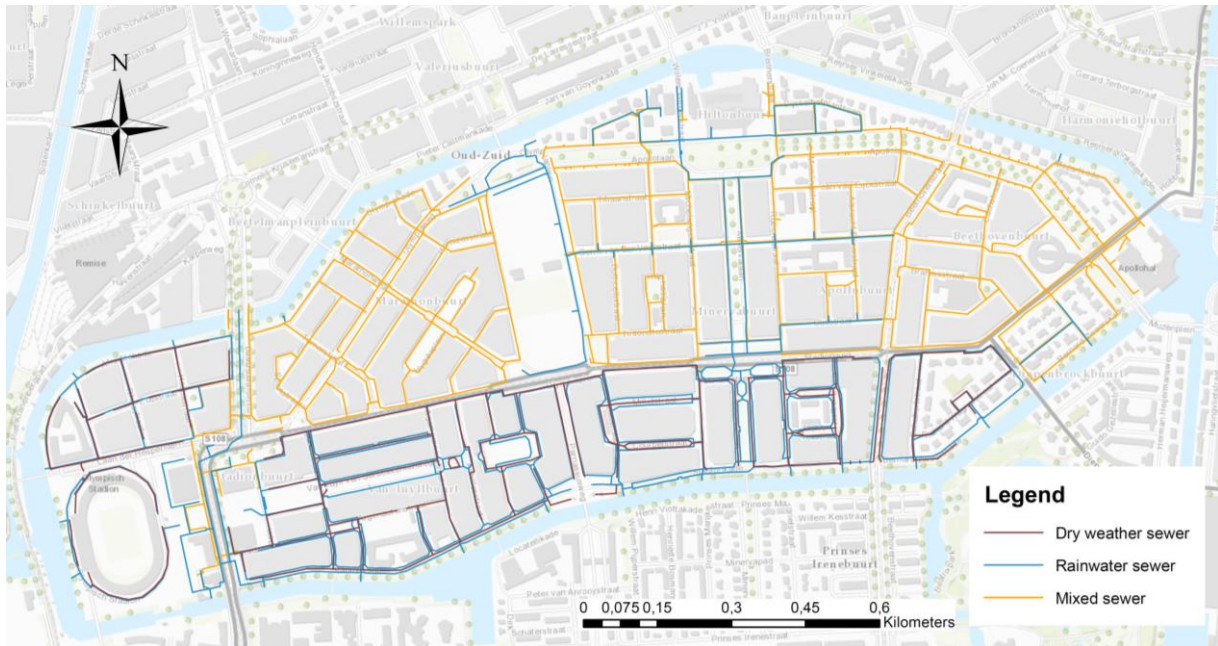


Figure 2.5 Sewage systems of the Stadioneiland with a mixed sewage system in area 5190 and separated dry weather and rainwater sewage in areas 5271 and 5050 (Adapted from Waternet database, 2018).

2.4 Time Series Analysis of groundwater observations

Whether the model has a good fit will be evaluated by comparing the calculated heads with piezometer observations. Waternet has close to a hundred piezometers within the research area. The measurement frequency differs per piezometer: on average, hand measurements are done every three months, whereas a pressure transducer logs every month up to five minutes, with a standard frequency of four times a day (Waternet Database, 2018). If these observations are used unprocessed, the optimization will be dominated by the more frequent observations. Besides, some piezometers – especially the higher frequency pressure transducers - are placed projects or experiments, such as construction work or an infiltration test (Graafstra et al., 2017). These periods do not reflect representative heads. Time series analysis is used to smooth out differences in measurement frequencies and determine the accuracy and precision of observation data (Graafstra et al., 2017). Heads are related to precipitation and evaporation using an empirical time series model (Knotters & Bierkens, 2000). The precipitation series P_t in mm day^{-1} and evaporation series E_t in mm day^{-1} are transformed as follows:

$$Y1_t = a1 Y1_{t-1} + (1 - a1)P_t \quad (2.6)$$

$$Y2_t = a2 Y2_{t-1} + (1 - a2)E_t \quad (2.7)$$

where smoothing factors $a_1 = e^{(-1/T_1)}$ and $a_2 = e^{(-1/T_2)}$, with time constants T_1 and T_2 in days (Janse & Graafstra, n.d.). From the transformed series Y_1 and Y_2 , a series of daily groundwater levels Z_t is simulated which has the best fit to the observations and the precipitation series by:

$$Z_t = b_0 + b_1 Y_{1t} + b_2 Y_{2t} \quad (2.8)$$

with b_0 as the regression parameter in meters and b_1 and b_2 being the regression coefficients of Y_1 and Y_2 , respectively.

Observations exceeding five times the standard deviation from the mean are considered outliers and are excluded from subsequent time series analysis (Janse & Graafstra, n.d.). An important result of the time series analysis is a measure of how well the time series model can replicate the variance of the observation: the explained variance. As groundwater levels are a linear function of precipitation and evaporation, the correlation coefficient for this data set is equal to the explained variance. The variance of variable X is defined as s_x^2 (Burt et al., 2009):

$$s^2 = \frac{\sum_{i=1}^n (X_i - \bar{X})^2}{n-1} \quad (2.9)$$

with the residual X_i , the mean of residual \bar{X} and n as the number of observations. For two variables X and Y , the correlation between their respective variances S_X or S_Y is determined by the Pearson's product-moment correlation coefficient r (Burt et al., 2009):

$$r = \frac{S_{XY}}{S_X \times S_Y} \quad (2.10)$$

On Stadioneiland, Waternet has checked piezometers in 2007. Therefore, observations since 2007 are more reliable than before and will be used for time series analysis. Climate data is used of the KNMI meteorological station at Schiphol. In stationary optimization, average head of 2007-2016 is compared to calculated stationary heads at piezometers. In transient optimization the 10-day or daily value of the time series heads is compared to calculated heads.

2.5 Stationary parameter optimization and calibration

Parameter optimization is the search for the least erroneous set of values for parameters not known exactly in the model. A measure of valuing the parameter sets is the error between the modeled values (m_i) and the observation values (o_i). The sum of all these squared errors (RMSE) is called the objective function (Φ). If n is the number of observations used in calibration, the objective function is given by (Doherty, 2002):

$$\Phi = \sum_{i=1}^n (m_i - o_i)^2 \quad (2.11)$$

The lower the objective function, the better the model calculations fit the observations. In parameter optimization uncertain parameters can be adjusted to reduce the objective function. Parameter optimization is only a part of model calibration process which is an iterative

loop of parameter optimization, analyzes of results, adjustments to model schematization and again parameter optimization (figure 2.1). Optimization will be done with the automated optimization routines of MicroFEM and PEST.

2.6 Sensitivity analysis

Part of the parameter optimization and calibration process is the sensitivity analysis. All parameters which are assumed to be uncertain are analyzed in order to determine the sensitivity of the model to each. Insensitive parameters can be left out of the optimization to increase calculation time. After each model run, PEST calculates the Jacobian matrix or the change in objective function (Φ) as a change in parameter values (x_n) (Weisstein, 2018):

$$J(x_1, \dots, x_n) = \begin{bmatrix} \frac{\partial \Phi_1}{\partial x_1} & \dots & \frac{\partial \Phi_1}{\partial x_n} \\ \dots & \dots & \dots \\ \frac{\partial \Phi_n}{\partial x_1} & \dots & \frac{\partial \Phi_n}{\partial x_n} \end{bmatrix} \quad (2.12)$$

The sensitivity of a parameter can be calculated through use of a scaling matrix S of the normal matrix of Jacobian $J^t Q J$ (Doherty, 2002):

$$S_{ii} = (J^t Q J)_{ii}^{-\frac{1}{2}} \quad (2.13)$$

Doherty (2002) defines sensitivity in two different ways:

- 1) Composite sensitivity, being V_{ii} , the inverse of the scaling matrix from equation 2.13, divided by the number of observations m .
- 2) Relative sensitivity, which is the composite sensitivity by multiplying it by the magnitude of the parameter value.

Composite sensitivity is used to determine which parameters the model is insensitive to and might be eliminated from the optimization to improve calculation time. Relative sensitivity can assist in determining the effect of parameters of different type and magnitude.

2.7 Quantification of sewage leakage flux

Information on groundwater infiltration would allow better determination of the leaky sewage resistances. Yet, quantification of infiltrating groundwater flux remains a challenge in urban water management (STOWA, 2003). During this research, an extensive effort is made to quantify this flux for area 5271. Unfortunately, it had to be concluded that the measurements are not reliable enough to be used for optimization. Both the specifically for this research area designed methodology and the results are described in annex 10.1.

2.8 PEST stationary parameter optimization and calibration

2.8.1 Introduction to PEST

PEST (**P**arameter **E**stimation) is a program designed to be coupled to any type of model and assist in data interpretation, model calibration and predictive analysis (Doherty, 2002). It optimizes parameters using the Levenberg-Marquardt algorithm. Similar to parameter optimization in MicroFEM, the objective function is minimized. The objective function (Φ) in PEST is calculated as follows:

$$\Phi = \sum_{i=1}^n (w_i r_i)^2 \quad (2.14)$$

where w_i is the weight of observation i ; r_i is the difference between the i 'th observation and the model outcome and n is the number of observations (Doherty, 2002).

The advantages of using automatic optimization over manual optimization in MicroFEM are numerous. First of all, optimization in PEST can be done fluxes in addition to head observations. Also, instead of all observations being equally important, they can be given a certain weight, for example based on location or measurement certainty. If observations with different units are used, for example head (m) and fluxes ($\text{m}^3 \text{day}^{-1}$) it is essential to correct for this difference in the observations weight (NHV, 1997). Furthermore, PEST provides a useful module for analyzing sensitivity. One of the most important reasons to decide on automatic optimization is the increase in efficiency over manual calculations, which leads to a much quicker and more effective calibration. PEST also provides a module through which parts of the PEST calculations can be run parallel on different computers or computer cores. In the process of optimization, PEST calculates more statistics than sensitivity alone, for example correlation matrix and group residuals. These statistics can partly be analyzed during optimization in order to halt useless optimizations.

2.8.2 Comparison MicroFEM vs PEST optimization

Before utilizing the added possibilities of PEST, an initial base run is done to compare optimization in PEST to MicroFEM. For this purpose, input and method of both optimizations has to be equal. In MicroFEM, the strong concentrations of observations around the project area of the Argonautenstraat was reduced by omitting certain observations. In PEST, the same set of observations is used by making the weight of the omitted observations zero.

2.8.3 Weighting of observations

Analysis is done using surface of the Voronoi diagram (the area represented by a location) as weight and using explained variance of time series analysis as weight. The weighting with the best fit - based on, among others, the distribution of residuals and run time - will be used in further model runs in PEST. By making Voronoi polygons, Stadioneiland is divided into piezometer regions of which all points within the region are closest to piezometer (figure 2.6).

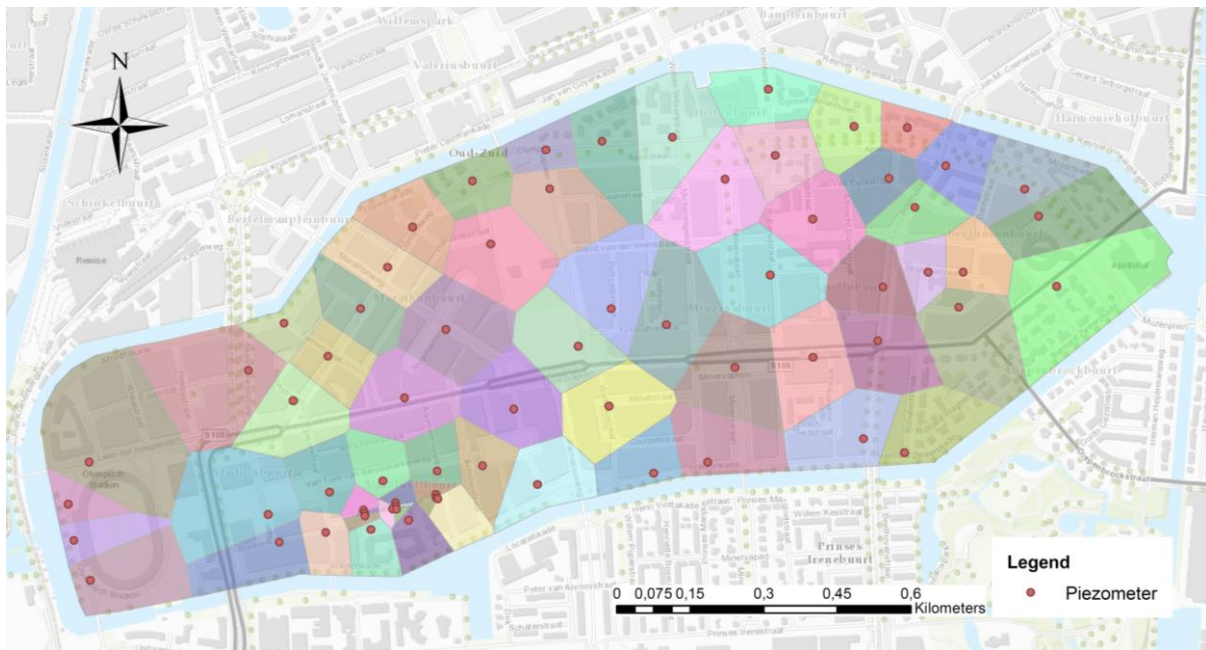


Figure 2.6 Stadioneiland divided into Voronoi diagrams around the corresponding piezometers.

2.9 PEST transient parameter optimization and calibration

For transient calculations, adjustments have to be made to the model regarding calculation period, storativity and groundwater recharge. In order to reduce calculation times of transient calculations, parts of a PEST optimization are run parallel.

2.9.1 Calculation period

The calculation period used in transient calculations is determined mainly by data availability. With time series analysis it appeared groundwater level observations are most reliable in the period from October 2013 until April 2018. In this research, a transient model run starts with calculating the stationary situation. To ensure there is no sudden jump from the stationary to the transient calculations and the initial head levels do not influence the optimization, the model is then run transiently for half a year from July to end of 2014 before optimization begins (table 2.1). Subsequently, optimization is done on two years, 2015 and 2016. The year 2017 will deliberately not be used for optimization so it can be used in validation of the model. To decrease model run time, the transient calculations are performed in time steps of 10 days.

Table 2.1 Time periods of calculation, optimization and validation periods. The first time period is preceded by a stationary calculation.

Time period	Purpose
Average of 2007-2016	Stationary calculations
2014-07-01 until 2014-12-31	Transient calculations without optimization
2015-01-01 until 2016-12-31	Transient calculation and optimization
2017-01-01 until 2017-12-31	Validation

Table 2.2 Historical climate data of temperature (yearly average) and precipitation (yearly sum) for the Netherlands and Schiphol climate station in the period of 2014-2017 (KNMI, 2018c)

Year	The Netherlands			Schiphol	
	Description	Temperature [°C]	Precipitation [mm]	Precipitation [mm]	Evaporation [mm]
2014	Exceptionally warm, very sunny and relatively dry	11.7	776	825.6	605.3
2015	Warm, sunny and normal amount of precipitation	10.9	831	885.1	623.2
2016	Very warm and sunny, relatively dry	10.7	757	862.6	602.8
2017	Very warm and sunny and relatively wet	10.9	862	932.6	610.9

Table 2.2 and figure 2.7 show climate conditions in terms of temperature, precipitation and evaporation in the calculation period from 2014-2017. Annual average precipitation in the Netherlands ranges between 700 – 900 mm per year, with an average of 849 mm over the

period of 1906 until 2003 (Buishand et al., 2010). Average precipitation of the years described in table 2.2 is 857 mm and is slightly higher than the long-term average.

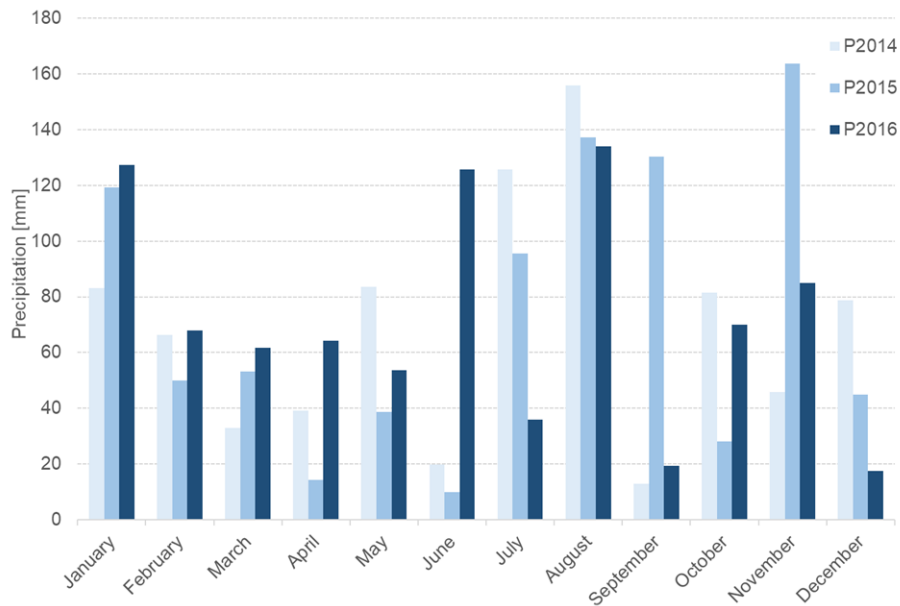


Figure 2.7 Monthly precipitation as recorded at Schiphol meteorological station for 2014 until 2016 (KNMI, 2018a).

Another indicator of climate conditions is the precipitation deficit: the difference between net precipitation and calculated evapotranspiration based on Makkink reference equation summed over the summer period from April 1st until September 30th (KNMI, 2018d). Figure 2.8 displays this deficit for the year 2015 with the all-time median in blue, whereas the average for the period of 1906-2000 is 144 mm per summer (KNMI, 2006).

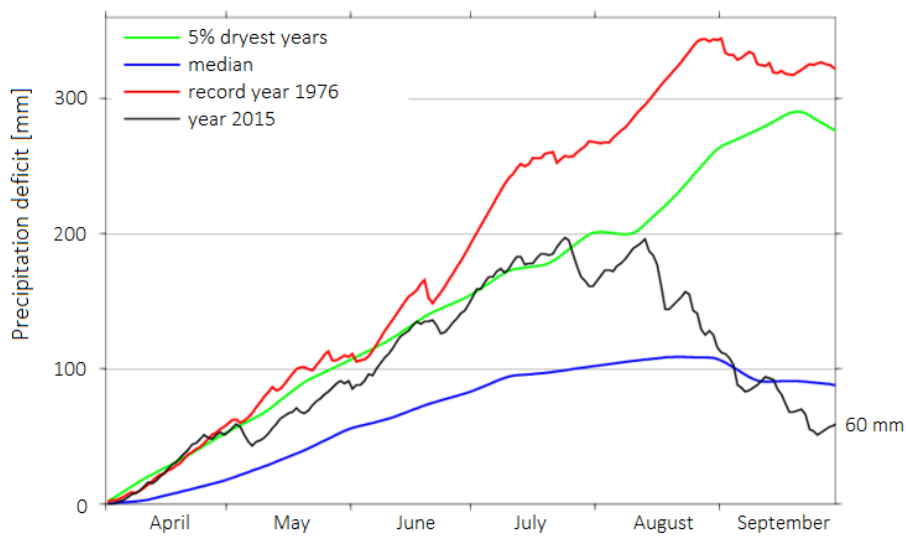


Figure 2.8 Precipitation deficit in 2015 in black relative to the median in blue, the 5% driest years of all-time in green and the record year in red (KNMI, 2018d).

2.9.2 Storativity

Storativity (S) is 'the increase or decrease in volume of water stored beneath the unit area per unit increase or decrease in head' (Dingman, 2015). The mechanisms for storativity differ for unconfined or confined aquifers. For an unconfined aquifer, storativity is defined as specific yield S_y or 'the volume of water that the unconfined aquifer releases from storage per unit surface area of aquifer per unit decline of the water table' (Kruseman & De Ridder, 2000). Specific yield is mostly determined by the type of soil material. The first aquifer of the research area is medium fine sand and will have a S_y of 0.28 (Bot, 2011; Kruseman & De Ridder, 2000). For a confined aquifer, storativity is defined as $S = S_s D$, where S_s is the specific storage (m^{-1}) and D the thickness of the aquifer (m). Specific storage for confined aquifers is mainly determined by the elastic storage coefficient. For confined aquifers around 20 m of depth, this global elastic storage coefficient is $4 \cdot 10^{-5} m^{-1}$ per meter of aquifer thickness (Bot, 2011). The second aquifer (the clayey sand of the Naaldwijk Formation) is around 8 m thick, resulting in a storativity of $3 \cdot 10^{-4}$. For the fine sand of the third aquifer (section 1.3.1) of 15 meters thick, the storativity will be $6 \cdot 10^{-4}$.

2.9.3 Groundwater recharge

Similar to the stationary calculations, groundwater recharge is determined for unpaved, semi-permeable and impermeable surfaces with the following formulas:

$$GWA_{unpaved} = P - E \quad (2.15)$$

$$GWA_{semi-permeable} = 0.15 * P \quad (2.16)$$

$$GWA_{permeable} = 0 \quad (2.17)$$

Now, instead of taking the average precipitation and evaporation to calculate the average groundwater recharge, calculations are made per 10 days.

2.10 Scenarios

Once the model is sufficiently optimized, it will be used to run three different scenarios:

- I. Climate change Wh scenario of KNMI
- II. Permeable paving
- III. DIT sewage and variable drainage depth

2.10.1 Scenario I - Climate change

In the first scenario, changes in climate are tested on the model. Adaptations to the system are designed for the future and climate conditions are not similar to those today. Therefore, the model is used to explore projected changes in precipitation and evaporation as predicted by the KNMI (2014). The effects of climate change are analyzed both on the long-term as in the case of extreme events.

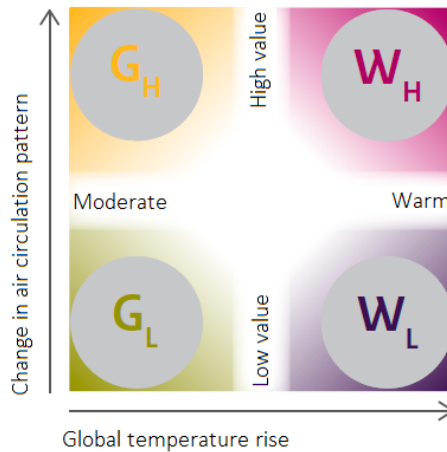


Figure 2.9 Four climate scenarios developed by the KNMI for the Netherlands based on the IPCC report of 2014 (KNMI, 2014).

For the year 2050, four different scenarios are set out, varying from low to high changes in air circulation patterns and 1 to 2 °C change in global air temperature compared to 1990 (figure 2.9). Scenario Wh has large changes in air circulation and a 2 °C temperature change. This most extreme scenario will be used in model exploration. KNMI provides a transformation tool in which a historical precipitation series can be converted to a series of a certain climate scenario. The precipitation series of mid-2014 until end 2016 is thus transformed to a Wh series with +15% per degree more precipitation in winter, -12% per degree less precipitation in summer and year-round more intense and frequent extreme precipitation events (KNMI, 2014). A transformation tool is also available for temperature, but evaporation is determined by more factors than temperature alone. To transform the current measured evaporation series for 2014-2016 to a future scenario, the precipitation deficit is used as calculated in the 2006 scenarios of KNMI, as no recalculations of the predicted precipitation deficit are done in the 2014 scenarios. For the period of 1906-2000 the average maximum precipitation deficit was 144 mm for the Netherlands and is projected to rise to 220 mm by 2050 according to the W+ scenario. The evaporation series of 2014-2016 are increased by 17% resulting in a net precipitation deficit of 220 on average for the transformed series.

Currently, the sewage system in Amsterdam is designed to withstand a precipitation event of 20 mm hour⁻¹ (Van Assenbergh et al., 2016). According to recent calculations of STOWA (2018), this represents a precipitation event with a repetition time of 2 years. The design target of 60 mm hour⁻¹ will occur once every hundred years based on data from 2003-2016. No predictions are made on the future repetition time of this target per hour. Though according to most recent calculations of KNMI (2018b) for the city of Amsterdam, the highest climate scenario for 2050 indicates precipitation of 60 mm in one day will occur a factor 2.5 more frequent (figure 2.10).

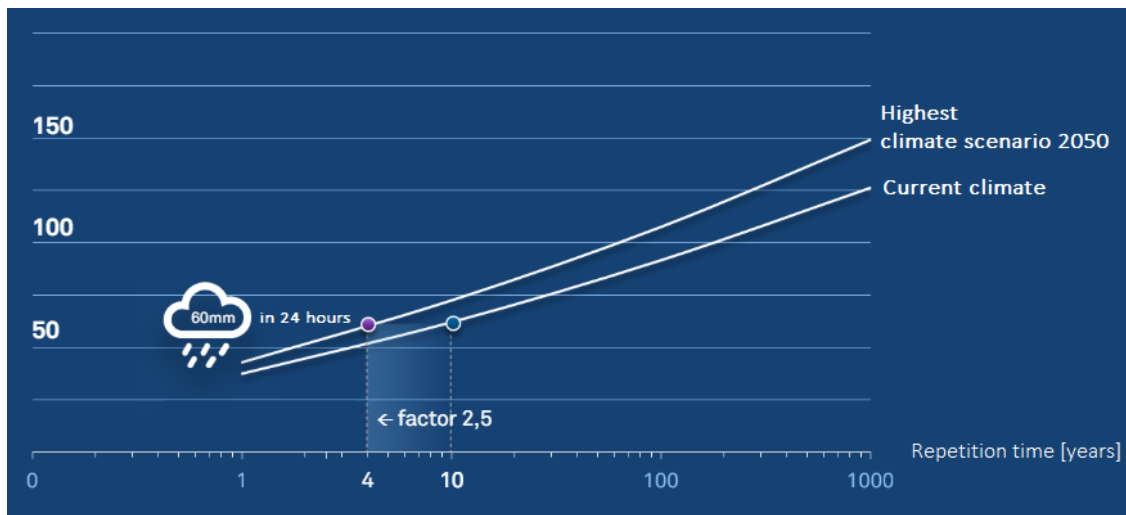


Figure 2.10 Repetition time of precipitation [mm day^{-1}] for Amsterdam in the current climate compared to the highest climate scenario in 2050 (KNMI, 2018).

2.10.2 Scenario II - Permeable paving

The second scenario is aimed at climate proofing the research area, focussing on infiltrating precipitation through permeable paving to the groundwater. The advantages of which are both to reduce pressure on the rainwater sewage during extreme precipitation and make better use of the scarce precipitation during periods of drought. Countless types of permeable paving are available, though many face the problem of clogging by street dirt or other pollutants (Pötz & Bleuzé, 2016). Consequently, the infiltrating capacity of the paving reduces and maintenance or replacement is needed. One particular type of permeable paving, the Drainvoeg, seems to minimize this advantage as dirt collects on the street level of the joint and can be cleaned partly by road sweepers (figure 2.11). To test the materials functioning, especially after exposure to street dirt and other sources of clogging, an infiltration test is performed.

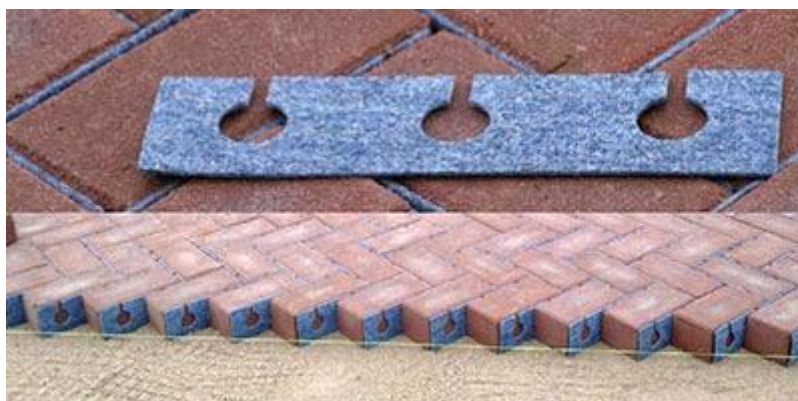


Figure 2.11 Permeable paving by use of Drainvoeg joint material, during construction (MKB, 2018).

2.10.3 Scenario III - DIT sewage and variable drainage depth

Similar to the previous scenario, this scenario aims to make Stadioneiland more climate proof. In order to prevent heads to drop to hazardous levels for foundation poles, two different adjustments to the drainage system are explored. First drainage level of the current drainage sewer can be heightened by designing an attachment piece to the drainage tube (figure 2.12). For example, during the end of the winter (February 1st) the drainage level can be raised to NAP -0.20 m to allow for a higher starting level when the drop in groundwater levels starts in summer. The hypothesis is the heads will increase during summer using this new design.

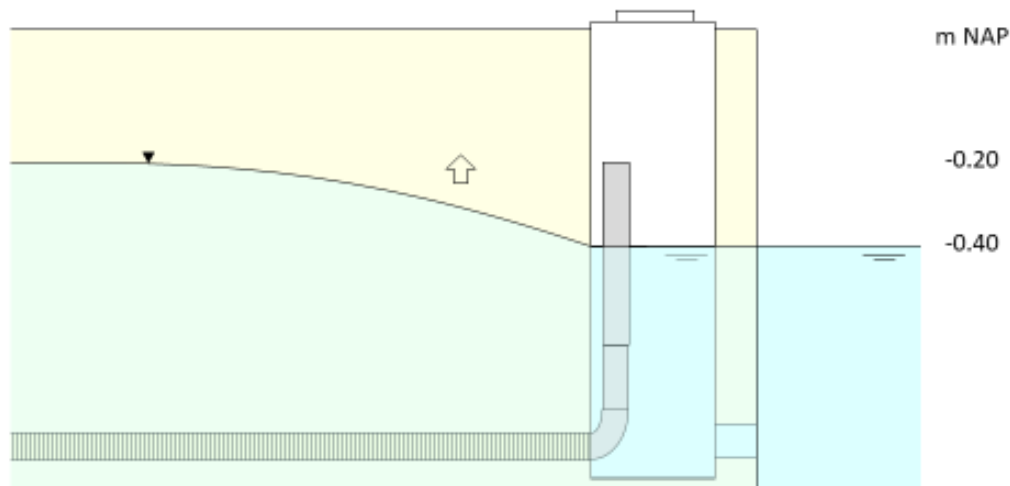


Figure 2.12 Design of drainage, infiltration and transport sewer with an attachment piece to elevate the drainage level to NAP -0.20 m.

An addition to this design could replace drainage with drainage, infiltration and transportation (DIT) sewers. It is presumed these pipes could drain high groundwater level in winter and infiltrate water from the canals during summer. If a higher drainage level is set than the surface water level, no infiltration can occur, but still it is hypothesized groundwater levels will be higher at the start of summer. When groundwater levels drop below NAP -0.40 m, the attachment piece can be removed, thus draining again at the NAP -0.40 m level, but also allowing for infiltration at level. During long periods of drought, this infiltration can supply vegetation with sufficient water for evapotranspiration whilst still preserving the standard of 40 cm of foundation water coverage. In this scenario, the moment at which the attachment is removed is at May 1st, but the moment at which groundwater levels drop below NAP -0.40 m will vary per location.

3 RESULTS CALIBRATION

The model calibration results are presented in this chapter in the same order as the modeling process of section 2.2. Model conceptualization will recur throughout the results as schematization adjustments were made during calibration (figure 2.1). The scenario results will be presented in the subsequent chapter 4.

- 3.1 Pre-optimization fit
- 3.2 Stationary parameter optimization and calibration
- 3.3 PEST stationary parameter optimization and calibration
- 3.4 PEST transient parameter optimization and calibration
- 3.5 Final optimization

3.1 Pre-optimization fit

Figure 3.1 displays calculated heads in the phreatic aquifer using initial conditions before optimization. How these calculated heads compare to the observations at the piezometers is displayed spatially in figure 3.2. All piezometers west of the Olympic Stadium are underestimated up to 0.43 m whereas the other piezometers are overestimated. Figure 3.3 shows a wide spread of head points, with most point below the line indicating overestimation.

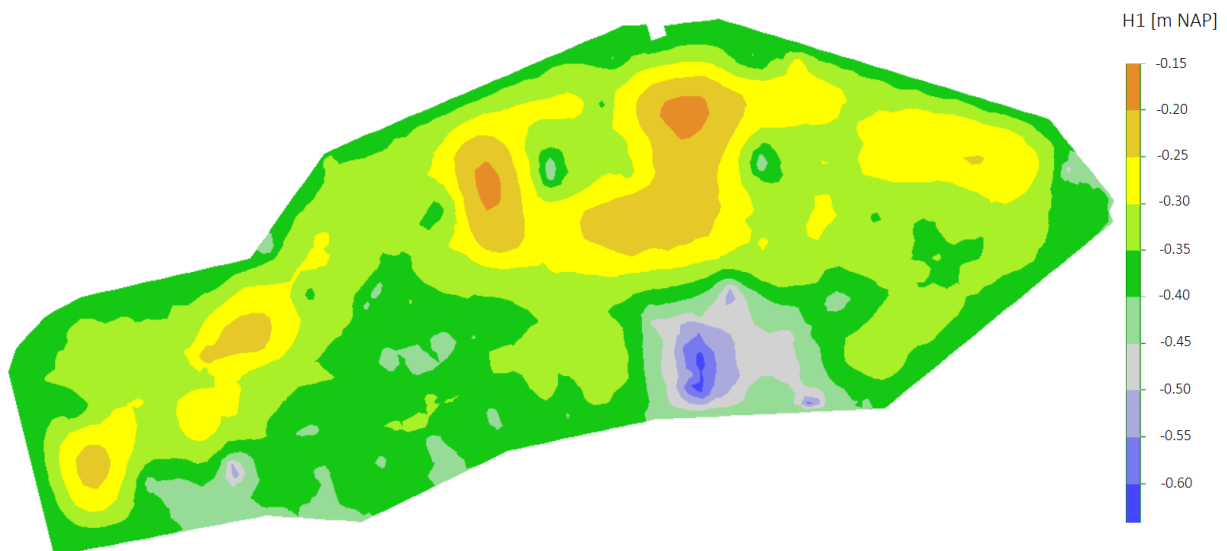


Figure 3.1 Calculated heads of the stationary model with the initial parameter values.

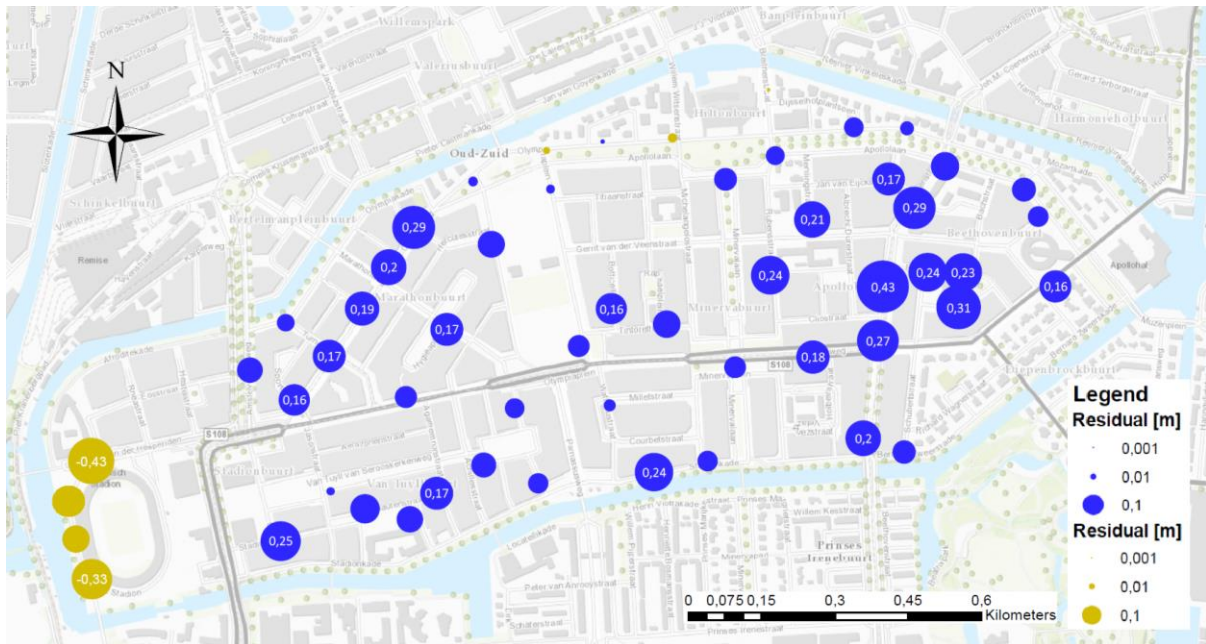


Figure 3.2 Residuals of the stationary model with the initial parameter values. Blue circles indicate calculated head is higher than the observed head and yellow circles indicate a calculated head lower than observed.

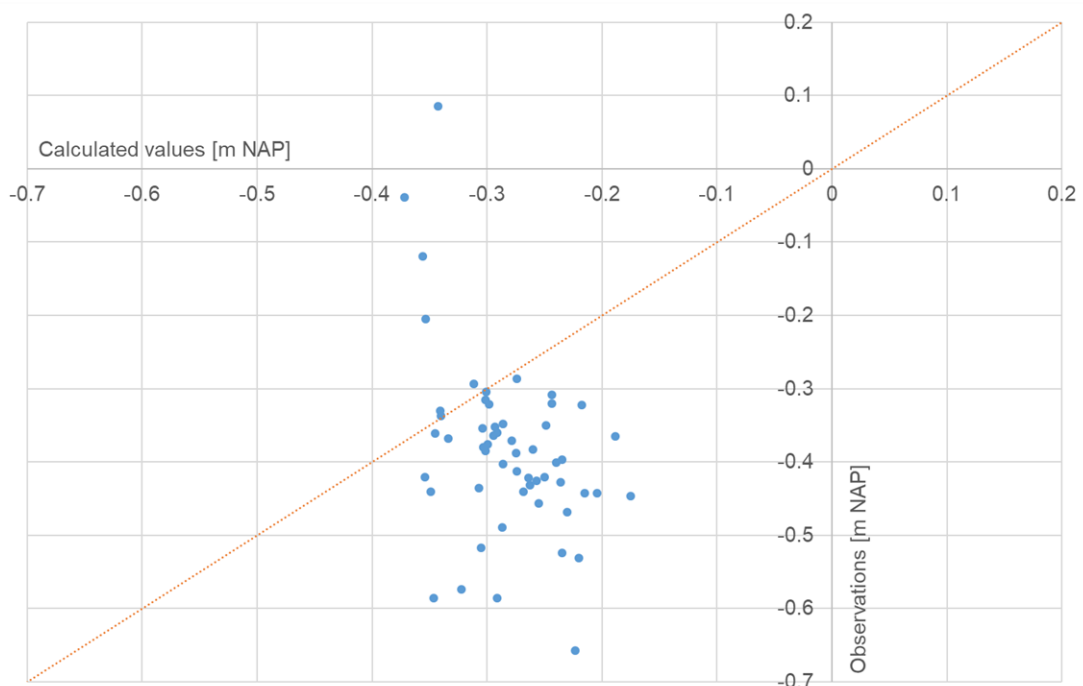


Figure 3.3 Calculated heads with the stationary model with the pre-optimization parameters compared to average observed heads at the piezometers.

3.2 Stationary parameter optimization and calibration

In order to improve the fit in figure 3.2 and 3.3, the stationary model is optimized on five parameters which are considered uncertain. Table 3.1 displays these parameters with their initial values and after optimization with MicroFEM. Transmissivity increases with factor 1.76, $rc1$ and $ri2$ decrease whereas $ri1$ and $rc2$ increase. The objective function is decreased with 19% to 0.74. The spatial distribution and quantity of residuals is displayed in figure 3.4. The residuals are smaller in magnitude and more randomly distributed, though the west of the Olympic Stadium are still underestimated. The fit of the calculated with observed heads improves (figure 3.5).

Table 3.1 Initial and optimized values for parameters of the stationary model.

Parameter		Symbol [unit]	Initial value
Transmissivity factor		$ft1$ [-]	1
Drainage	Drainage resistance	$rc1$ [d]	100
	Infiltration resistance	$ri1$ [d]	100
Leaky sewage	Drainage resistance	$rc2$ [d]	100
	Infiltration resistance	$ri2$ [d]	100
Objective function		Φ [-]	0.91

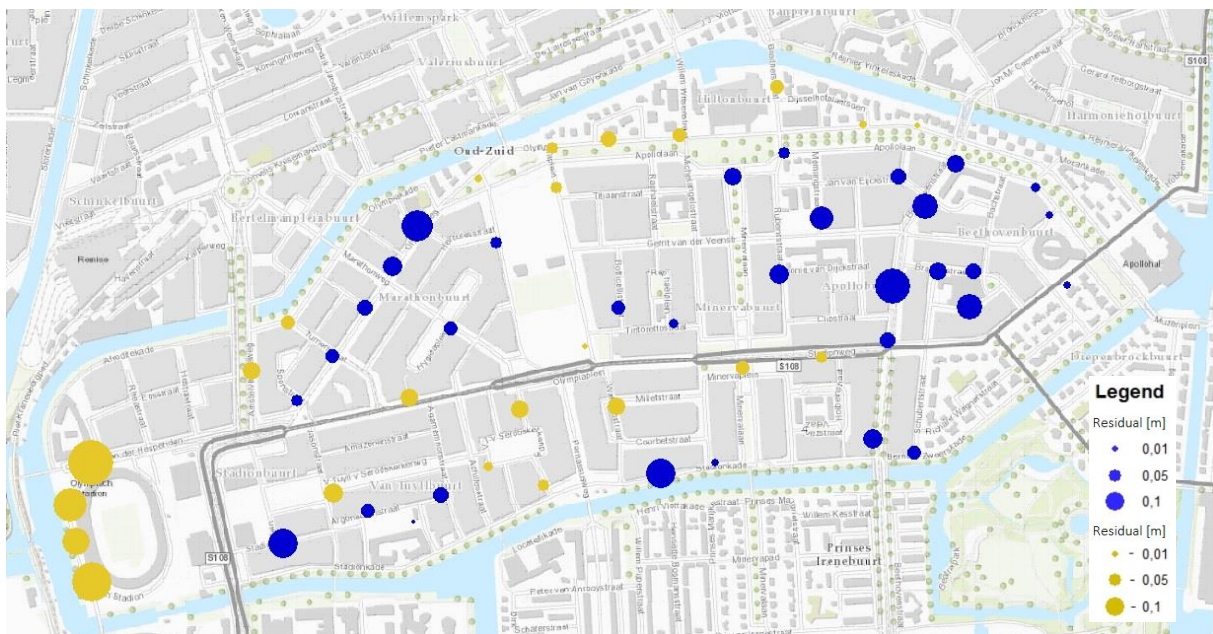


Figure 3.4 Calculated heads compared to observed heads after stationary optimization in MicroFem.

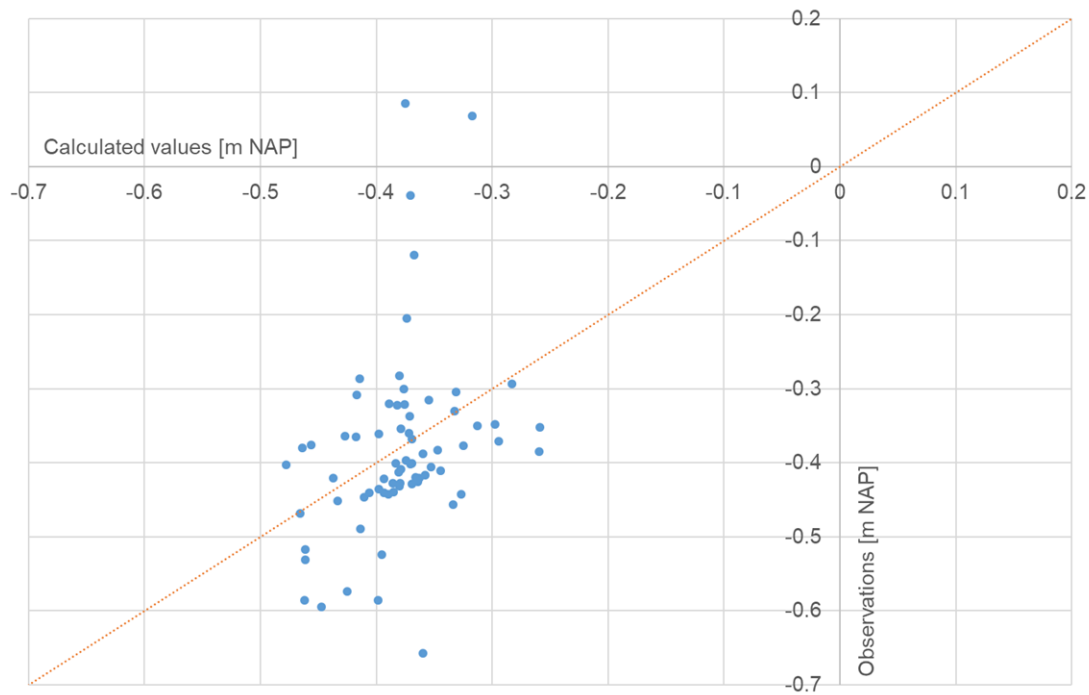


Figure 3.5 Calculated heads with the stationary model after optimization compared to average observed heads at the piezometers.

All five optimized parameters have composite sensitivities above $1E^{-02}$, with relative sensitivity of infiltration resistances $ri1$ and $ri2$ being the highest with 2.9 and 2.3 respectively. Throughout the following optimizations, composite and relative sensitivities are analyzed when interpreting results. During calibration, no parameters turned out to be sufficiently insensitive to be eliminated out of the optimization process.

3.3 PEST stationary parameter optimization and calibration

3.3.1 Comparison MicroFEM versus PEST optimization

The results of optimization with same initial values using either the optimization routine of PEST or MicroFEM is shown in table 3.2. The initial as well as the residual sum of squares in PEST is slightly higher than in MicroFEM, though PEST does manage to reduce to objective function by 10% more relatively. The difference might be caused by the rounded values MicroFEM returns to PEST during optimization. The ranges of optimized values differ per optimization routine. In MicroFEM the upper and lower range are determined by +/- one standard deviation and in PEST by the 95% confidence limits. It appears value ranges calculated in PEST are more narrow, but the two types of ranges cannot be compared at first sight. Increase in transmissivity might be due to the high initial value of the drainage resistance (100 days). Whilst reducing the drainage resistance, the hydraulic conductivity increases as well. Therefore, the initial value of $rc1$ is chosen to be 20 days from now onwards.

One of the motivations to use PEST for optimization is to be able to optimize on fluxes in addition to head observations. The measurements at the pumping station 5271 showed groundwater infiltration for the area was around a value of $90 \text{ m}^3 \text{ day}^{-1}$. If compared to the net

precipitation of $50 \text{ m}^3 \text{ day}^{-1}$, it can be concluded this value is unrealistic and will not be used for optimization. The full calculations are presented in annex 10.1.

Table 3.2 Results of optimization in PEST and MicroFEM.

Parameter	Symbol [unit]	Initial values	Stationary MicroFEM	Range	Stationary PEST	Range
Transmissivity factor	α_1 [-]	1	1.76	1.65-1.88	1.11	1.11-1.16
Drainage resistance drainage	rc_1 [d]	100	0.66	0.58-0.75	1.2	1.23-1.24
Infiltration resistance drainage	ri_1 [d]	100	113.7	108.0-119.7	100.6	100.4-100.8
Drainage resistance leaky sewage	rc_2 [d]	100	158.7	150.5-167.4	125.4	125.0-125.7
Infiltration resistance leaky sewage	ri_2 [d]	100	53.0	52.4-53.7	77.9	77.7-78.1
Objective function	Φ [-]	MicroFEM: 0.91 PEST: 1.07	0.74		0.76	

3.3.2 Weighting of observations

To determine the most suitable weight factor for the observations, several types of results are analyzed: the residuals between calculated and observed heads (figure 3.6 and 3.7), the initial and residual objective function (table 3.3) and the calculation time. The spatial distribution of calculated heads are shown in annex figure 9.4 and 9.5.

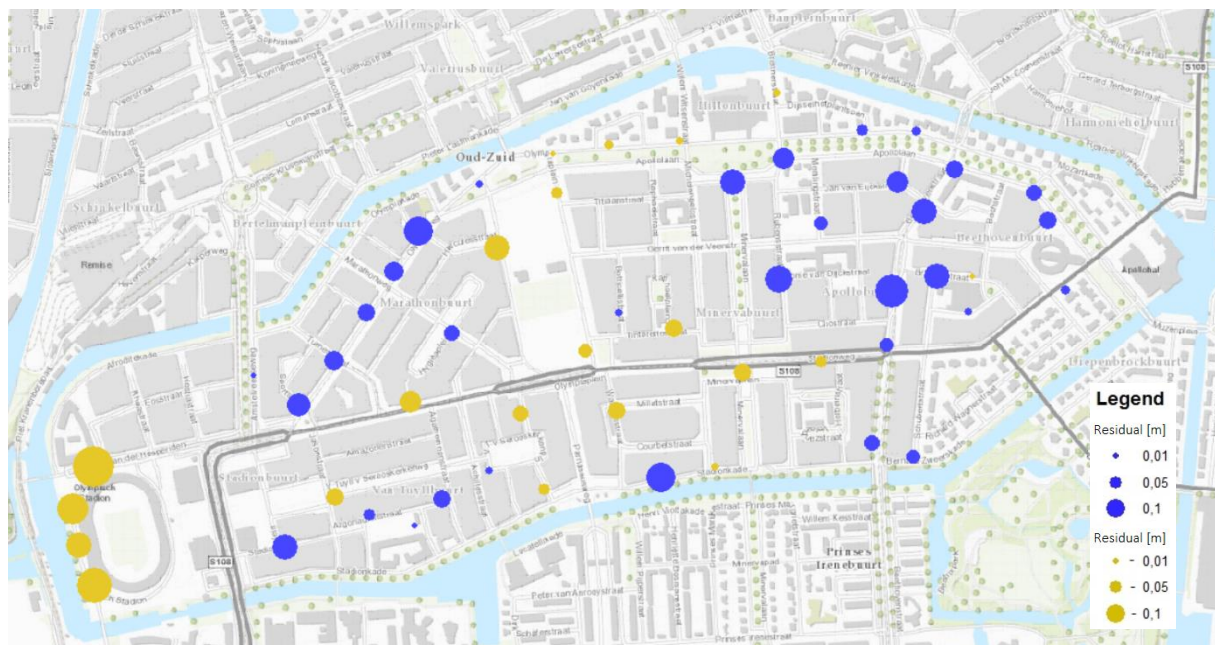


Figure 3.6 Residuals of calculated and observed heads using Voronoi area to weight the observations.

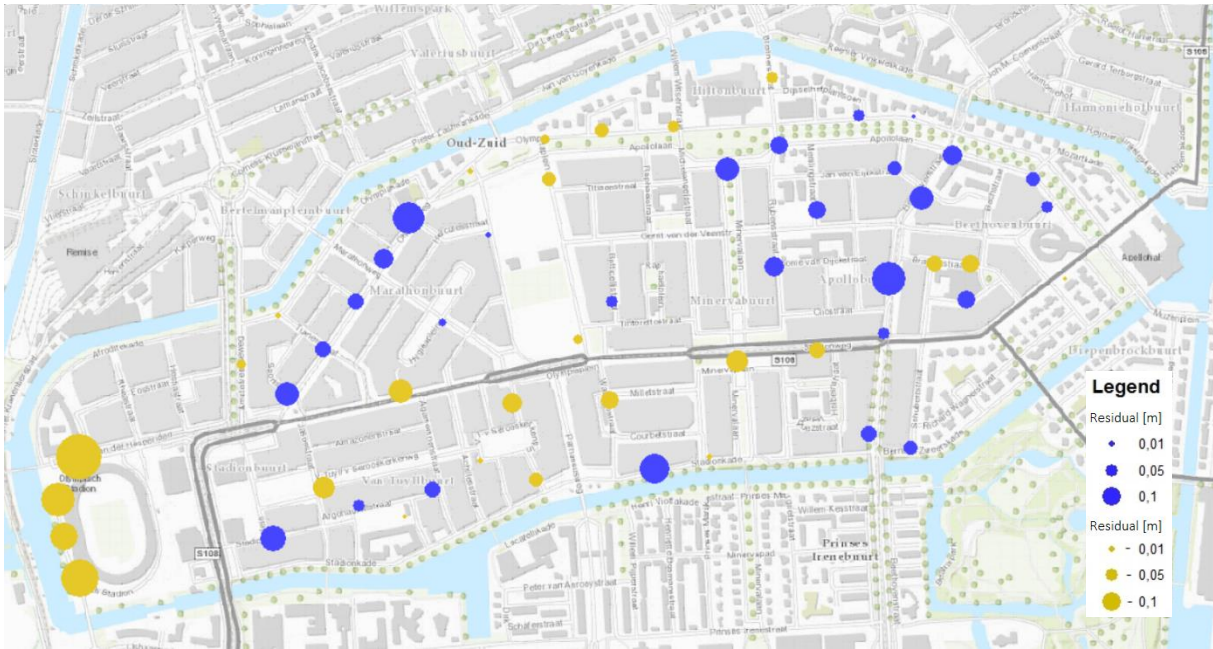


Figure 3.7 Residuals of calculated and observed heads using explained variance of the time series analysis area to weight the observations.

A non-random distributed pattern of residuals might indicate an error in the conceptual model (NHV, 1997). Residuals when using explained variance as a weighting factor are more randomly distributed, with underestimation varying with overestimations and large residuals close to small residuals. Objective functions of both weighting factors are displayed in table 3.3, but cannot be compared as weighting factors influence initial objective functions as well. When taken into account the lower calculation time and more randomly distributed heads of the phreatic aquifer (annex figure 10E-F), explained variance is chosen to weight the observations in following optimizations.

Table 3.3 Results of optimizing the model using Voronoi or explained variance to weight the observations.

Parameter	Symbol [unit]	Voronoi	Explained variance
Initial objective function	Φ [-]	3.18	1.21
Residual objective function	Φ [-]	2.80 (88%)	1.03 (85%)
Maximum correlation coefficient in matrix	r [-]	0.56	0.52

3.4 PEST transient parameter optimization and calibration

In stationary calculations, residuals were plotted as calculated heads minus average observed heads. This approach is no longer suitable when optimizing a transient model. Instead, residuals are plotted as the combined contribution per piezometer to the objective function Φ over the length of the calculation time. In addition, the *average* calculated head is plotted compared to the average observed head to be able to analyze model under- and overestimations. The objective function in PEST is calculated using a quadrate (equation 2.14) and is not a reliable measure when interpreting groundwater levels. The average residual in units of meters is easier to interpret, but evens out negative and positive residuals. A combination of the two visualizations, together with graphs of simulated and time analyzed series over time, provide insights to interpret the optimization results.

3.4.1 Division of canal walls, sewage and drainage parameters

Throughout all optimizations until now, the piezometers in pumping area 5271 (figure 1.8) on the west side are underestimated by the model. These persistent residuals led to the hypotheses that the canal wall around that side of the island might be less permeable than in the rest of the island.



Figure 3.8 Division of canal wall west (orange) from canal wall east (blue) with photo outsets from fieldwork displaying the typical wall construction of each region.

Fieldwork was initiated during which the canal walls all around the island were inspected and photographed. Also a discussion with colleagues of the Civil Engineering Department (IB) of the municipality of Amsterdam was held on this topic. It was concluded the canal wall around the western part is of different construction and probably less permeable (figure 3.8). Consequently, the canal walls are split in two regions and their resistances optimized separately.

Up until now, all sewage on the island is optimized together. As it was aimed to determine the discharge of infiltrating groundwater per pumping area, the resistance parameters rc_2 and ri_2 of the leaky sewage are split in three according to area (table 3.4). Similarly, drainage parameters were optimized for all drains combined. However, the state and draining capacity of the drains will not be equal. The main cause of reduced drainage is cluttering due to iron in the groundwater (Bos, 2004). When the dissolved iron Fe^{2+} is exposed to oxygen, it will oxide as Fe^{3+} and create flocks. Under influence of bacteria, a gel type of substance is created which sticks to drain openings and increases drainage resistances. The drainage is split into three age categories (figure 3.9) to test the hypothesis whether older, more clogged drainage will increase in resistances. Table 3.4 shows the optimized values for the separated sewage and drainage parameters.

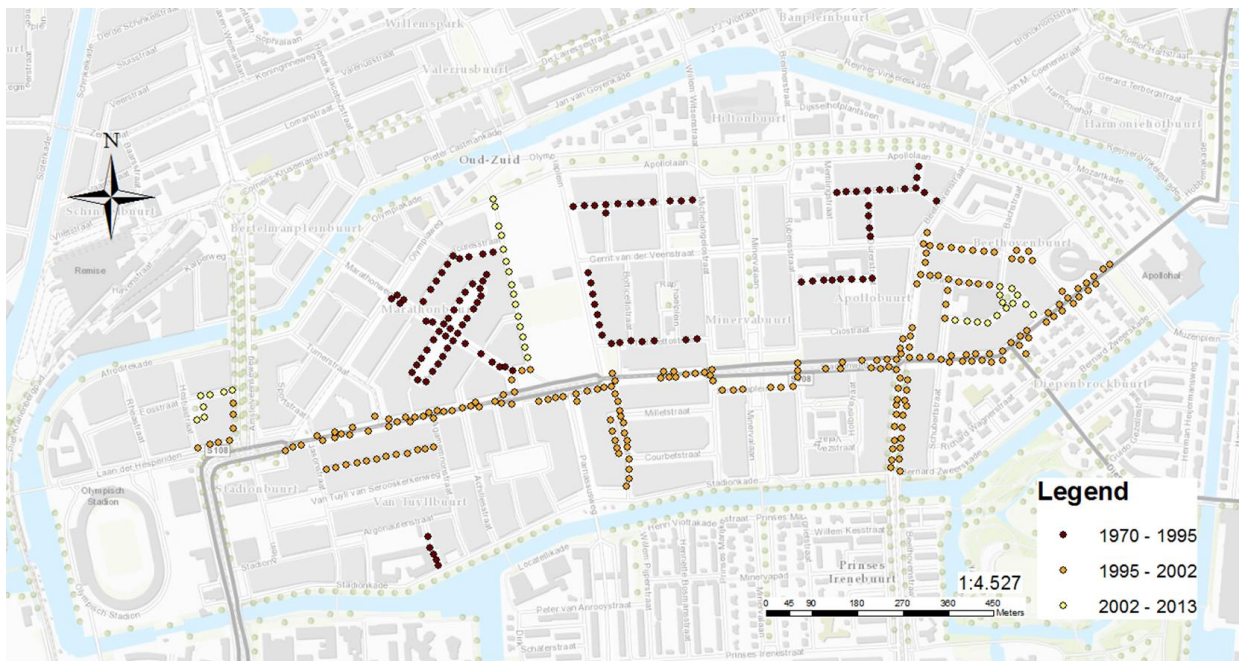


Figure 3.9 Categorization of drainage according to age with young drainage in yellow, medium aged in orange and old drainage in brown.

The results of the division of the canal walls into two regions, the sewage system into three regions and the drainage into three age categories are shown in table 3.4. In the area 5271 of underestimated heads, drainage resistance has a higher optimum value than in the other two regions and the infiltration resistance a very low optimum value of 0.15 days. The resistance of the west canal wall has a higher optimum value of 120 days compared to the east wall of 13 days at this point in the calibration. The hypothesis that older drainage has higher optimum values for resistances is not represented in the optimization. Possibly, this is caused by the age categorization or because older drainage is of a different, more robust type.

Table 3.4 Initial and optimized values for drainage, sewage and canal wall parameters after division into age category and area, respectively.

Parameter		Symbol [unit]	Initial value	Optimized value	
Transmissivity factor		$ft1$ [-]	1	7	
Drainage	Drainage resistance	Young	$rc1_young$ [d]	10	125
		Medium	$rc1_medium$ [d]	20	196
		Old	$rc1_old$ [d]	30	50
	Infiltration resistance	Medium	$ri1_medium$ [d]	100	8
		Old	$ri1_old$ [d]	100	13
Leaky sewage	Drainage resistance	Area 050	$rc2_050$ [d]	100	65
		Area 190	$rc2_190$ [d]	100	18
		Area 5271	$rc2_5271$ [d]	100	732
	Infiltration resistance	Area 050	$ri2_050$ [d]	100	50
		Area 190	$ri2_190$ [d]	100	7
		Area 5271	$ri2_5271$ [d]	100	0.15
Canal wall resistance		East	$c1east$ [d]	20	13
		West	$c1west$ [d]	30	120

3.4.2 Revision drainage schematization

In these transient optimizations, the residual of the largest magnitude no longer corresponds to piezometer F05249 north of the Olympic Stadium, but to piezometer F05309 in the Beethovenstraat (figure 3.10). In figure 3.11, the calculated heads are plotted along the observed heads at this location and those derived from the time series analysis. The rise and fall of groundwater levels seems roughly in accordance with the pattern of the TSA series, though with an overestimation of around 0.20 - 0.30 m. This is an indication to reassess the presence and depth of drainage in the surrounding area. During fieldwork, drainage level at the Gerrit van der Veenstraat was remeasured to be NAP -0.60 m instead of the NAP -0.40 m. Based on the type of drainage and time of installation, this lower drainage level is applied to a part of the connected drainage. The calculated heads with the corrected drainage depth of NAP -0.60 m is plotted in figure 3.12. As a result, the simulated series is slightly lowered, barely observable. The drainage located close to the Beethovenstraat is part of the medium-aged drainage from the period of 1995-2002. Even if the drainage depth is corrected, the drainage resistance will be optimized along with all other medium-aged drainage. An analysis is made of a separate optimization of the drains in the close perimeter of the Beethovenstraat. These drains structurally have a factor 4-10 lower optimized resistance value than medium drainage. Drainage around the Beethovenstraat is thus considered of a different type or in a more effective state than other medium-aged drainage.

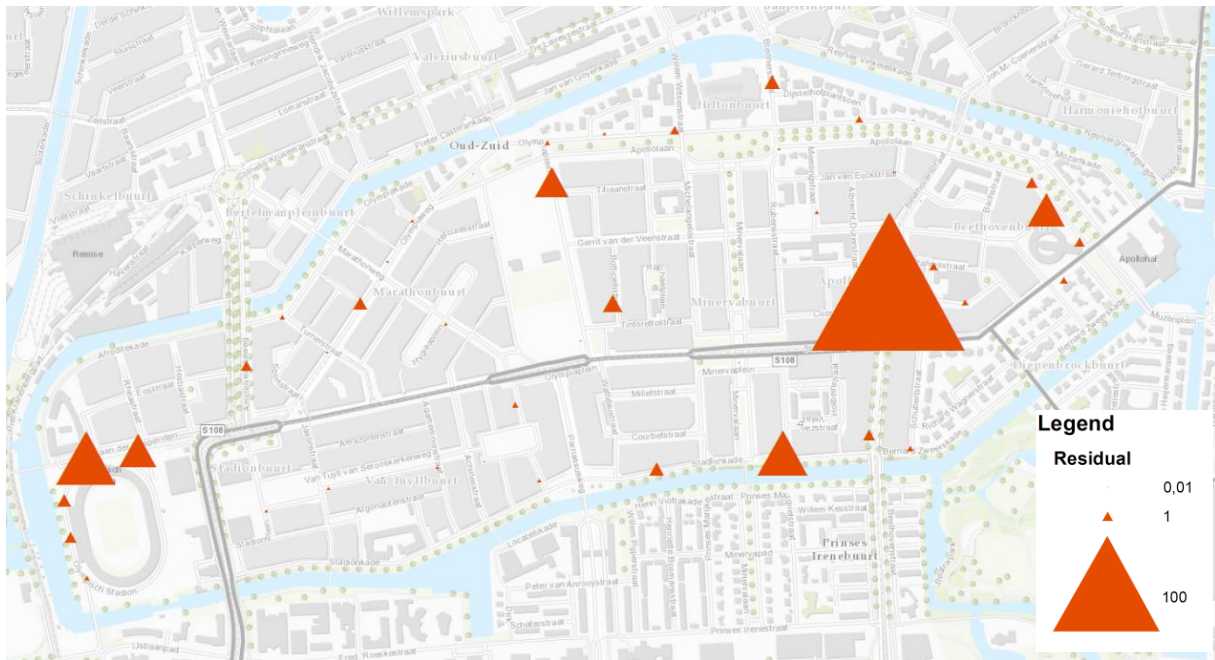


Figure 3.10 Contribution to the objective function at each piezometer location after transient optimization per 10 days. The largest residual is piezometer F05309 at the Beethovenstraat.

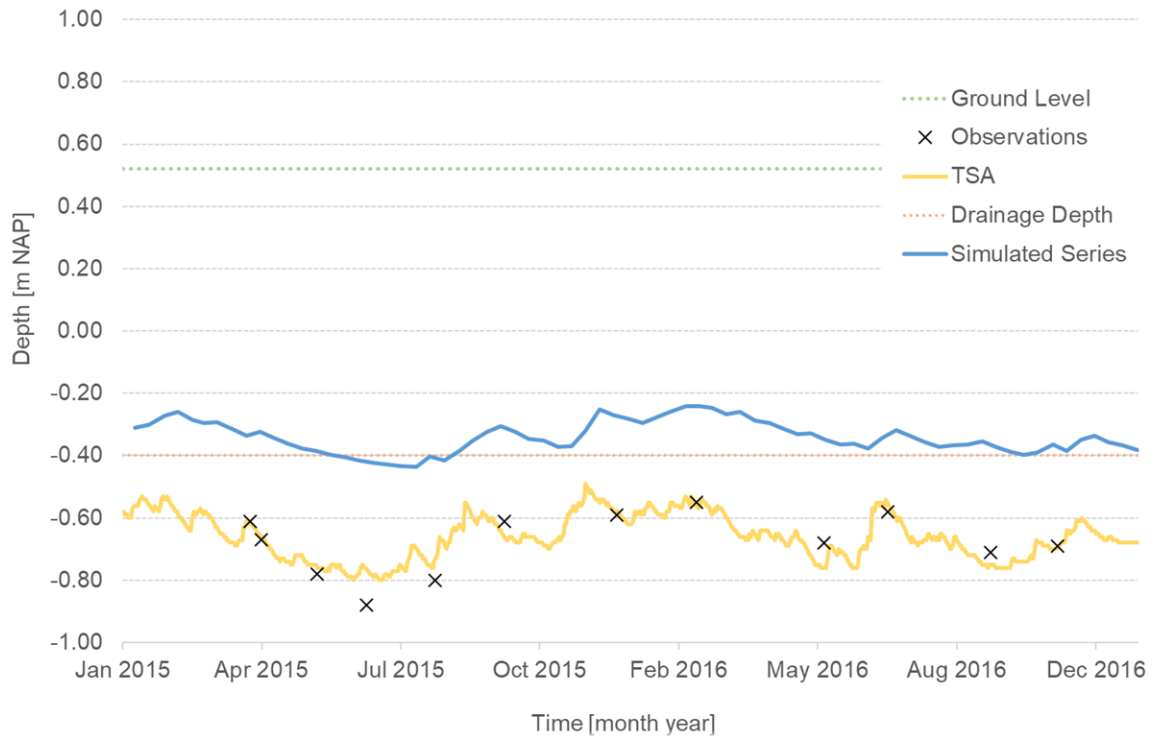


Figure 3.11 Transiently calculated groundwater level after optimization for piezometer F05309 (Beethovenstraat) from January 2015 until December 2016.

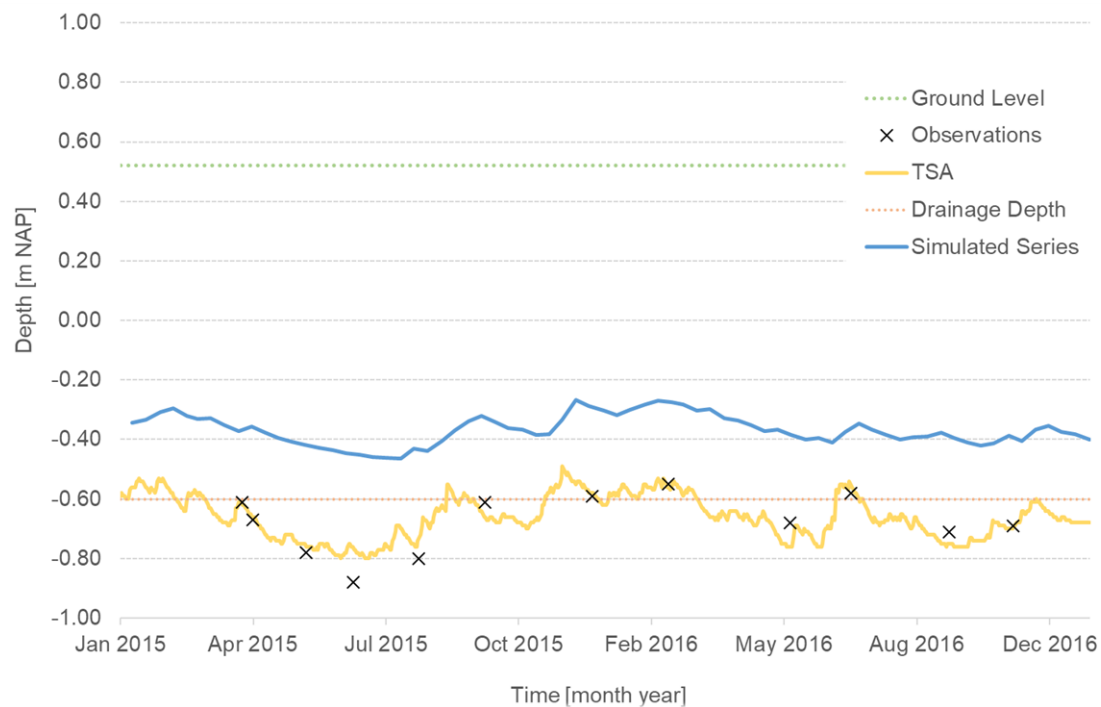


Figure 3.12 Transiently calculated groundwater level after correction of drainage level and optimization for piezometer F05309 (Beethovenstraat).

3.4.3 Incorporation of historical dyke body

Groundwater levels at the four piezometers in pumping area 5271 have been underestimated by the model for all runs so far. Even after fieldwork and the associated adjustments to the permeability of canal walls, all parameters are optimized in the direction of providing more water in this region of the island. For example, transmissivity goes up, drainage resistance of region 5271 is increased whereas the infiltration resistance is reduced and the resistance of the canal wall is maximized so no groundwater can seep towards the canals. But in these extreme and unrealistically optimized situation, groundwater levels are still too low, indicating more factors are at play.

This led to the discovery of a historical dike body located within the research area. In 1864, Rijkswaterstaat has made the first edition of the 'waterstaatkaart'. This map shows a large part of what currently is Amsterdam South was a polder at the time: the Binnendijsche Buitenveldersche polder (figure 3.13). The polder was enclosed by a dyke located at what now is the Amstelveenseweg (Van Manen & De Kleijn, 2017). No known records are found on the current state of this dyke, though from Waternet experience such bodies are rarely removed when a polder area is turned into a residential area. Before allowing residential construction work, ground level has to be heightened. Removing a dyke first would make this process costlier and result in more material needed as well. Therefore, chances are the dyke is still in place underneath the current Amstelveenseweg. As dykes (partly) consist of an impermeable clay layer, this part of the phreatic aquifer is expected to have a low hydraulic conductivity. The historical dyke body is incorporated in the model schematization by reducing the hydraulic conductivity K to 0.005 m day^{-1} , which is a general value for clayey loam (Bot, 2011). Hydraulic conductivity might even be lower when the dyke consists of (heavy) clay, but caution is made

not to exaggerate the dyke's presence. On top of the dyke, a small quantity of sand can still be available.

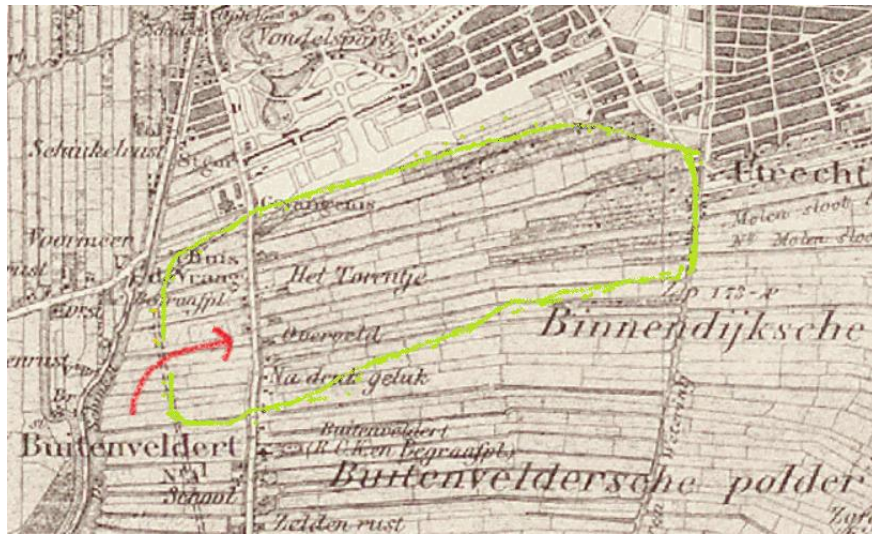


Figure 3.13 Topographical Military Map on which the first ‘waterstaatkaart’ of Rijkswaterstaat is based. Stadioneiland is encircled in green and the dyke of the Binnendijksche Buitenveldersche Polder is indicated with the red arrow (Van Manen & De Kleijn, 2017).

3.4.4 Construction work Stadionplein

Even after incorporation of the dyke body as described in the previous section, the model could not simulate the high groundwater levels west of the Olympic Stadium. After thorough research, the advice for the permit of the construction work at Stadionplein in 2015 showed the suggestion to return part of the dewatering and marked several possible return locations. No monitoring report on the activities is available, though on a historical view of Google Streetview the location of the injection wells can be spotted: on the west side of the Olympic Stadium. The injection wells can be seen to discharge to quickly, causing water to burst up to the surface, thus replenishing the top aquifer (figure 3.14). These injection wells can be the explanation for the high observed heads of the west piezometers, though without quantities of the return fluxes, the construction work cannot be simulated in the model. Therefore, the only option was to remove these four piezometers from the optimization.

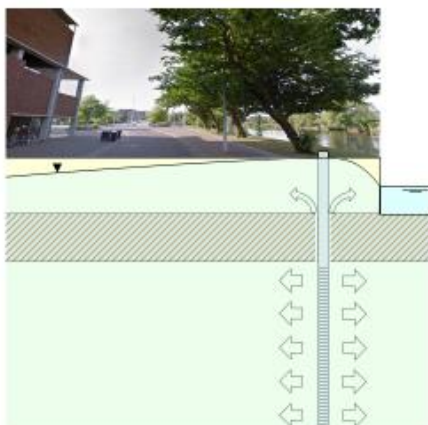


Figure 3.14 Bursting injection wells on the west side of the Olympic Stadium.

3.4.5 Refinements calculation steps and groundwater recharge

Towards the end of the optimization, two refinements are made to the model. First of all, the calculation steps are changed from 10 days to 1 day. As shown in figure 3.12, the precision of the time series analysis cannot be simulated by the model in steps of 10 days. If the model calculates heads per day, the fit with the observation series significantly improves (figure 3.15).

Secondly, groundwater recharge is assigned more accurately with a programmed routine. The summed up surface area per land use category in MicroFEM has a 99% correspondence with the total surface area distribution in the GIS land use map. Still, nodes are attributed to either of the three categories of land use, whereas their nodal area probably will consist of a mix of the three. The groundwater recharge per node is changed to be proportional to the percentages of land types within the nodal area.

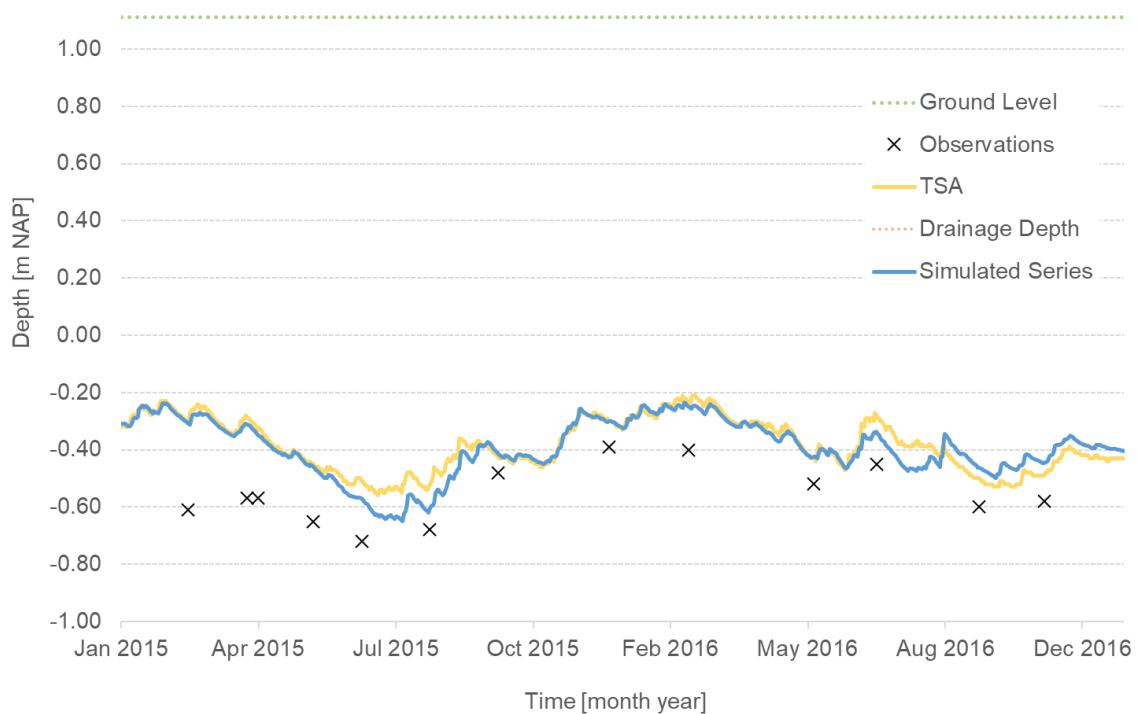


Figure 3.15 Transiently calculated groundwater level with refinement of calculation steps and groundwater recharge for piezometer F05134 (Apollolaan).

3.4.6 Reevaluation of weighting factors

Since the evaluation of the weighting factors as presented in 2.8.3, many adjustments to the model are made. The largest adjustments are the transition from stationary to transient calculation, from steps of 10 days to one day and all schematization corrections which finally led to the discovery of the retour pumping at area 5271 and the removal of the observation in that area from the observation set. These large changes led to believe it might be valuable to reevaluate the choice of the explained variance as a weighting factor for the observations. Besides, explained variance has disadvantages as a weighting factor, as described in the discussion. The optimized parameter values with the three different factors for weighting the observations are displayed in table 3.5. Equal weighting of the observations results in a better

fit when analyzing contributions to the objective function, residuals and parameter values than the explained variance used before. When using Voronoi area to weight to observations, transmissivity has an unrealistically high value. It can be concluded an equal weighting for the observation is the most suitable for the model in this stage.

Table 3.5 Optimized parameter values for transient model weighting the observations according to Voronoi, explained variance of time series analysis and with an equal weight.

Parameter			Symbol [unit]	Initial value	Equal weight	Voronoi Area	Explained variance
Transmissivity factor			$ft1$ [-]	1	1.9	43.7	2.5
Drainage	Drainage resistance	Young	$rc1_young$ [d]	10	96	150	40
		Medium	$rc1_medium$ [d]	20	58	224	14
		Old	$rc1_old$ [d]	30	18	76	106
	Infiltration resistance	Medium	$ri1_medium$ [d]	100	42	198	66
		Old	$ri1_old$ [d]	100	1.2	0.25	1.2
Leaky sewage	Drainage resistance	Area 050	$rc2_050$ [d]	100	139	475	166
		Area 190	$rc2_190$ [d]	100	60	6.68	65
		Area 5271	$rc2_5271$ [d]	100	127	27	75
	Infiltration resistance	Area 050	$ri2_050$ [d]	100	270	31	256
		Area 190	$ri2_190$ [d]	100	19	1.2	20
		Area 5271	$ri2_5271$ [d]	100	79	101	97
Canal wall resistance		East	$c1east$ [d]	20	12	146	37
		West	$c1west$ [d]	30	73	13	18
Objective function		Initial	Φ [-]	Depends on w	652	827	843
		Residual			513	402	634

3.5 Final optimization

This section presents the results of the optimization which has the best fit with observations and is considered the final optimization. The calculated optimum values are displayed in table 3.6, with a reduction of the objective function of 47% from 652 to 347. The contribution to the objection function randomly distributed and the magnitude reduced as compared to for example figure 3.10. The fit of the average calculated heads with the average observed heads has improved in comparison to the stationary fit (figure 3.5) and the pre-optimized fit (figure 3.3). The spatial distribution of the average residuals (figure 3.16) does not show a clear correlation in space or magnitude and could be described as a random distribution of residuals. The largest residual is 0.26 m in the Beethovenstraat, but the gross amount of residuals is below 0.10 m (figure 3.17). The dynamics of the groundwater systems and the effects for the wooden foundation poles, together with scenarios of climate adaptations, are presented in the next chapter.

Table 3.6 Initial and optimized parameter values for the final optimization.

Parameter			Symbol [unit]	Initial value	Final optimized value
Transmissivity factor			$ft1$ [-]	1	3.9
Drainage	Drainage resistance	Young	$rc1_{young}$ [d]	10	90
		Medium	$rc1_{medium}$ [d]	20	76
		Old	$rc1_{old}$ [d]	30	16.8
	Infiltration resistance	Medium	$ri1_{medium}$ [d]	100	44
		Old	$ri1_{old}$ [d]	100	18.7
Leaky sewage	Drainage resistance	Area 050	$rc2_{050}$ [d]	100	204
		Area 190	$rc2_{190}$ [d]	100	43.6
		Area 5271	$rc2_{5271}$ [d]	100	68.1
	Infiltration resistance	Area 050	$ri2_{050}$ [d]	100	138
		Area 190	$ri2_{190}$ [d]	100	7
		Area 5271	$ri2_{5271}$ [d]	100	94
Canal wall resistance		East	$c1_{east}$ [d]	20	4
		West	$c1_{west}$ [d]	30	11
Objective function			Φ [-]	652	347

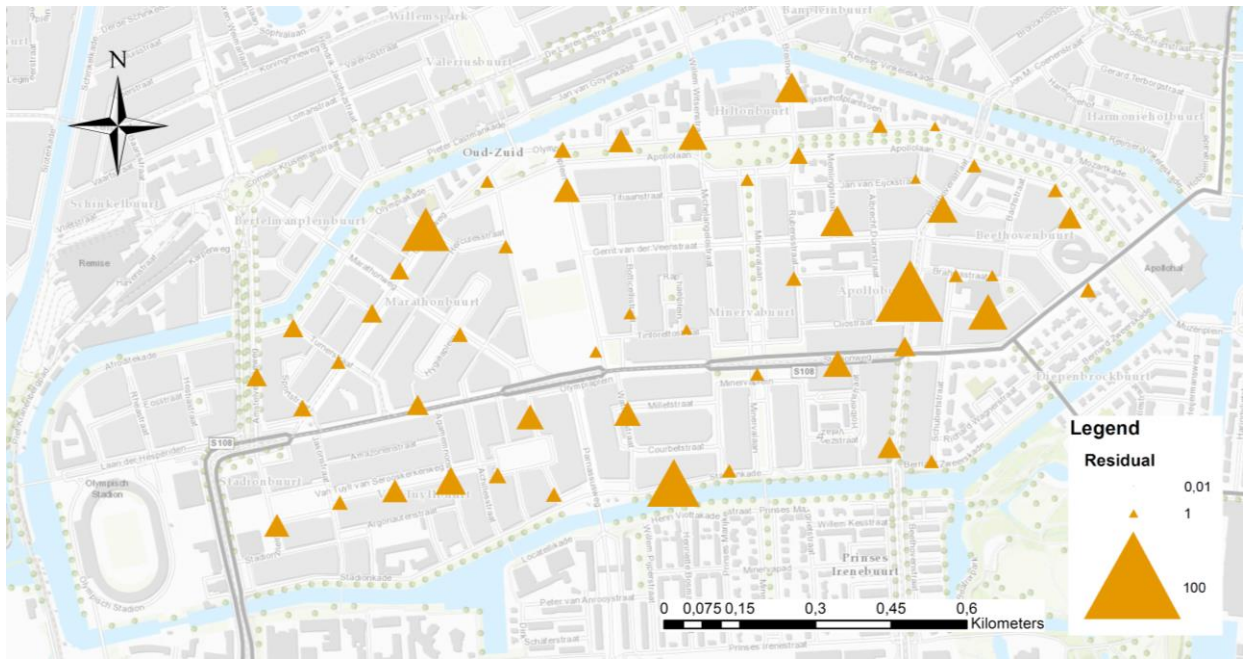


Figure 3.16 Contribution to the objective function at each piezometer location after transient optimization per day.

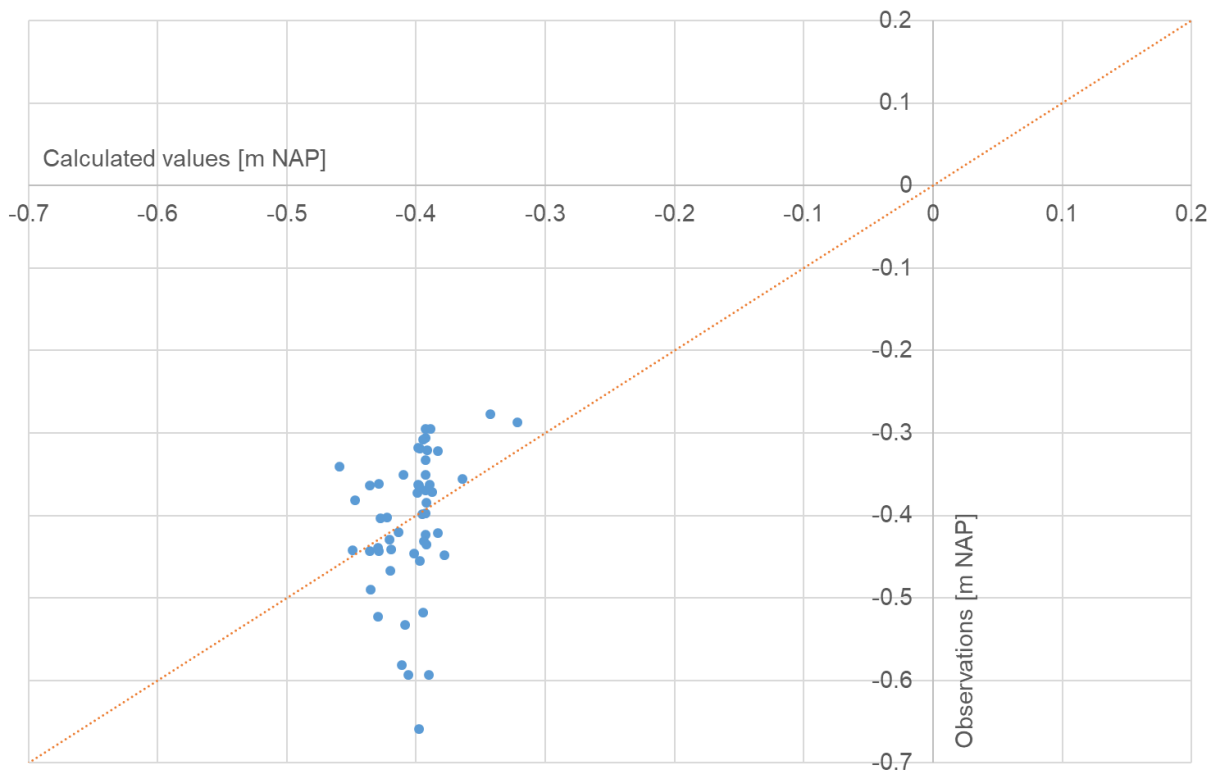


Figure 3.17 Calculated average heads with the transient model after optimization compared to average observed heads at the piezometers.

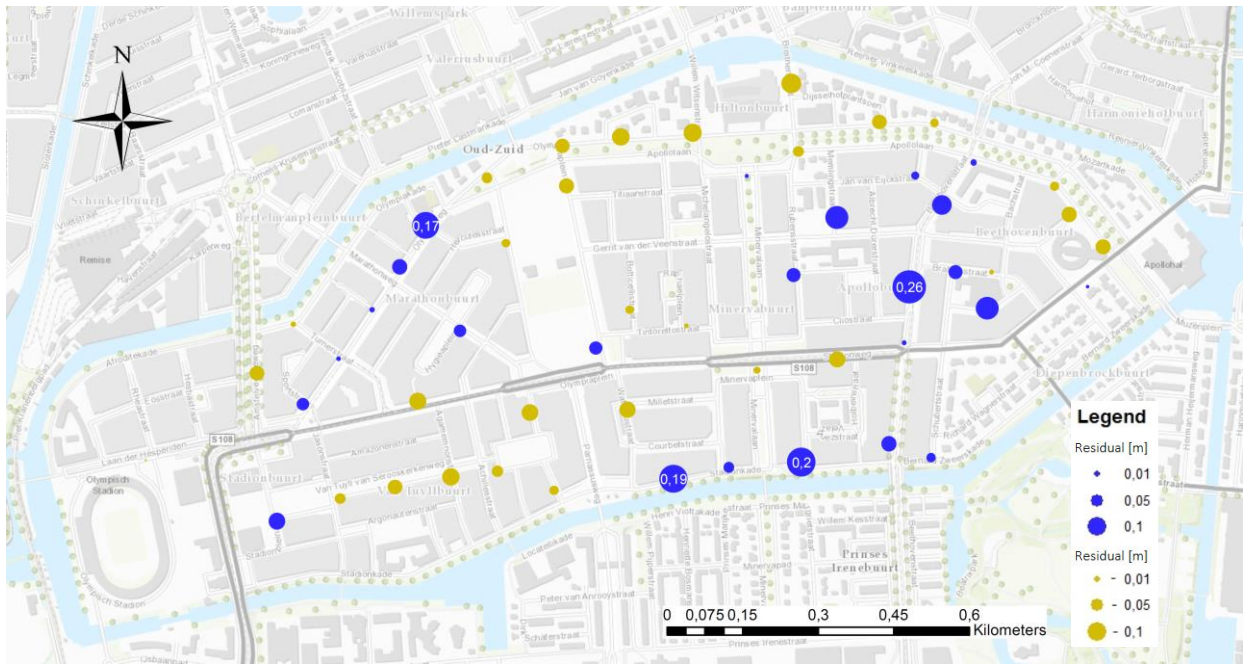


Figure 3.18 Residuals of calculated and observed heads with equal weight of the observations and refinement of groundwater recharge. Model overestimations are displayed in blue and underestimations in yellow.

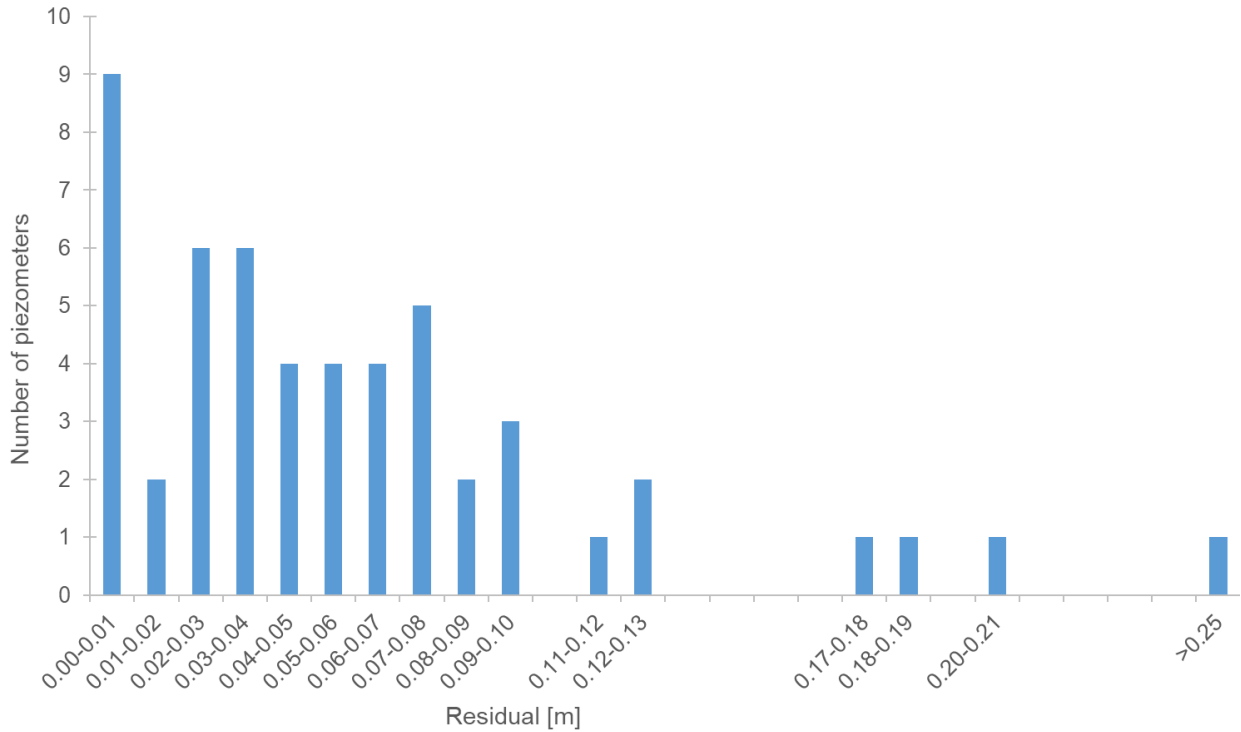


Figure 3.19 Frequency distribution of residuals after final optimization.

4 RESULTS SCENARIOS

4.1 Water coverage of foundation poles

A normative depth for analyzing when heads are too low is the depth of wooden foundation poles (Waternet, 2018). First of all, it has to be stated data on foundation depth has a large range of uncertainty (annex, figure 10G). However, this data is used to interpret to severity of low heads throughout this chapter. Waternet aims at safeguarding sufficient water coverage, so analysis is made with the data of best quality available.

The calculated lowest heads per node of the model with the optimized parameter set described in section 3.5 are displayed in figure 4.1, showing a drop in groundwater level up to NAP -0.82 m. An analysis is made which of the foundation poles will not be covered with water during these lowest calculated heads (figure 4.2). Only the poles marked green comply to the demand of a minimum of -0.40 m. The orange marked poles do not reach this target throughout the two calculated years, but water coverage does not drop below 0 m either. Figure 4.2 shows already only a small fraction of the poles are covered with water sufficiently in the current calculated situation. In the next section, the effect is calculated in a scenario of a changed climate.

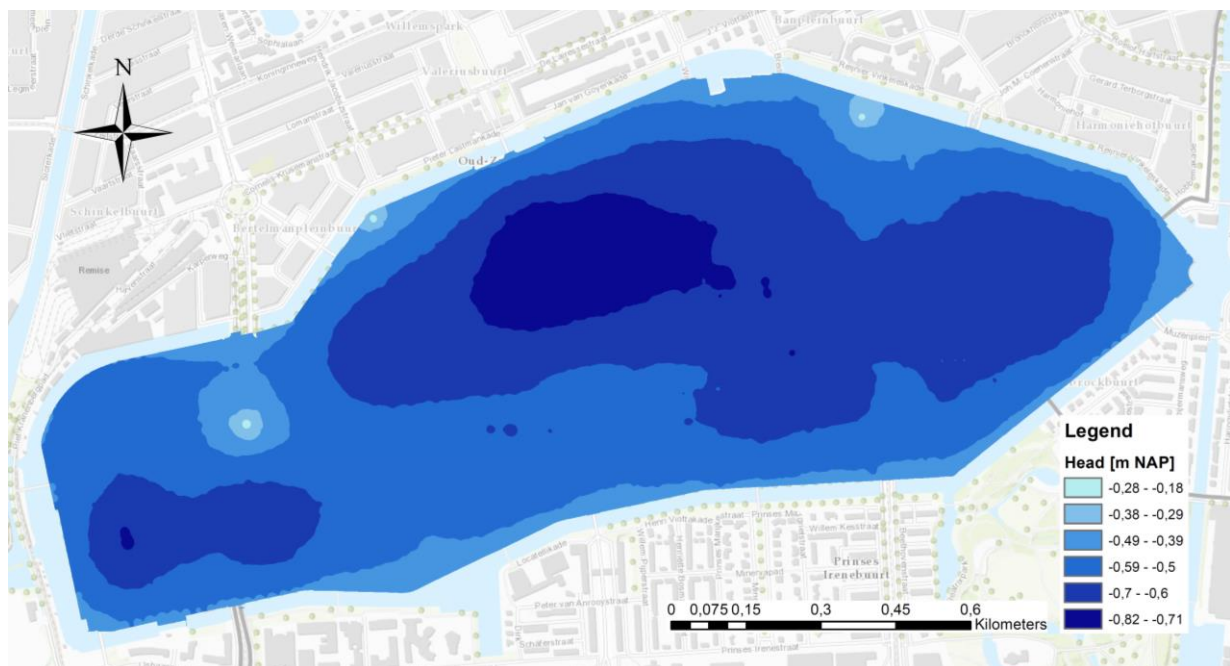


Figure 4.1 Calculated lowest heads in the top aquifer reached during the optimization period of 2015-2016.

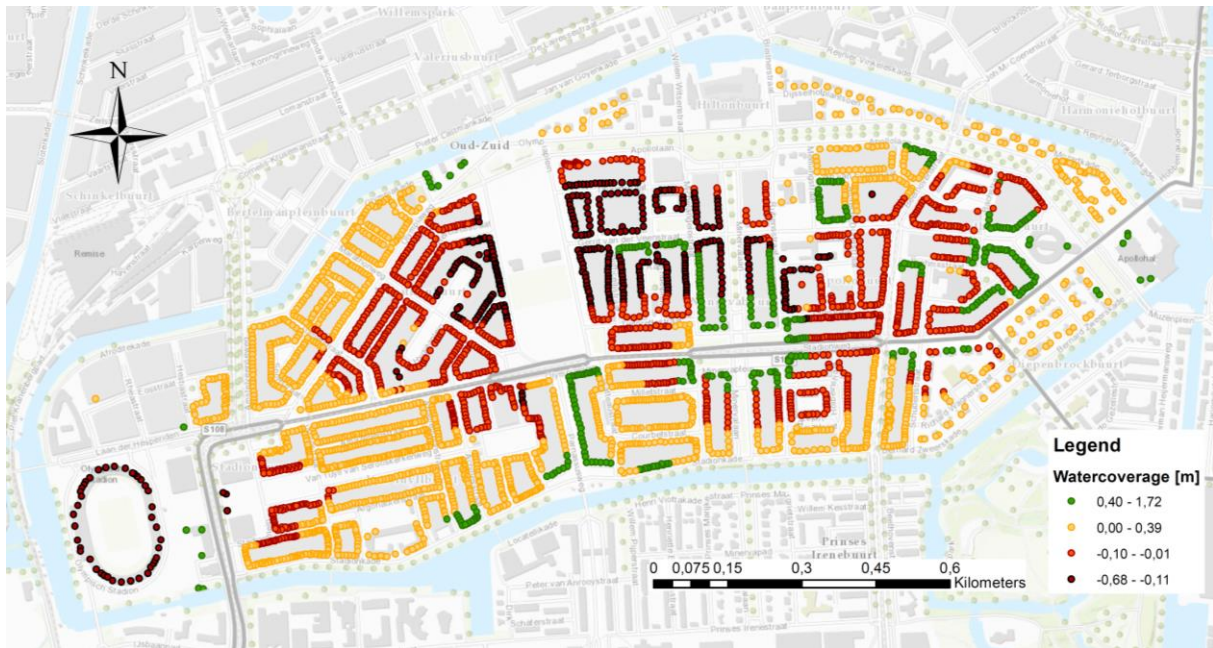


Figure 4.2 Water coverage of foundation poles during the calculated lowest heads in the current situation.

4.2 Scenario I – Climate change

In a scenario of climate change according to the Wh scenario predicted by the KNMI for the year 2050, lowest groundwater levels reached in the area become even lower. The decrease between the current lowest groundwater levels (figure 4.1) and the scenario Wh in 2050-2051 is displayed in figure 4.3, indicating a decrease of groundwater levels up to 10 cm. In this scenario, 64% of the foundation poles will be dry at one point during the two years, instead of the 47% currently. Besides, the number poles in the category of the severest lack of water coverage (< -0.10 m) increases with 270%. This indicates measures to safeguard foundation with sufficient water coverage are needed not only now, even more so in the future with the predicted Wh climate scenario.

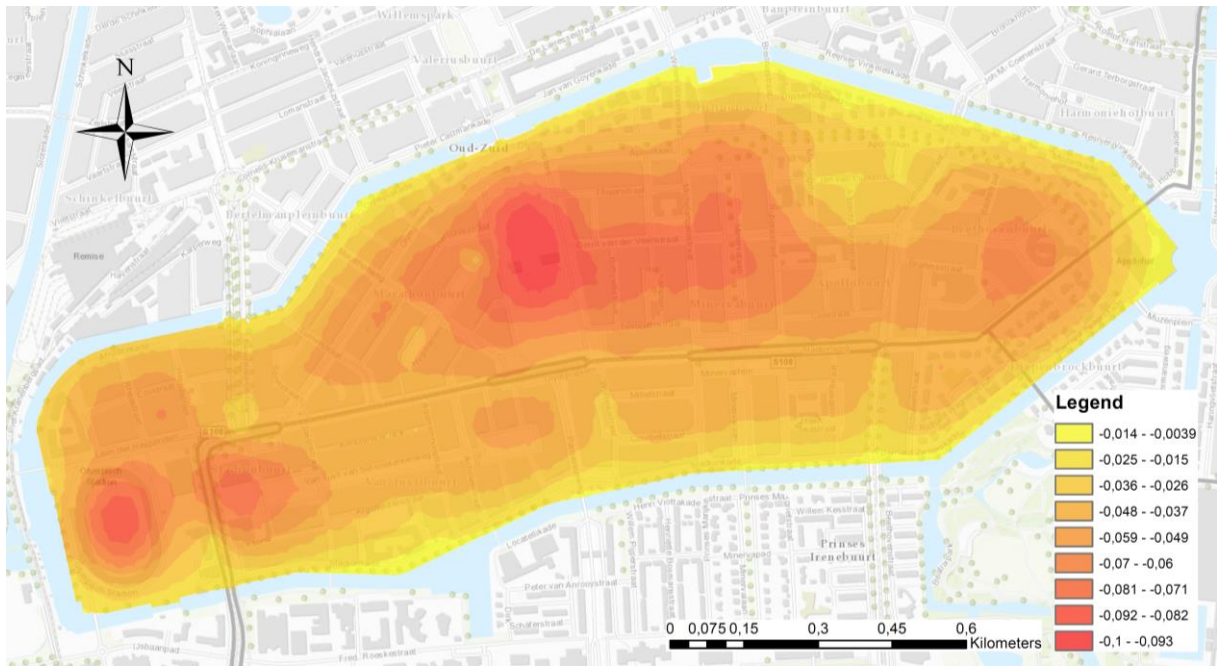


Figure 4.3 Difference between calculated lowest heads reached during the optimization period of 2015-2016 in the current situation and in the scenario of Wh in 2050-2051.

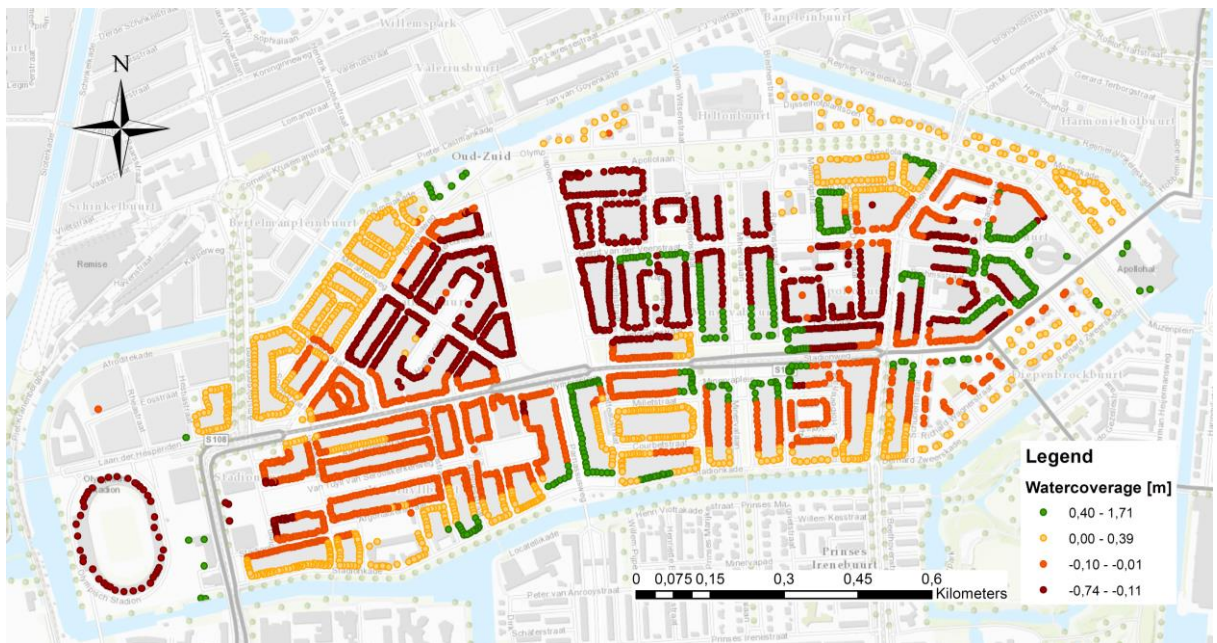


Figure 4.4 Calculated water coverage of foundation poles during the lowest groundwater level in climate change scenario Wh of 2050.

4.3 Scenario II - Permeable paving

The infiltration test on the permeable paving with Drainvoeg in Egmond (figure 4.5) determined the infiltration capacity was 40 mm hour^{-1} after a lifespan of five years. The hypothesis that Drainvoeg material functions as a barrier to small particles from the streets seems valid when looking at figure 4.6. A rough translation of measured infiltration capacity to the permeability of semi-permeable streets is made by increasing the groundwater recharge from 15% of precipitation to 30% of precipitation. When compared to climate scenario Wh, highest calculated groundwater levels rise with up to 0.62 m (figure 4.7), whereas the lowest calculated heads only increase with a maximum of 0.06 m (figure 4.8).



Figure 4.5 Infiltration test of permeable paving with Drainvoeg in Egmond aan Zee (2018).



Figure 4.6 Drainvoeg after 5 years of use, with pollutants in black limited to the top few centimeters of the material (2018).

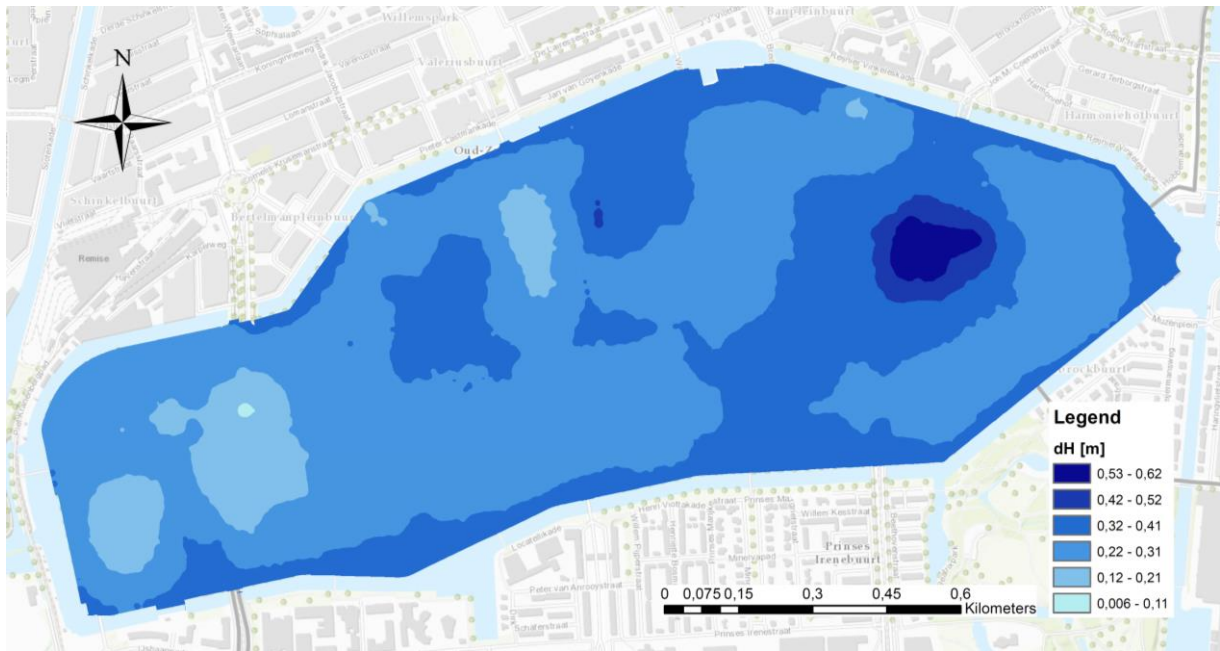


Figure 4.7 Difference between calculated highest groundwater levels reached with a permeable paving and in the climate scenario Wh in 2050-2051.

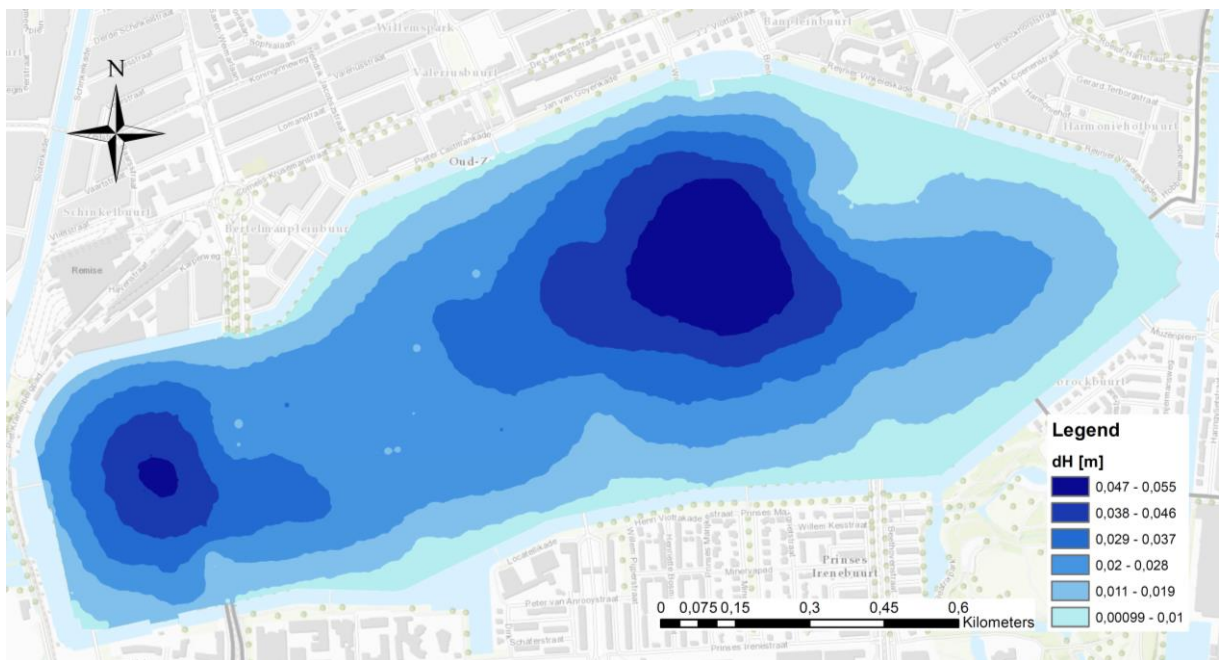


Figure 4.8 Difference between calculated lowest groundwater levels reached with a permeable paving and in the climate scenario Wh in 2050-2051.

Figure 4.9 shows the required 0.90 m between surface level and groundwater level is just met for the Cliotraat in scenario of climate change Wh. When applying more permeable paving, groundwater levels rise more in winter, when more precipitation occurs. Consequently, the range of 0.90 m is exceeded in winter. It can be concluded that permeable paving as

calculated in this scenario is not sufficient to protect foundations with water coverage and is more likely to cause problems for tree growth and other water nuisance due to heightened groundwater levels.

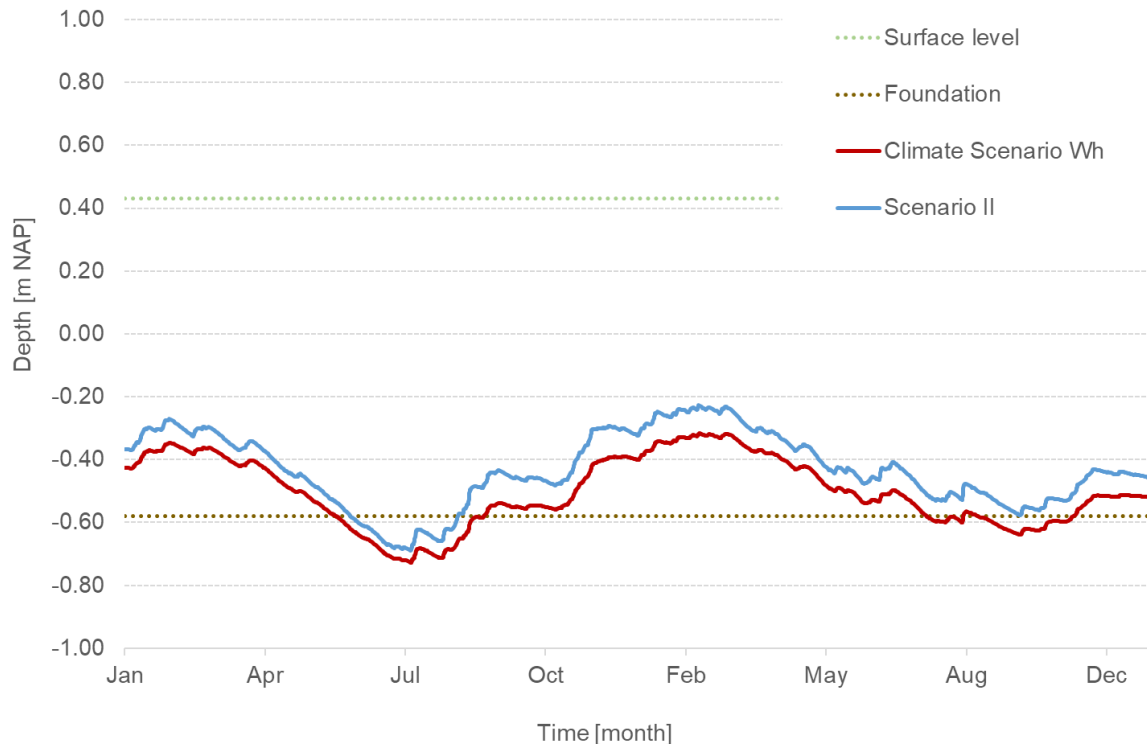


Figure 4.9 Difference between calculated lowest groundwater levels reached with a permeable paving and in the climate scenario Wh in 2050-2051 in the Cliostraat.

4.4 Scenario III - DIT sewage and variable drainage depth

In scenario III, all drainage is replaced by a drainage, infiltration and transportation (DIT) sewage and drainage level is variable between NAP -0.20 m in February until May and NAP -0.40 m during the rest of the year. Drainage resistance is 1 day and the resistance of infiltration, if it occurs, is 10 days. This adaptation increases the lowest groundwater level up to 0.34 m compared to groundwater levels during the climate scenario Wh (figure 4.10). At the piezometer of the Beethovenstraat, neighboring wooden poles at a depth of NAP -0.50 m will not be covered with water during roughly half the simulated period in the climate scenario of Wh in 2050-2051 (figure 3.22). The calculated heads with DIT-sewage of variable depth show this is an efficient climate adaptation to ensure sufficient water coverage of wooden poles for Stadioneiland.

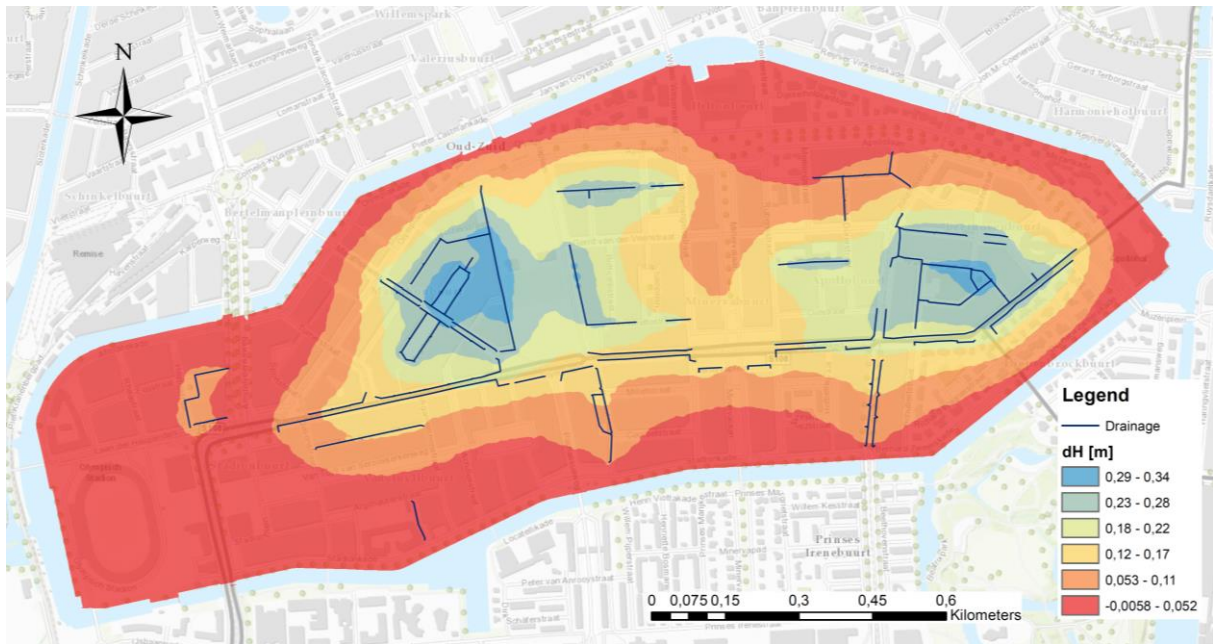


Figure 4.10 Difference between calculated lowest groundwater levels reached with a variable drainage depth of DIT-sewage and in the climate scenario Wh in 2050-2051.

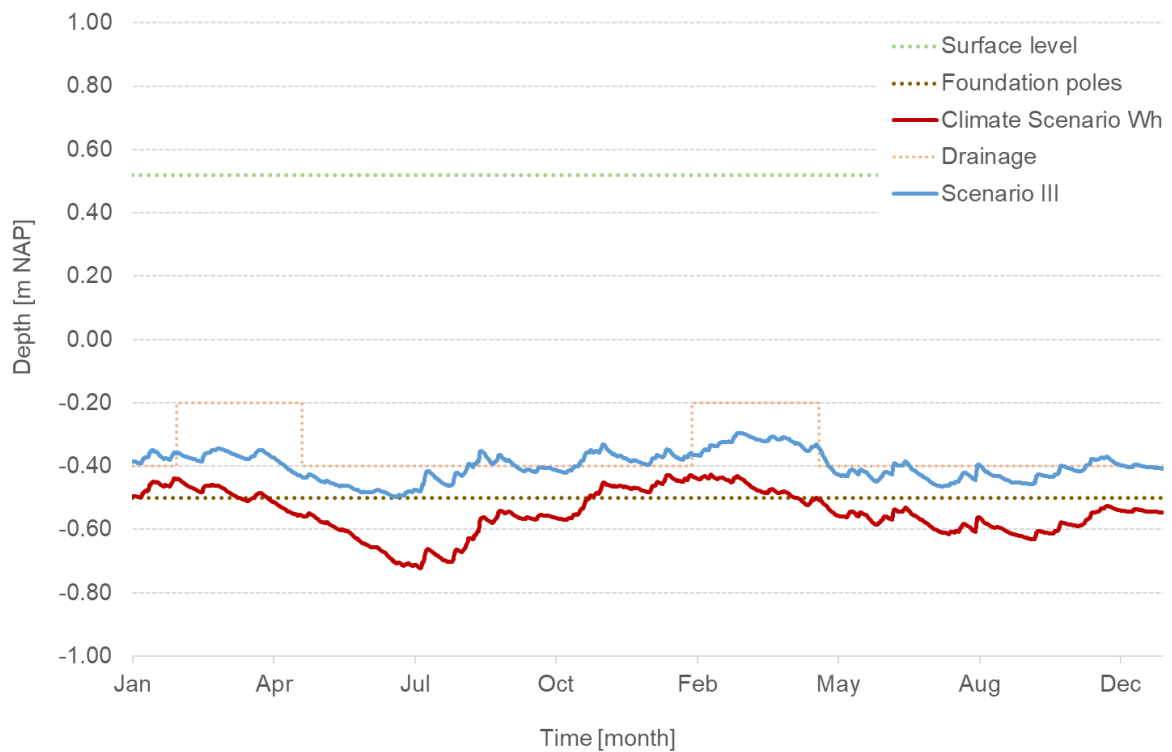


Figure 4.11 Calculated groundwater level with a variable drainage level (solid blue line) as compared to the groundwater level in climate scenario Wh (solid red line) for piezometer F05309 (Beethovenstraat).

5 DISCUSSION

In this chapter, the results presented in the previous chapters, will be discussed. The assumptions and limitations are taken into account, a comparison is made to previous work and the research relevance highlighted.

5.1 Assumptions in model schematization

Several assumptions are made to schematize the sewage system into the model. Locations of groundwater infiltration are based on sewage inspections. Through personal experience and according to research of Dirksen (2013), it can be said these inspections use advanced technology, but are open to interpretation of the sewage investigator. Groundwater infiltration can be identified by iron deposition around fractures, but the amount of groundwater infiltrating is hard to quantify. If the camera registers direct infiltration, an estimation might be done visually. Still the rate is dependent on the groundwater level at that time. Besides, even if the inspection records indicate the correct position of possible infiltration, their accuracy is not sufficient. Whether damage is found at one location within a string or at several locations, in the inspection record the entire length of the string and will be labeled as damaged. Consequently, in the model the sewage will be able to take in water along the total length of the string, whereas infiltration might only occur at a single point in reality.

Subsequently, in the modeling process, leakage of the sewage is assumed to be constant. But, the degradation of the sewer is a continuous process, so leakage is probably increasing over time. The latest inspections of Stadioneiland in 2015 are used for this research, though time passes, both in the model and in reality.

The drainage system specifically offers a modeling challenge. If drainage is connected to the surrounding surface water, it can be presumed to be draining at the same level of NAP -0.40 m. But a large part of the drainage is connected to the manholes of the mixed sewage system. During fieldwork a part of these drains were inspected and drainage depths were remeasured. Drainage was found which was sealed off or not present where it should be according to most recent information in the database. This suggests the presence and depth of the drainage is not accurately registered, though it is an important component in the model.

During the research it was discovered the research area used to be a polder area of which the outer dyke ran from north to south along what now is the Amstelveenseweg. The dyke was incorporated in the model as a line element with a low hydraulic conductivity of 0.005 m day^{-1} , a general value for clayey loam (Bot, 2011). The fit of the model to the observations improved with the addition of the dyke body, but no more evidence on the presence was found than an old map. Also the exact height of the dyke, now assumed to be close to surface level, is uncertain. Eventually, pumping area 5271 was not included in the optimization, making these assumptions of less concern. But these constraints are important to keep in mind if a modeling effort or an intervention in the groundwater system is made for this part of Stadioneiland.

5.2 Measurement of groundwater infiltration

A lot can be discussed on this topic. Theoretically, an indication of leakage quantities can be measured during low discharges in a dry weather system (STOWA, 2003). In practice, the measured flux appeared unrealistically high. This might have several causes. Firstly, it is assumed dry weather discharge is at a minimum with only 5-10% of the daily drinking water consumption between 3:00 and 4:00 a.m. This time period is in accordance with the minimum in discharge measured at the pumping station, though the percentage of drinking water consumption at that time might be higher for this area. Besides, drinking water consumption is not known exactly for large parts of the city, this research area included. For some houses, water meters are in place, which provides an accurate yearly consumption of drinking water. Still, one assumes drinking water consumption is average each day and remains equal in the calculated year (2018) compared to the years of which consumption is known (2016-2017). Even more uncertain is the consumption of houses without a water meter, of which the yearly consumption is estimated based on the amount of residents.

5.3 Weighting of observations

Both for the stationary as for the transient model, a variety of weighting factors for the observations was analyzed. Equal weighting of the observations proved most useable for the transient model. No information is given to the spatial and temporal correlation of the observation when applying equal weighting. A weighting according to spatial correlation is provided in the use of Voronoi area, which assigns a higher weight to observations representing a larger area of the island. A disadvantage is that a larger area will consist of more variety, for example in type of drains and land use, than what are factors of influence to the groundwater levels of the observed location. Finally, weighting according to explained variance of the time series analysis provides temporal information in the optimization and weights better explained observations higher than observations which might be less reliable. The disadvantage of this weighting technique is caused by time series analysis being a response function. Consequently, if the fit of the observation is explained according to evaporation and precipitation, it will be assigned a high weight. Though the time series analysis does not take physical factors into account, such as drainage depth, which are modeled in MicroFEM. Explained variance seems to be an unsuitable weighting factor. Still, time series analysis remains an important tool for pre-processing the observation data on trends, measuring errors and outliers.

5.4 Model validation

For the year 2017, suitable time series analyzed observations and climate data are available, but are deliberately not used for calibration. These time series could be used for validation of the model. Unfortunately, the research period did not allow for this validation procedure in the end. It is recommended to either use this time period to extend the optimization period with this extra year of measurements or use it for validation of the model.

5.5 Interpretation of optimization results

The transmissivity is uncertain in both its components hydraulic conductivity K and depth of the aquifer D . The initial value of the K is 5 m day^{-1} , as is the estimated hydraulic conductivity of the aquifers material. Aquifer depth D is extracted from the interpolated model of TNO which is based on bore profiles and cone penetration tests. Both properties have a relatively large range of uncertainty. The origin of the sand used for the first aquifer is unknown and if it is coarser, the hydraulic conductivity will be higher. Similarly, if the aquifer is thicker than assumed in the model, transmissivity will increase as well. The optimized value of transmissivity is a factor 3.9 higher than the initial value from the regional model, but still within the range of acceptable values.

5.6 Research relevance

This research of analysing the groundwater system of the Stadionbuurt has begun before the initiation of sewer replacement in the area. The calibrated model can therefore be used to explore possibilities of climate adaptations, not only to advice on plans already made. Furthermore, the model can be used to dimension the measurements to be taken. For example, it can be calculated which locations are suitable for permeable paving and what the effects are during high groundwater levels in winter. The model can also be used to explore more adaptations, for example a combination of scenario II and III.

Increase in drought and extreme precipitation will face challenges not only for Stadioneiland, but for the entire city of Amsterdam. The soil properties and wooden pole foundation are rather specific to Dutch cities, but climate adaptations need to be designed in all urban areas. The technique of calibrating a transient groundwater model for highly urbanized neighbourhoods could be used as a template to design other local models. Furthermore, half of the world's population live in delta regions like the Dutch delta and face similar challenges (VHL, 2018). Water management as modeled in this research might be a source of inspiration for other delta regions.

6 RECOMMENDATIONS

6.1 Determination of hydrological parameters

As described in section 1.4, Waternet has performed infiltration and drainage experiments in the Argonautenstraat, Stadioneiland. These tests can be used to determine the local hydraulic conductivity K of the top aquifer. It is recommended to retrieve more borehole profiles and cone penetrations tests from the geotechnical department to have the most precise data of the local top aquifer depth D . Together this results in a locally redetermined transmissivity T . Consequently, the Stadioneiland model can be better optimized by extrapolating this local value of transmissivity to the rest of the island. The infiltration and drainage experiments also provide better insights into the drainage and infiltration resistances of DIT-sewage. These values are now estimated in scenario III and can then be recalculated.

6.2 Recommendations for improved schematization

Observations show a strong decline in groundwater levels during droughts, which will be mainly caused by the evapotranspiration of trees. As the lowest heads are a threat to wooden foundations, it is important to be able to model these drought more accurately. Currently, the evapotranspiration is only incorporated for unpaved surface, but evapotranspiration could occur from underneath semi-permeable paving as well. Research on urban transpiration is sparse (Liu et al., 2017), therefore it is recommended to measure the transpiration on Stadioneiland in an experimental set-up further elaborated upon in annex 10.2).

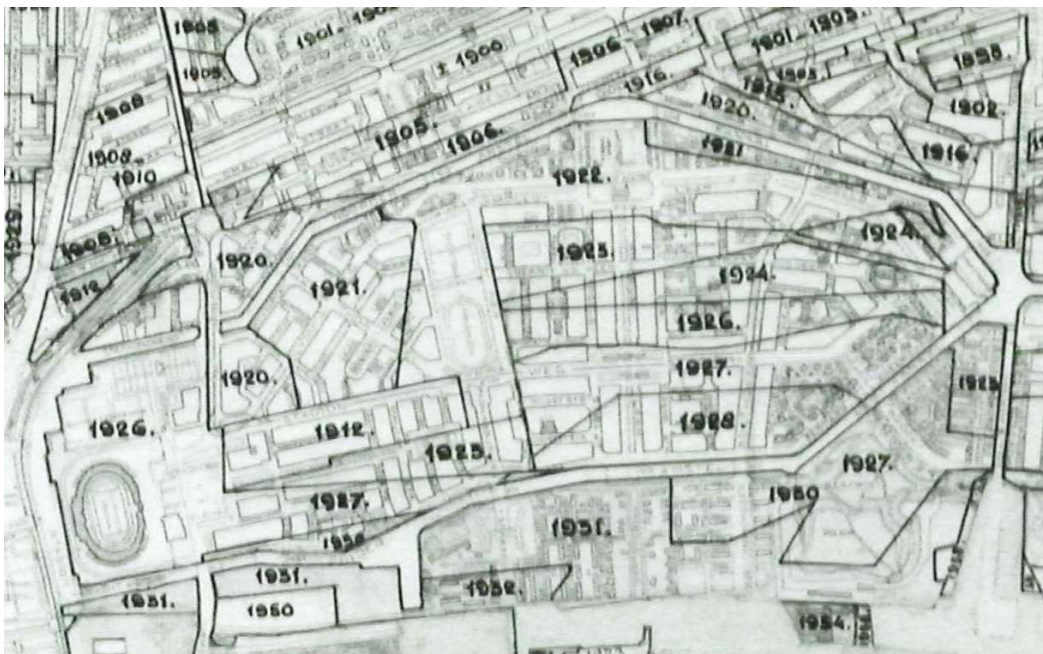


Figure 6.1 Historical map of year of surface level raise in south of Amsterdam (Waternet, n.d.).

Corrections to the sewage schematization could be made if the coordinates are recorded of the damaged locations during sewage inspections. Besides, it is recommended to perform fieldwork aimed at updating the database on drainage presence and depth.

Probably the model will improve when build in more detail, for example with a finer grid and division of drainage and sewage into more categories. Besides, it might be legitimized to divide the transmissivity according to construction period of each parcel (figure 6.1).

Furthermore, it is recommended to incorporate the presence of cellars, as far as this is properly documented, into the model. For example, the Olympic Stadium is known to have a crawling space and these barriers to groundwater flow can cause a rise in groundwater levels. The increase of cellars and the effects on the groundwater system is a concern of the municipality and could be a scenario tested in the model.

6.3 Recommendations for improved optimization

Transient optimization can better be performed on the observations than on the analyzed time series. Unfortunately, the frequency of observations is low and varies over time. It is recommended to program a routine in order to be able to optimize directly on the observations. Besides, the recommendation is made to measure groundwater level more frequent.

An optimization improves when performed not only on head values, but on fluxes as well (NHV, 1997). The measurement of leakage at 5271 should have only reflected dry weather sewage and groundwater infiltration. Water height measurements in the pumping station indicated precipitation could enter the upstream sewer. In order to trace the source of this precipitation, an analysis can be made of the precipitation peak versus the increases in pump frequency of the pumping station. If the delay between the peaks is long, precipitation will probably travel through the groundwater towards the station. If the delay is short, the route will more likely be through the sewage system. It can be recommended to check whether there are accidental connections of the neighboring mixed sewage system onto this pumping station. Besides, if the drinking water consumption of the connected houses and businesses can be measured more precisely, a better estimate can be made of which fraction of the measurement discharge can be attributed to groundwater infiltration. For the other two areas, 050 and 190, leakage can possibly be measured using a salt dilution method (STOWA, 2009).

The observations west of the Olympic Stadium were taken out during optimization as it was not possible to simulate the construction work at the Stadionplein. If the quantities returned to the surface water and especially injected near Olympic Stadium were known, it would not have been needed to remove these observations. In a city which is continuously renewing and construction works take place regularly, it would be difficult to identify a period of sufficient length without any interventions. Ideally, more information would be registered on projects in a monitoring rapport set up by constructors and documented by Waternet. This would also assist in proper enforcement of the permits granted.

6.4 Recommendations for further research

In this research, the water coverage of foundation poles at the lowest calculated head is presented. The duration of time that the water coverage does not meet the required height is more important for the degradation of the poles, so it is recommended to make that analysis.

The model could be used to determine the radius of influence of drainage and leaky sewage. This information can be useful in designing climate adaptations using drainage, similar

to scenario III. With the normative depth of the foundation poles, PEST can be used to calculate the desired drainage levels. To reach these groundwater levels, dimensioning of different climate adaptations can be tested in the model. For example, it can be calculated what the effects are of an increase in surface waters, the application of permeable paving in only a part of the area, the construction of wadis or an infiltration system only infiltrating during extreme precipitation, to name a few. Besides, further research into the infiltration of surface water and the effects of clogging are recommended to better explore scenario III.

The research has focused more on climate adaptations to protect pole foundation from drought, than the effects of extreme precipitation. If the model would be build in smaller time steps, an extreme precipitation event can be simulated. This can be useful to analyze and optimize on the retardation between the peak in precipitation, the peak in groundwater levels and the resulting peak in discharge from the groundwater to the surface water.

Amsterdam Rainproof has made so-called solution maps for several neighborhoods in Amsterdam to indicate the possible rainproof adaptations (figure 6.2). Until now, the groundwater system and its possible contribution is not taken into account. With further expansion of the model results, the solution map of Stadioneiland can be complemented with possibilities and risks of the groundwater system.

A local model as presented in this research for the Stadioneiland could be very valuable for other neighborhoods as well. For most areas, only the stationary regional model is available. If sufficiently optimized, transient models were to be made of each neighborhood before construction work begins, risks, possibilities and climate adaptations can be calculated and dimensioned. The solution maps of Amsterdam Rainproof for each neighborhoods can then be complemented with the solutions for the groundwater system.

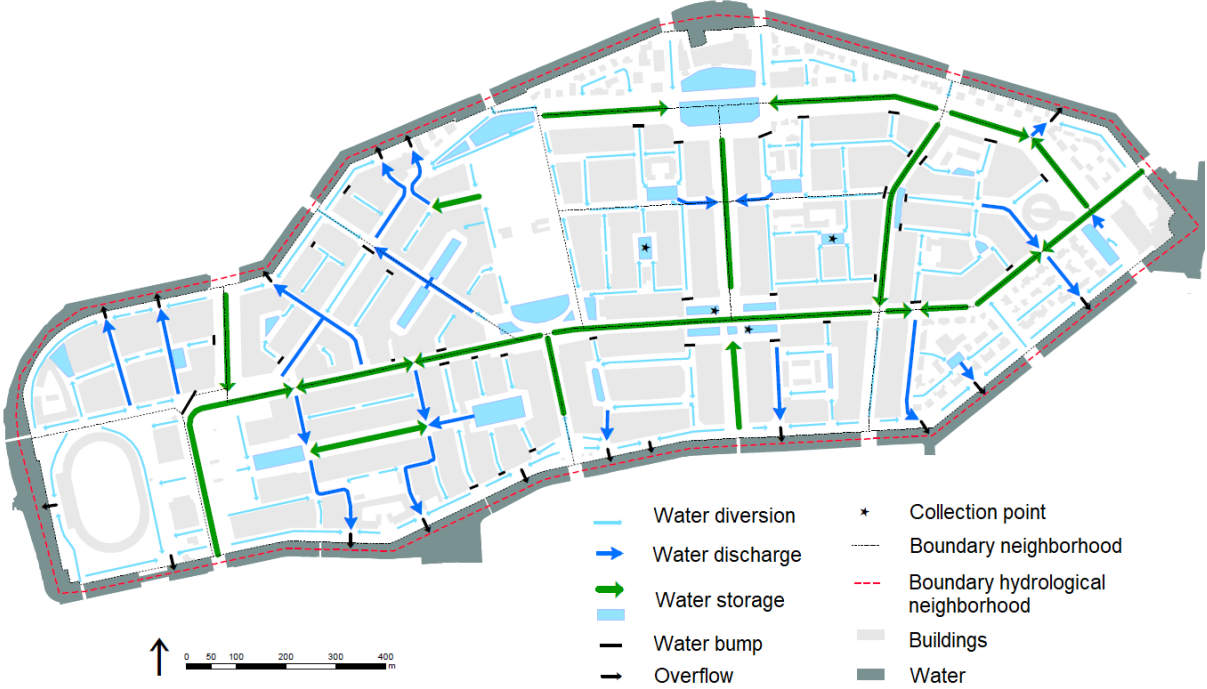


Figure 6.2 Solution map with possible rainproof adaptations for Stadioneiland (Waternet, 2018).

7 CONCLUSIONS

For the Stadionbuurt in Amsterdam, a groundwater model is built in MicroFEM which is extensively calibrated using both MicroFEM and PEST for parameter optimization. The observation data of groundwater levels are pre-processed on trends, measuring errors and outliers. Data of almost hundred piezometers are filtered to 71 suitable observation series. Throughout the calibration process and with aid of fieldwork, adjustments to the initial model schematization are made. The most notable of which are the division of canals walls into two types according to permeability, the incorporation of an old dyke body, the exclusion of observation data based on construction work and corrections in drainage sewage. The resulting model has an optimum set of parameter values (table 3.6) with transmissivity being a factor 3.9 higher than was optimized with the regional groundwater model. Drainage resistances of leaky sewage vary from 44 to 204 days and resistances to infiltration from 7 to 138 days, depending on the area. The hypothesis that more recently constructed drainage has lower resistances to drainage and infiltration cannot be proved with the results of this research.

Subsequently, the calibrated model is used for exploration of scenarios. The first scenario of the KNMI climate change scenario Wh for the year 2050 shows an decrease in lowest calculated groundwater levels up to 0.10 m. Consequently, 64% of wooden foundations would lack water coverage compared to 49% now at a certain point during the calculated two years. In order to prevent these low groundwater levels and the potentially harmful effects on wooden foundations, scenarios are created to analyze the effects of a climate adaptive design. For scenario II, an infiltration experiment is performed and the infiltration capacity of the Drainvoeg permeable paving is determined to be 40 mm hour⁻¹ after a lifespan of five years. A scenario is explored of constructing this type of permeable paving instead of the current semi-permeable paving. This adaptation results in groundwater levels of a height that can be damaging to trees and cellars while not raising the groundwater significantly during drought. In scenario III, DIT-sewage is constructed where currently drainage is located on the island. The sewage has a variable drainage depth of NAP -0.20 m at the end of winter until beginning of summer and NAP -0.40 m to allow for infiltration during the rest of the year. At locations where foundations is threatened in a scenario of changed climate, this renewed DIT-sewage design can ensure a sufficient water coverage (for example, figure 4.11).

Finally, the analysis of the previously described scenarios leads to the main research question of how the shallow groundwater system of the Stadionbuurt can contribute to climate adaptations. The capacity between surface level and groundwater levels indicates possibilities for infiltrating surface water or precipitation. Scenario III shows the shallow groundwater system can contribute to climate adaptations, at least sufficiently for minimizing negative effects of drought. The balance between too high and too low groundwater levels remains delicate and caution has to be taken to the disadvantages of climate adaptations, as shown in scenario II.

The calibrated shallow groundwater model developed in this research for the Stadionbuurt has proved useful for climate exploration as well as analyzing the effects, both positive as negative, of adaptations. Many more scenarios can be explored by Waternet, for example scenarios of increase in cellars or the expansion of surface waters in the area. In addition, the model can be used to dimension the adaptations.

Increase in drought and extreme precipitation will face challenges not only for Stadioneiland, but for the entire city of Amsterdam. Soil properties and wooden pole foundations are rather specific to Dutch cities, but climate adaptations need to be designed in all urban areas. The technique of calibrating a transient groundwater model for highly urbanized neighbourhoods could be used as a template to design other local models. Furthermore, half of the world's population live in delta regions like the Dutch delta and face similar challenges (VHL, 2018). Water management as modeled in this research might be a source of inspiration for other delta regions.

8 ACKNOWLEDGEMENTS

I would like to thank my thesis supervisors, Frank Smits from Waternet and Steven de Jong from Utrecht University. Special thanks to Frank with his unparalleled dedication and endless enthusiasm for the research.

Furthermore, my gratitude goes out to all the people at Waternet who contributed to my research internship: Najim el Ayadi, Torben Tijms, Koen Tromp, Jos Beemster, Rob Tijssen, Bas de Nijs, Lisette Beets, Jeroen Ponten, Ab Visser, Iris van Wielink, Volkert van der Keelen, Raymon Sanou, Boudewijn de Jong, Mohamed Boughlala, Juan Bonillo Martinez, Stefan Fritz, Ferry Devilee, Jan Willem Voort, Arne Bosch, Danny Jongejeugd, Martijn Haselaar, Driss Mahfoudi, Marcel van der Blom, Tom Kind, Ernst Bontjes, Peter Beemsterboer, Cornelis Peperkamp, Johan Prenger, Ben Staring, Arie de Beer, Robert Heuving, Joyce Dankelman, Sara Giorgi, Thijs Visschers, Reinier Kuipers & Maarten Plug.

9 REFERENCES

Abas, I. (2017). Onderzoek naar een nieuw infiltratiesysteem in de Argonautenstraat, Amsterdam Zuid. *Technische Universiteit, Delft*.

AHN: Actueel Hoogtebestand Nederland (2018). AHN Viewer. Retrieved from <http://www.ahn.nl/common-nlm/viewer.html>.

Amsterdam Rainproof (2014). Programmaplan Amsterdam Rainproof juni 2014. Retrieved from: <https://www.rainproof.nl/sites/default/files/programmaplan-amsterdamrainproof.pdf>.

Amsterdam Rainproof (2018). Omgekeerde drainage/IT-riool. Retrieved from: <https://www.rainproof.nl/toolbox/maatregelen/omgekeerde-drainageit-riool>.

Anderson, M.P. & Woessner, W.W. (1992). Applied Groundwater Modeling. Simulation of Flow and Advective Transport. *Academic Press, Inc., San Diego*.

Beemster, J. (2016). *Hydrologisch Onderzoek Museumkwartier*. Waternet, Amsterdam.

Boerma, E. & Boogaard, F. (2012). Test waterpasserend verharding 'Drainvast'. *Tauw*, Amsterdam.

Bos, E. (2004). Controle en onderhoud van drainagevoorzieningen. Wageningen UR E-depot, retrieved from: <http://edepot.wur.nl/161878>.

Bot, B. (2011). *Grondwaterzakboekje*. Bot Raadgevend Ingenieur, Rotterdam.

Buishand, A, Jilderda, R. & Wijngaard, J. (2010). Regional differences in the extreme rainfall climatology in the Netherlands. Retrieved from: <https://www.knmi.nl/kennis-en-datacentrum/achtergrond/regional-differences-in-the-extreme-rainfall-climatology-in-the-netherlands>.

Burt, J.E., Barber, G.M. & Rigby, D.L. (2009). *Elementary Statistics for Geographers*. The Guilford Press, New York.

Commissie Waterbeheer 21^e eeuw. (2000). Water beleid voor de 21e eeuw: geef water de ruimte en de aandacht die het verdient.

De Boer, B. (2014). Bestraten met de Drainvast en de Drainbrick - Innovatie zorgt voor snellere afvoer van water op bestratingen. *Stad + Groen*, 6, 26-29.

De Mulder, E.F.J. & Bosch, J.H.A. (1984). Holocene geologische geschiedenis van Centraal en Noordelijk Noord-Holland. *Grondboor en Hamer*, 3, 75-107.

Dingman, S.L. (2015) *Physical Hydrology*. Waveland Press, Inc, United States of America.

Dirksen, J. (2013). Monitoring ground settlement to guide sewer asset management. TU Delft. Retrieved from: <http://doi.org/10.4233/uuid:26116a82-51be-4474-853b-926f1a8f16f7>.

Doherty, J. (2002). *Manual PEST: Model-Independent Parameter Estimation*. Watermark Numerical Computing.

Drainvast (2017). Bestektekst Drainvoeg en DV-B1 bestekbijlage drainvoeg 19-09-2017. Retrieved from: <http://www.drainvast.nl/producten/bestek/>.

Drainvast (2018). Website Drainvast B.V. Retrieved from <http://www.drainvast.nl/>.

Dynamax (2017). Thermal Dissipation Probe. Retrieved from: http://dynamax.com/images/uploads/papers/TDP_Presentation.pdf.

Fraenkel, F.F. (1974). Berlage's Amsterdamse Plan Zuid (1905-1917) en de daaraan voorafgaande 19de-eeuwse uitbreidingsplannen. *Netherlands Yearbook for History of Art*, 25, 181-275.

Gemeente Amsterdam (2018). *Datasets kaarten van Amsterdam*. Retrieved from kaart.amsterdam.nl/datasets.

Geoheritage NL (2009). *Het ontstaan van het Nederlandse landschap: een canon*. Buro voor Explanation Design, Haarlem.

Göbel, P., Starke, P. & Coldewey, W.G. (2008). Evaporation measurements on enhanced water-permeable paving in urban areas. *11th International Conference on Urban Drainage, Edinburgh, Scotland, UK*.

Goedbloed, D. (2018). *Personal communication*.

Graafstra, P., Smits, F., & Janse, T. (2017). Incorporating insights from Time Series Analysis in groundwater modelling for the urban area of the city of Amsterdam. *Proceedings of the MODFLOW and More 2017 Conference: May 21 - 24, 2017, Golden, USA*.

Hemker, K, Van den Berg, E. & Bakker, M. (2004). Ground Water Whirls. *Groundwater*, 42(2), 234-242.

Hendriks, M.R. (2010). Introduction to Physical Hydrology. *Oxford University Press Inc., New York*.

Hoogheemraadschap van Rijnland. (2018). Peilbesluiten. Retrieved from: <https://www.rijnland.net/plannen/extra-paginas-plannen/peilbesluiten>.

IAHS: International Association of Hydrological Sciences (1990). Hydrological Processes and Water Management in Urban Areas. *IAHS Press, Institute of Hydrology, Wallingford, Oxfordshire, UK*.

IPCC (2014). Climate Change 2014: Synthesis Report. Contribution of Working Groups, I, II and III to the Fifth Assessment Report of the Intergovernmental Panel on Climate Change. *IPCC, Geneva, Switzerland*, 151p.

Janse, T. & Graafstra, P. (n.d.) *How to get the most out of your historical groundwater data using a basic time series approach*. Waternet, Amsterdam.

Janssen, G. & Hemker, K. (2004) Groundwater models as civil engineering tools. *FEM_MODFLOW, Karlovy Vary*, 35-38.

Kibler, D.F. (1982). Urban Stormwater Hydrology. *American Geophysical Union, University of Michigan*.

Klaassen, R.K.W.M. (2008). Bacterial decay in wooden foundation piles – Patterns and causes: A study of historical pile foundations in the Netherlands. *International Biodeterioration & Biodegradation*, 61, 45-60.

Klimaatatlas (2018). De Bilt, langjarige gemiddelden, tijdvak 1981-2010. Retrieved from: http://www.klimaatatlas.nl/tabel/stationsdata/klimtab_8110_260.pdf.

KNMI (2006). *KNMI Climate Change Scenarios 2006 for the Netherlands*. Scientific report WR2006-01, KNMI, De Bilt, The Netherlands.

KNMI (2014). *KNMI'14: Climate Change scenarios for the 21st Century – A Netherlands perspective*. Scientific Report WR2014-01, KNMI, De Bilt, The Netherlands.

KNMI (2018a). Klimaatatlas: Klimatogram station Schiphol (240). Retrieved from: http://www.klimaatatlas.nl/grafiek/stationsdata/klimgram_8110_240.pdf.

KNMI (2018b). Ons Klimaat verandert – Facts & figures voor klimaatadaptatie in het beheersgebied van Waterschap Amstel, Gooi en Vecht en de Metropoolregio Amsterdam. Retrieved from: <https://www.knmi.nl/over-het-knmi/nieuws/klimaatverandering-in-de-regio-amsterdam>.

KNMI (2018c). Klimatologie: Maand-en-seizoenoverzichten 2014-2017. Retrieved from: <https://www.knmi.nl/nederland-nu/klimatologie/maand-en-seizoenoverzichten>

KNMI (2018d). Background information precipitation deficit. Retrieved from: <https://www.knmi.nl/kennis-en-datacentrum/achtergrond/achtergrondinformatie-neerslagtekort>.

Knotters, M. & Bierkens, M.F.P. (2000). Physical basis of time series models for water table depths. *Water Resources Research*, 36(10), 181-188.

Kruseman, G.P. & De Ridder, N.A. (2000). Analysis and Evaluation of Pumping Test Data. *International Institute for Land Reclamation and Improvement, Wageningen*.

Liu, X. Li, X., Harshan, S., Roth, M & Velasco, E. (2017). Evaluation of an urban canopy model in a tropical city: the role of tree evaporation. *Environmental Research Letters*, 12, 2-12. <https://doi.org/10.1088/1748-9326/aa7ee7>.

MKB (2018). MKB Innovatie Top 100: Innovatie-etalage van de Kamer van Koophandel. Retrieved from: <https://www.mkbinnovatietop100.nl/site/Drainvast-oplossing-voor-wateroverlast>.

NHV: Nederlandse Hydrologische Vereniging (1997). Modelkalibratie: het automatisch ijken van grondwatermodellen. *Secretariaat NHV, Groningen*.

Nerem, R.S., Beckley, B.D., Fasullo, J.T., Hamlington, B.D., Masters, D. & Mitchum, G.T. (2018). Climate-change-driven accelerated sea-level rise detected in the altimeter era. *Proceedings of the National Academy of Sciences*, Feb. 2018, DOI: <https://doi.org/10.1073/pnas.1717312115>.

Nicolaas, J.S. (2012). Kunststof strook houdt straat droog. *Cobouw*, 175, 11.

Nienhuis, P.R. & Hemker, C.J. (2010). MicroFEM Tutorial. Amsterdam, Netherlands. Retrieved from: <http://www.microfem.com/download/microfem-tutorial.pdf>.

Olympic Stadium Foundation (2018). *Aerial Photo Olympic Stadium*. Retrieved from: <https://olympischstadion.nl/nl>.

Pötz, H. & Bleuzé, P. (2016). *Green-Blue Grids: Manual for Resilient Cities*. Atelier GroenBlauw, Delft.

Reedijk, P. (2012). Waternet: de integrale waterketen in de praktijk. *Waterspiegel*, September 2012, 18-22.

Rijkswaterstaat (2018). IJsselmeer: zoetwatervoorraad op peil. Retrieved from: <https://www.rijkswaterstaat.nl/water/projectenoverzicht/ijsselmeer-zoetwatervoorraad-op-peil/index.aspx>.

RIONED Foundation (2018). RIONEDInnovatieprijs. Retrieved from: <https://www.riool.net/2276/rionedinnovatieprijs>.

SERC (2018). Photo retrieved from: <http://fotos.serc.nl/noord-holland/amsterdam/>.

Smith, D.M. & Allen, S.J. (1996). Measurement of sap flow in plant stems. *Journal of Experimental Botany*, 47(305), 1833-1844.

Smits, F. (2002). Afstudeerverslag Koppeling DufLOW-MicroFEM. Vrije Universiteit.

Smits, F. (2018). *Personal communication*.

Smits, F. & Hemker, C.J. (2004). Modelling the interaction of surface-water and groundwater flow by linking DufLOW to MicroFEM. FEM_MODFLOW, Karlovy Vary, Czech Republic, 433-436.

STOWA (2003). Rioolvreed water: onderzoek naar hoeveelheden en oorsprong afvalwater. STOWA, Utrecht.

STOWA (2009). Handboek debietmeten in open waterlopen. STOWA, Utrecht.

STOWA (2018). Neerslagstatistieken voor korte duren. STOWA, Amersfoort.

Streetcare (2013). Granudrain information brochure. Retrieved from: <http://streetcare.nu/140-015-Infobrief-Streetcare.pdf>.

TNO, Geologische Dienst Nederland (2018). DINOloket: data and information of the Dutch Subsurface. Retrieved from: <https://www.dinoloket.nl/en/subsurface-models>.

Van Assenbergh, E., Baars, E., Dirksen, J., Van Esch, K.J. & Schaart, N. (2016). *Gemeentelijk Rioleringsplan* (GRPA). Retrieved from: <https://www.waternet.nl/ons-water/rioolwater/>.

Van Baaren, M. (2010). *Amsterdam Waterbestendig*. Waternet and Gemeente Amsterdam.

Van Manen, N. & De Kleijn, M.T.M. (2017). Geodatabase Waterstaatskaart ten behoeve van Cultuurhistorie Nederlands. Rijkswaterstaat.

Van de Ven, F.J.M. (2011). Water Management in Urban Areas. *Technische Universiteit, Delft*.

VHL, Van Hall Larenstein University of Applied Sciences (2018). *Delta Areas and Resources*. Retrieved from: <http://www.vhluniversity.com/about-vhl/profile-vhl/delta-areas-and-resources.aspx>

Visser, A.L. (2009). Technical Drainage Research Rapport Stadionbuurt. *Sector Research & Advice, Waternet*.

Waternet (2018). Website Waternet – Waterschap Amstel, Gooi & Vecht – Gemeente Amsterdam. Retrieved from <https://www.waternet.nl/>.

Waternet database (2018). Non-published data. Retrieved from local Waternet servers.

Weisstein, E.W. (2018). Jacobian. Retrieved from: <http://mathworld.wolfram.com/Jacobian.html>.

Zagwijn, W.H. (1986) Nederland in het Holoceen. Geologie van Nederland, Deel I. Rijks Geologische Dienst, Haarlem.

10 ANNEXES

The annexes elaborate on the methodology of sewage leakage quantification (10.1), research proposed for measuring urban tree evapotranspiration (10.2), additional figures to support the main thesis (10.3) and the Python codes written for the research (10.4).

10.1 Quantification of sewage leakage methodology

10.1.1 Methodology

As described in section 1.3.3, the research area is part of three pumping areas (figure 1.7). A methodology for the quantification of sewage leakage in pumping area 5271 is described in this section. Pumping area 5271 is a relatively small area (164.000 m²) which is located in its entirety within the research area. All the piping within this pumping area might be of influence to the groundwater system under research.

For determining the impact of leaky sewage in the region more accurately, a methodology is set out aimed to quantify the leakage flux. It is assumed little dry weather flux is discharged during night time, therefore a large fraction of discharge can be contributed to infiltration of groundwater at that time. The flux of groundwater can be measured in the pumping station basin, where all the dry weather discharge is collected before pumped to the pressure pipe. Unfortunately, data collected at the pumping station basin is only the water height, not the flux. Besides, the frequency of the water height measurement (every 5 minutes) in combination with the window of the data base to receive data makes the series of measured water heights unsuitable for calculation the flux. Therefore, an additional measurement is placed for the purpose of this research. The Keller data logger measures and registers every minute and data will be read locally. From the basin dimensions and relevant storage within the sewage system, the discharge to the basin can be calculated.

Possibly, some of the rainwater sewage might be wrongly connected to the dry weather sewage system. Or precipitation might enhance the infiltration of groundwater as the groundwater tables rises. Therefore, calculations of the leakage flux are made with the increase in water height during 03:00 and 04:00 AM at dry days. A dry day is defined as a day on which no precipitation occurred the day before, that day itself and the day after, or precipitation was so little it had no impact on the sewage system (STOWA, 2003).

The assumption is made little dry weather flux is discharged between 03:00 and 04:00 AM. Which fraction of the measured flux within at that time period can be contributed to dry weather flux is determined by the consumption profiles from Waternet research. In that research, discharges of several different type of users are measured throughout the week and weekend and converted into consumption profiles. Of area 5271, drinking water consumption is mainly at the Olympic Stadium (similar to a sport centrum). The rest of consumption belongs to a small housing block. The residential profile shows 7% of the average use as minimum usage in the night or even down to 0%, depending on the amount of persons in the household. For a sport centrum, the lowest consumption can still be 10% of the average consumption. A conservative percentage of 10% is used in the leakage calculations of area 5271.

With the calculations of leakage during night time the model can be optimized on this flux as well. Unfortunately, it is not possible to optimize on a flux in MicroFEM, which is one of the argumentations of using the model-independent parameter estimation program PEST.

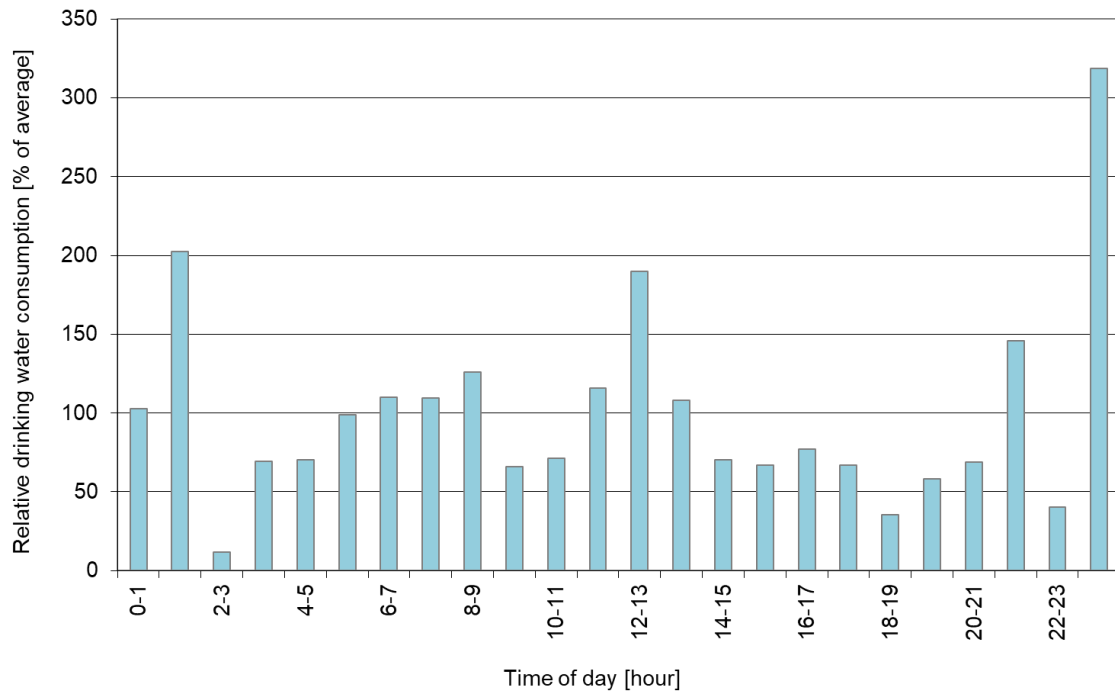


Figure 10.1 Profile of daily drinking water consumption for a sporting facility (Adapted from Waternet database, 2018).

10.1.2 Results

In the measurement at the sewage pumping station it is assumed that there is little production of dry weather sewage between 03:00 and 04:00 AM. In order to estimate the discharge as accurately as possible, the drinking water consumption is analyzed. The yearly drinking water consumption (both measured and theoretical consumption for unmeasured housing) is shown in the table below. From these yearly figures, the drinking water consumption per day, and per hour is calculated, based on drinking water use of 12 hours per day. As described in section 3.6.3, the fraction of the average consumption expected to be used during 03:00 and 04:00 AM is 10%.

Pumping Area	271 Olympic Stadium	190 - section 1e Weteringplantsoen	050 - section Cornelis Dopperkade
Area [m ²]	163.979	(total 7.551.639)	(total 1.886.181)
Pumping station			
Surface area basin [m ²]	3,61		
Pump start level [m NAP]	-2,00		
Pump off level [m NAP]	-2,50		
Drinking water consumption			
Yearly [m ³]	99342.06	611215.92	389897.56
Daily [m ³]	272.17	1674.56	1068.21
Hourly, based on 12h usage [m ³ hour ⁻¹]	22.68	139.55	89.02

Sewage leakage			
Normalized drinking consumption between 03:00 and 04:00 AM [%]	10		
Measured flux [$\text{m}^3 \text{ day}^{-1}$]	115		
Estimated sewage leakage [$\text{m}^3 \text{ day}^{-1}$]	90		

Table 10.1 Figures pumping stations and drinking water consumption per pumping area (Calculations with data from Waternet Database, 2018). For pumping area 190 and 050, only the part which lies within the research area is represented in these figures.

10.2 Experiment tree evapotranspiration

Trees play an important role in the urban water balance. As described in section 10.2, little is known on the transpiration of trees in an urban setting. For modeling purposes it is possible to estimate the evapotranspiration with correction factors or to calibrate the model on it. Quantification research of the flux could result in more accurate modeling of groundwater as well. Therefore, a field experiment will be done on the transpiration of trees in the research area.

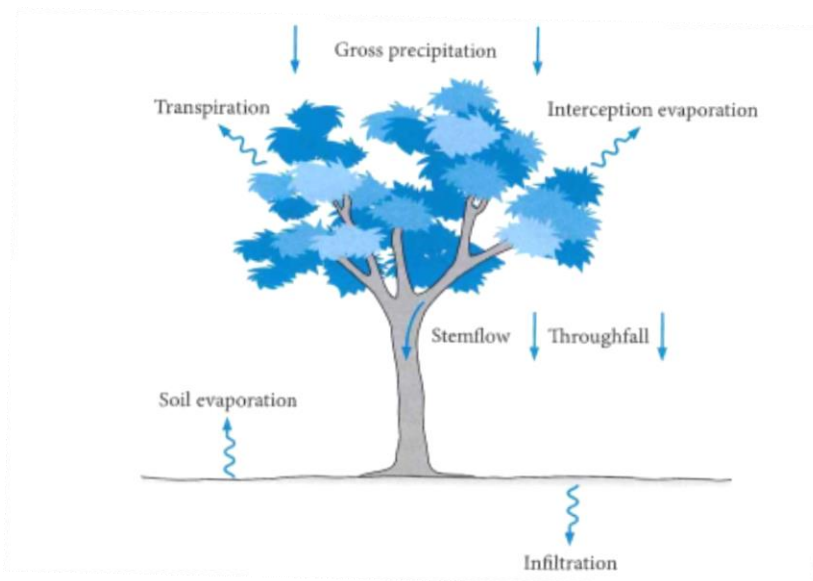


Figure 10.2 Water balance of a tree. Evapotranspiration is the combination of transpiration and interception evaporation (Adapted from Hendriks, 2010).

The evapotranspiration flux as illustrated in figure 1.3 is in fact a combination of multiple fluxes. Evaporation is the change of water in a liquid state to water vapor and if evaporation occurs in the stomata of plant leaves, it is called 'transpiration' (Hendriks, 2011). The

combination of fluxes of transpiration and evaporation from surfaces is called evapotranspiration (figure 2.2).

Trees use water to transport nutrients from the soil to the leaves. The water is taken up through plant roots by making use of groundwater. Therefore, urban tree transpiration is essential in modeling urban water requirements, however urban transpiration measurements and estimates are sparse (Liu et al., 2017). In the Argonautenstraat, several large trees are located: field elms (*Ulmus minor 'Sarniensis'*) and horse chestnut (*Aesculus hippocastanum 'Baumannii'*) (Gemeente Amsterdam, 2018). The transpiration of these trees will be measured by the use of sap-flow measurement (figure 3.1). By applying heat to one injected sensor and measuring the heat transfer to a sensor lower in the tree trunk, the sap flow can be measured (Dingman, 2015). At least 10 trees will be measured to provide an accurate estimate of transpiration flux. For the sap flow measuring equipment a cooperation with the University of Gent can be started.

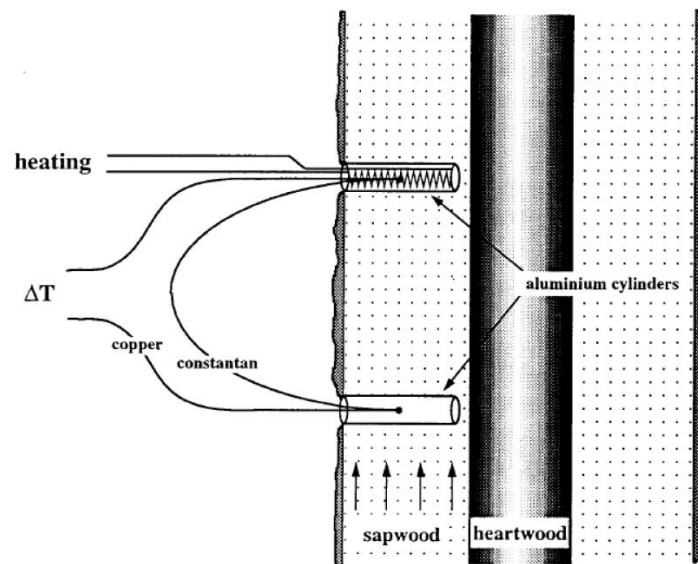


Figure 10.3 Sap-flow measurement in trees using thermal dissipation (Dynamax, 2017).

10.3 Additional figures

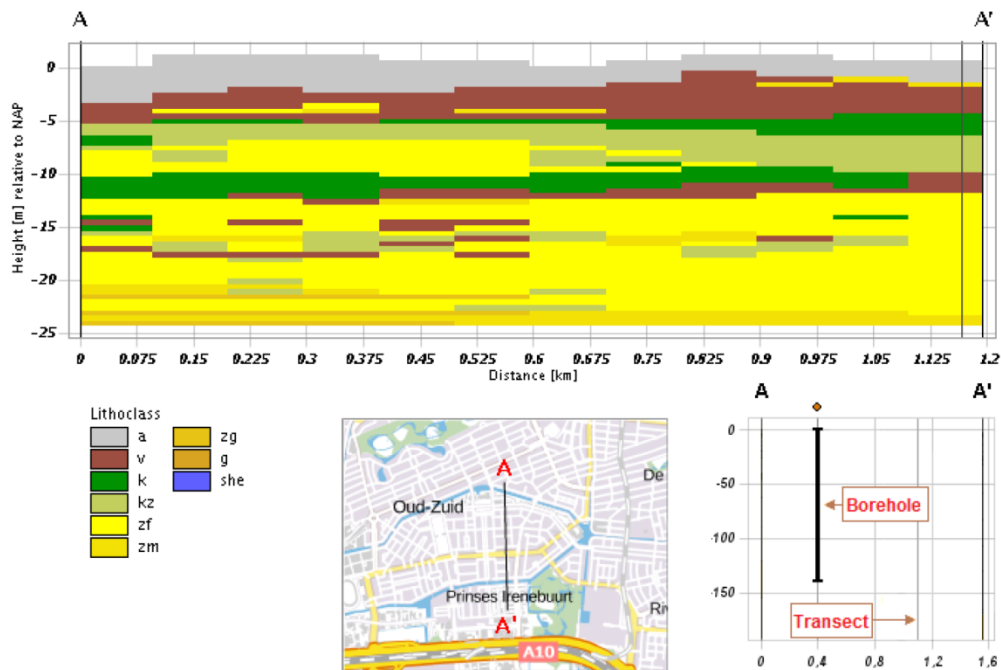


Figure 10A Cross section of geology research area, from A to A'. a = anthropogenic. v = peat. k = clay. kz = clayey sand. zf = fine sand. zm = moderately coarse sand. zg = coarse sand. g = gravel, she = shells (TNO, 2018).

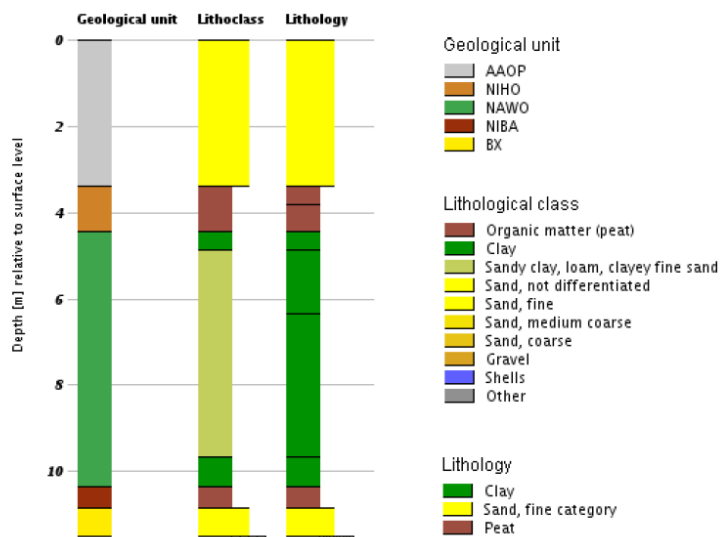


Figure 10B Borehole with description at coordinate location 119160,484170 (Van Tuyll van Serooskerkenweg) in research area. AAOP = Anthropogenic deposits. NIHO = Nieuwkoop Formation, Hollandveen Member. NAWO = Naaldwijk Formation, Wormer Member. NIBA = Nieuwkoop Formation, Basisveen Bed. BX = Boxtel Formation (TNO, 2018).

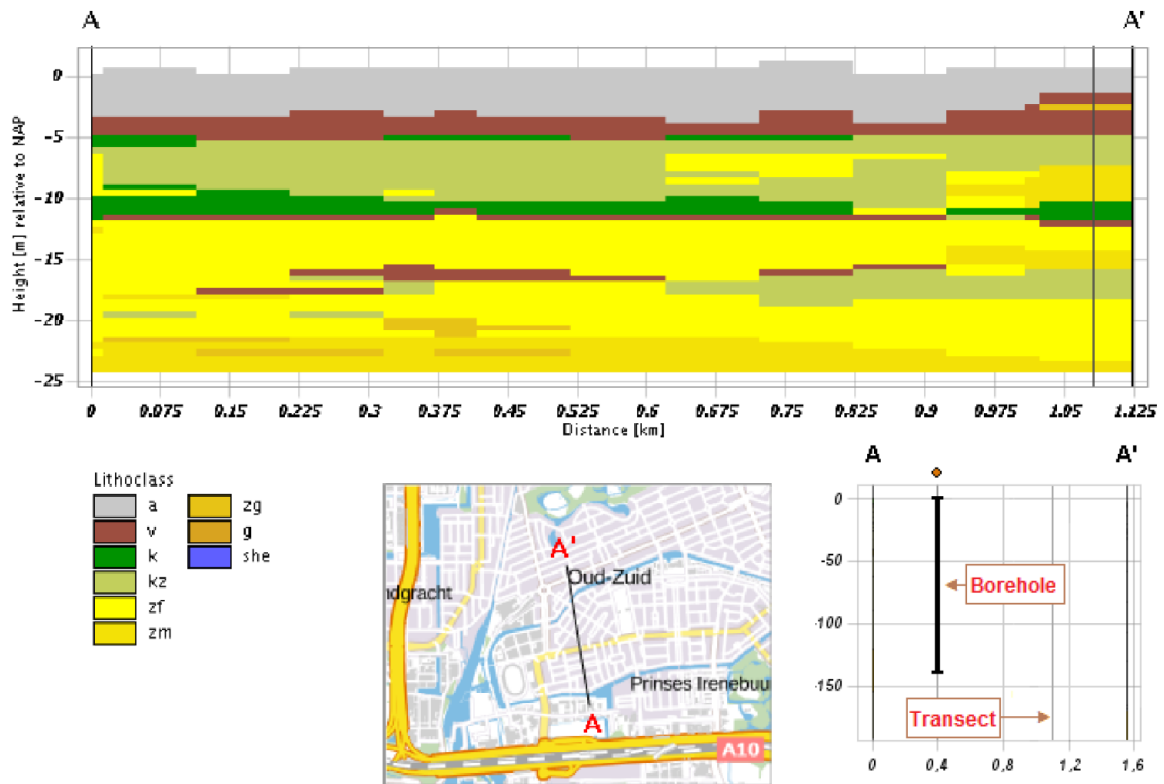


Figure 10C Cross section of geology research area, from A to A'. a = anthropogenic. v = peat. k = clay. kz = clayey sand. zf = fine sand. zm = moderately coarse sand. zg = coarse sand. g = gravel, she = shells (TNO, 2018).

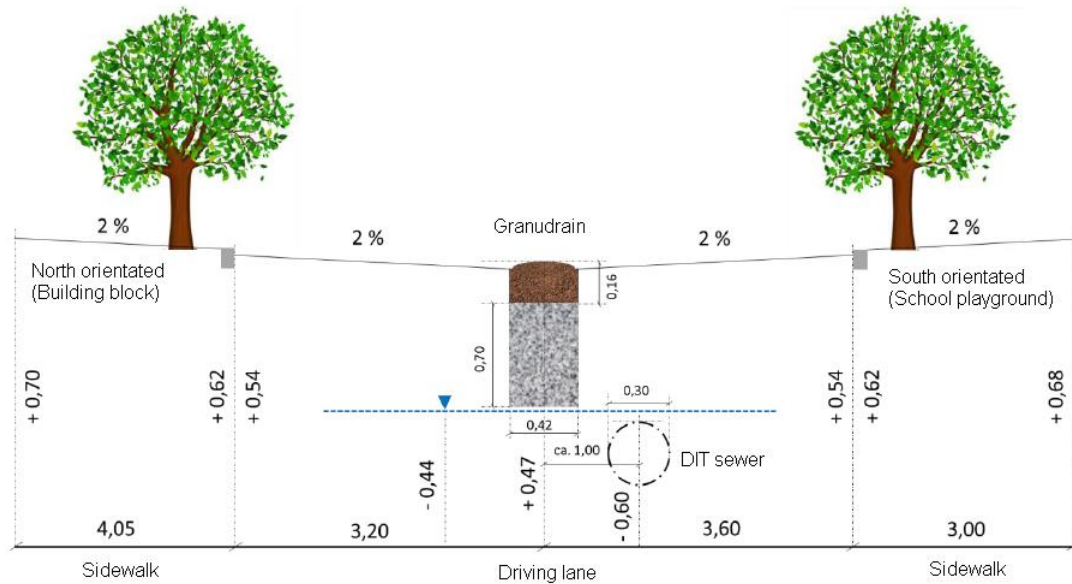


Figure 10D Cross section of the Granudrain and DIT sewer in the Argonautenstraat. Horizontal values are distances in meters and vertical numbers are depths in meters NAP (Adapted from Abas, 2017).

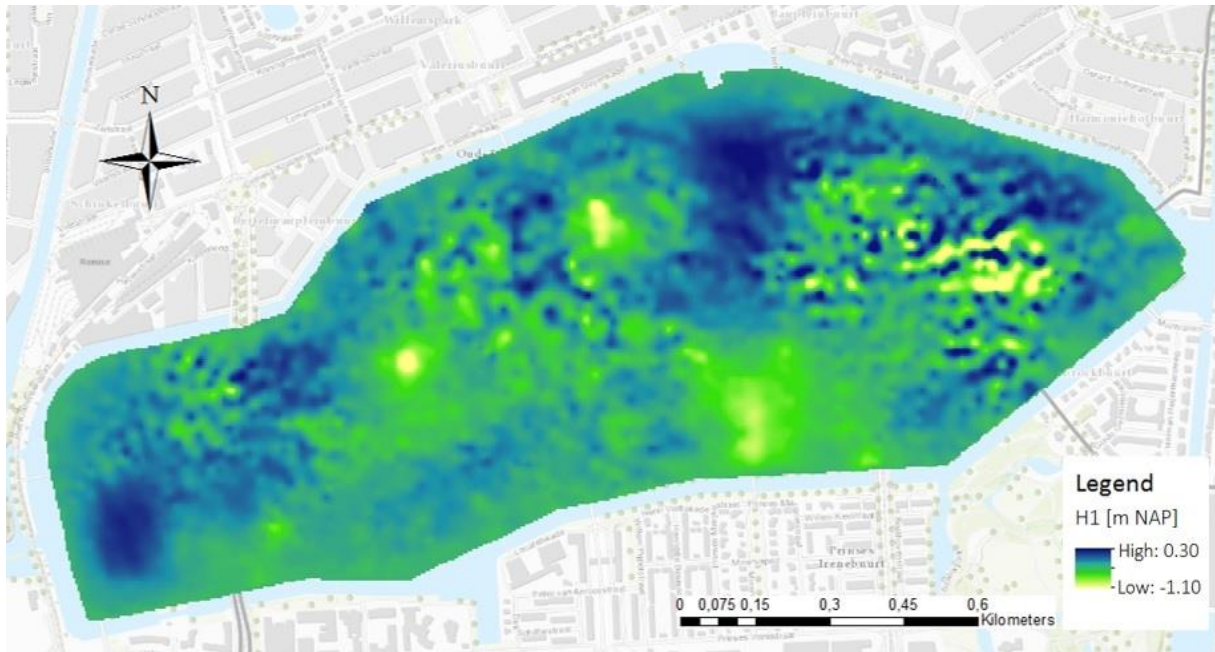


Figure 10E *Calculated hydraulic head values of the top aquifer using the Voronoi area to weigh the observations in stationary optimization.*

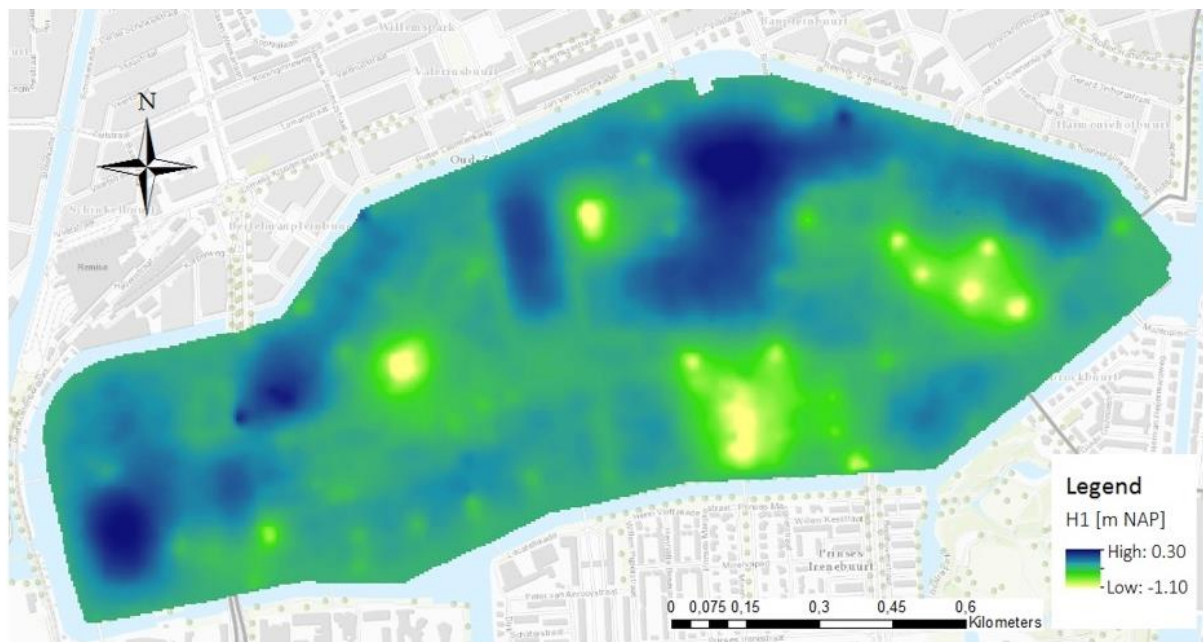


Figure 10F *Calculated hydraulic head values of the top aquifer using the explained variance of the time series analysis to weigh the observations in stationary optimization.*

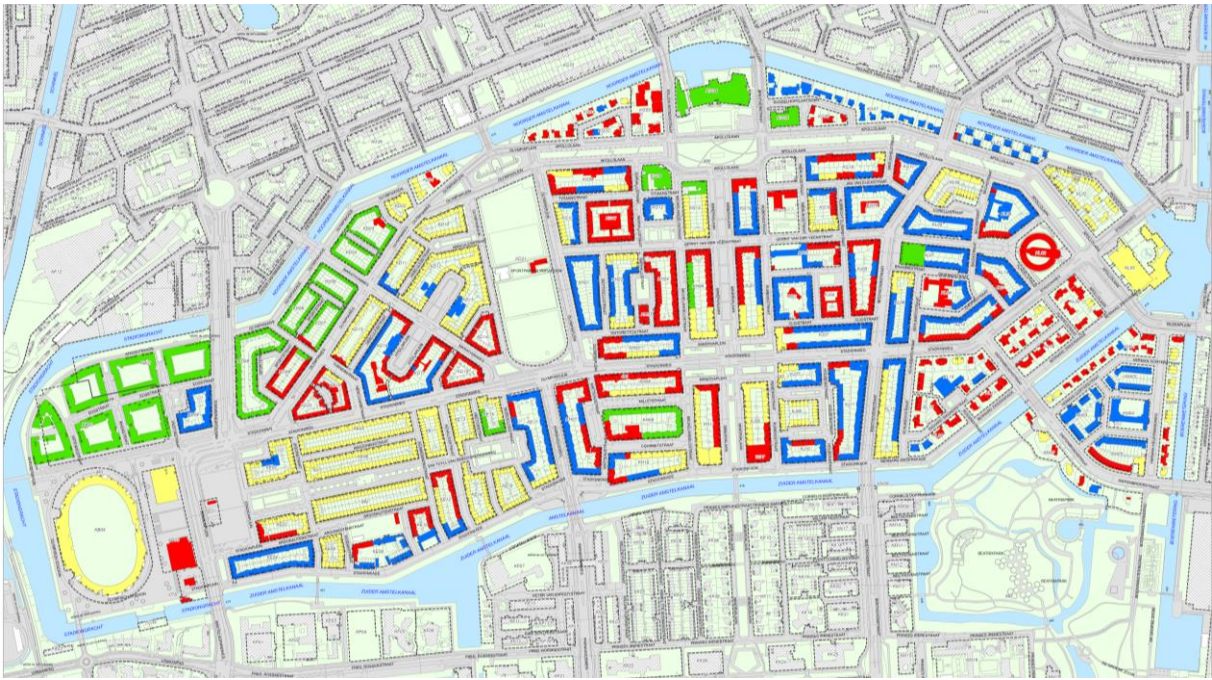


Figure 10G Uncertainty of wooden pole foundation depth data (Waternet, 2012)

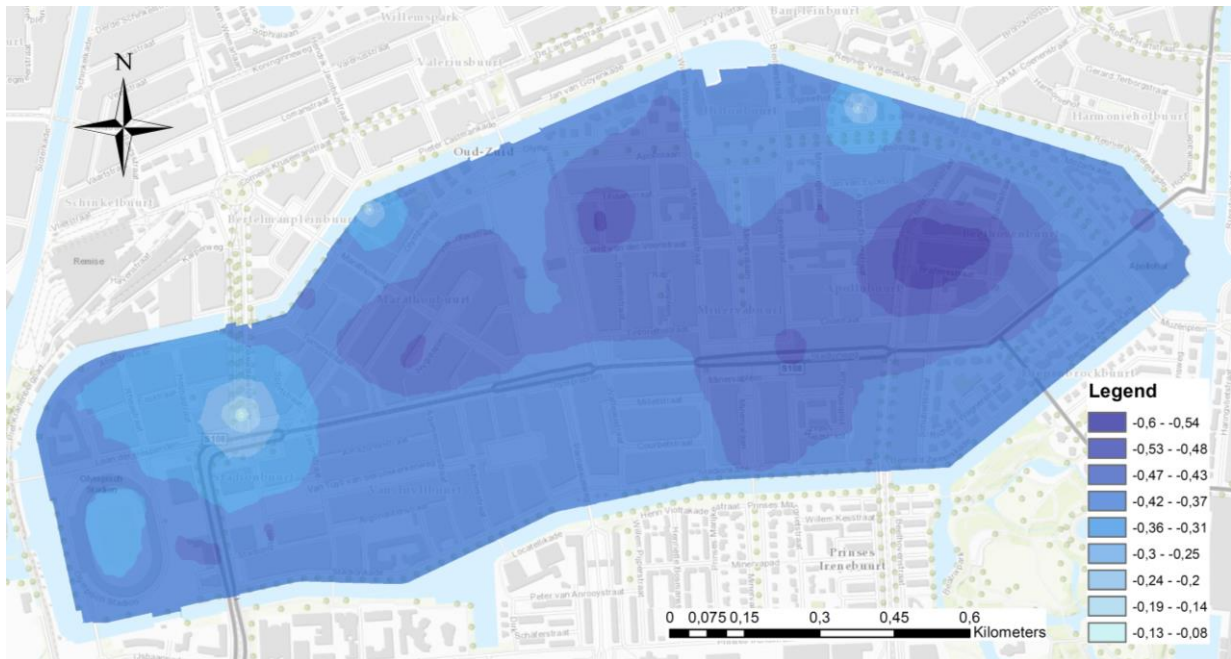


Figure 10H Calculated average groundwater levels reached during the optimization period of 2015-2016.

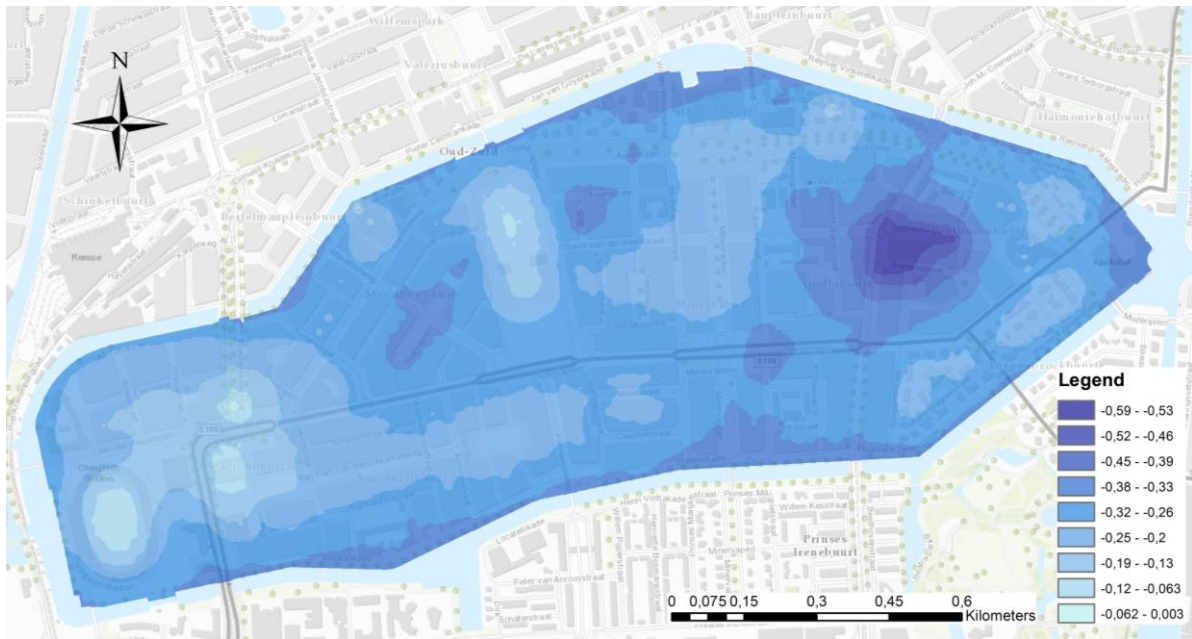


Figure 10I Calculated highest groundwater levels reached during the optimization period of 2015-2016.

10.4 Python code

This section provides the Python coding used in the research. The functional design of the coding is made by the author and the programming by Frank Smits. The code to create groundwater recharge input files are shown in 10.6.1, for creating transient pest control files in 10.6.2 and for processing the transient hydraulic head output files of all nodes in 10.6.3. Adjustments on the code are made according to calculation steps, weighting factor and in the scenarios.

10.4.1 Python code for groundwater recharge

```
# aanmaken van ppn-bestanden met de netto grondwater aanvulling voor in-stationaire berekeningen in
MicroFEM
# Frank Smits, Waternet & TU Delft, 31-03-2018
```

```
# definiëren van de paden en de bestandsnamen:
```

```
invoer_bestand_landgebruik = "D:/Jora/PEST/scriptje voor ppn/P4FEM.lgb"
# in dit bestand staat in de eerste regel de unieke ID-code voor de MicroFEM-parameter-file
# daarna volgt per regel tot welke klasse elk knooppunt behoort
# de opbouw van dit bestand wordt overgenomen voor de opbouw van het ppn-bestand
invoer_bestand_neerslag = "D:/Jora/PEST/scriptje voor ppn/neerslag.txt"
# in dit bestand staat per regel de dagelijkse neerslag voor de verschillende klassen
# het is een tekst-bestand dat bijvoorbeeld vanuit Excel wordt weggeschreven
# belangrijk is dat als decimaalscheidingsteken een punt wordt gebruikt
```

```
basis_uitvoer_bestand_ppn = "D:/Jora/PEST/scriptje voor ppn/ngwa"
# 'ngwa' staat voor 'netto grondwater aanvulling'
# per regel in het invoer_bestand_neerslag wordt er een ppn-bestand aangemaakt
# de basisnaam van het uitvoerbestand wordt per ppn-bestand aangevuld met een dagnummer
```

```
# bestand voor landgebruik regel voor regel inlezen naar de array landgebruik,
# het bestand wordt na dit commando automatisch weer afgesloten:
```

```
with open(invoer_bestand_landgebruik) as ibl:
    landgebruik = ibl.read().splitlines()
# print (landgebruik)
# print (landgebruik[3])
# for k in range(len(landgebruik)):
#     print (landgebruik[k])
```

```
# neerslagtabel genereren uit het invoer-bestand-neerslag:
```

```
import csv
f = open(invoer_bestand_neerslag,'r')
c = csv.reader(f,delimiter='\t')
neerslagtabel = []
for row in c:
    neerslagtabel.append(tuple(map(float, row)))
neerslagtabel = tuple(neerslagtabel)
f.close()
# print (neerslagtabel)
# print(neerslagtabel[1][1])
# for l in range(len(neerslagtabel)):
#     print(neerslagtabel[l])
```

```
dagnummer = 1
```

```
for n in range(len(neerslagtabel)):
```

```

dag = str(dagnummer)
# voorlooppnullen in de naam van het bestand regelen:
if (dagnummer > 0) and (dagnummer < 10):
    dag = '000' + dag
if (dagnummer >= 10) and (dagnummer < 100):
    dag = '00' + dag
if (dagnummer >= 100) and (dagnummer < 1000):
    dag = '0' + dag

# naam uitvoerbestand aanmaken:
uitvoer_bestand_ppn = basis_uitvoer_bestand_ppn + dag + '.ppn'

## uitvoerbestand openen om te schrijven:
ubppn = open(uitvoer_bestand_ppn, "w")

for i in range(len(landgebruik)):
    if i == 0:
        # eerste regel met ID-nummer onveranderd overnemen:
        ubppn.write(landgebruik[i])
        # harde return na de eerste regel (kan dat niet in één keer?):
        ubppn.write('\n')

    if i != 0:
        if (landgebruik[i] == '1':
#         print (neerslagtabel[dagnummer-1][0])
            ubppn.write(str(neerslagtabel[dagnummer-1][0]))
            ubppn.write('\n')
        if (landgebruik[i] == '2':
#         print (neerslagtabel[dagnummer-1][1])
            ubppn.write(str(neerslagtabel[dagnummer-1][1]))
            ubppn.write('\n')
        if (landgebruik[i] == '3':
#         print (neerslagtabel[dagnummer-1][2])
            ubppn.write(str(neerslagtabel[dagnummer-1][2]))
            ubppn.write('\n')
#         als er meer dan drie klassen zijn, dan moet het hier worden aangevuld

ubppn.close()

dagnummer = dagnummer + 1

```

10.4.2 Python code for creating transient pest control file

```

# aanmaken van observation data voor in pst-bestand voor in-stationaire berekeningen met MicroFEM
# Frank Smits, Waternet & TU Delft, 03-06-2018

# definiëren van de paden en de bestandsnamen:
invoer_bestand_peilbuizen = "D:/Jora/Python/scriptje voor pst/peilbuizen met gewicht en groep.txt"
# in dit bestand staat per regel de peilbuiscode, het gewicht en de groep

map_invoer_bestanden_meetreeksen = "D:/Jora/Python/scriptje voor pst/TRA/csv/"
# in deze map staan csv-bestanden met de uitkomsten van de tijdreeksanalyse
# elke peilbuis heeft zijn eigen csv-bestand

uitvoer_bestand_observation_data = "D:/Jora/Python/scriptje voor pst/observation_data.txt"
# per peilbuis worden de volgende gegevens per regel naar dit bestand weggeschreven:
# - een unieke code (WE/WF, peilbuisnummer & de datum)

```

```

# - de meting uit de tijdreeksanalyse van dat bewuste tijdstip
# - het gewicht van de peilbuis
# - de groep van de peilbuis

# begin- en einddatum opgeven:
startdatum = '2015'
einddatum = '2017'

# bestand met peilbuizen regel voor regel inlezen naar de list peilbuizen,
# het bestand wordt na dit commando automatisch weer afgesloten:
with open(invoer_bestand_peilbuizen) as ibp:
    peilbuizen = ibp.read().splitlines()
# print (peilbuizen)
# print (peilbuizen[-1])
# for k in range(len(peilbuizen)):
#     print (peilbuizen[k])

# de namen van alle bestanden in de TRA-map inlezen:
import os
bestandsnamen = os.listdir(map_invoer_bestanden_meetreeksen)
# for k in range (len(bestandsnamen)):
#     print (bestandsnamen[k])
# print (bestandsnamen[-1])

## uitvoerbestand openen om te schrijven:
ubod = open(uitvoer_bestand_observation_data, "w")

# elk bestandje met de meetreeksen uit de TRA apart openen:
for k in range (len(bestandsnamen)):
    bestand_tijdreeks = map_invoer_bestanden_meetreeksen + (bestandsnamen[k])
    # print (bestand_tijdreeks)
    code_peilbuis = 'W'+ bestandsnamen[k][0:6]
    print(code_peilbuis)

# bijbehorende gewicht en groep vinden uit het invoer_bestand_peilbuizen:
for m in range(len(peilbuizen)):
    if (peilbuizen[m][0:7]) == code_peilbuis:
#         print ('hebbes !!!!!')
#         print(code_peilbuis)
#         print(peilbuizen[m][0:7])
#         print(peilbuizen[m][7:])
        gewicht_en_groep = (peilbuizen[m][7:])
#         print("gewicht_en_groep", gewicht_en_groep)

with open(bestand_tijdreeks) as btr:
    tijdreeks = btr.read().splitlines()
    # komma's door punten vervangen ('range(1,...' daarmee wordt de eerste regel overgeslagen):
    for n in range(1,(len(tijdreeks))):
        tijdreeks[n]=tijdreeks[n].replace(',','.')
    # print (tijdreeks)

# alleen de waarden uit de tijdreeks overnemen tussen begin- en einddatum:
print('startdatum =', startdatum)
print('einddatum =', einddatum)
tussen_start_en_eind = False

for p in range(1,(len(tijdreeks))):
    # print (tijdreeks[p])
    # print(tijdreeks[p][0:10])

```

```

#print(tijdreeks[p][8:10])
#print (tijdreeks[p][0:4])
if (tijdreeks[p][0:4]) == startdatum:
    tussen_start_en_eind = True
if (tijdreeks[p][0:4]) == einddatum:
    tussen_start_en_eind = False

if tussen_start_en_eind:
    if (tijdreeks[p][8:10]) == '10':
        code_meting = code_peilbuis + tijdreeks[p][2:4] + tijdreeks[p][5:7]+'1'
        #print(code_meting)
        # gemeten waarde op de 10e dag van de maand inlezen tussen de ;-tekens:
        regel_list = tijdreeks[p].split()
        #print(regel_list)
        # van regel_list een string maken om het te kunnen splitsen op de ;-tekens:
        hele_regel_als_string = str(regel_list)
        import re
        regel = re.split(';','hele_regel_als_string)
        #print(code_meting + ' ' + regel[1])
        #print(gewicht_en_groep)
        #print(code_meting + ' ' + regel[1] + gewicht_en_groep)
        # regel[1] is de meting:
        ubod.write(code_meting + '\t' + regel[1] + gewicht_en_groep)
        # harde return na de eerste regel ( kan dat niet in één keer ? ):
        ubod.write('\n')

    if (tijdreeks[p][8:10]) == '20':
        code_meting = code_peilbuis + tijdreeks[p][2:4] + tijdreeks[p][5:7]+'2'
        regel_list = tijdreeks[p].split()
        hele_regel_als_string = str(regel_list)
        import re
        regel = re.split(';','hele_regel_als_string)
        ubod.write(code_meting + '\t' + regel[1] + gewicht_en_groep)
        ubod.write('\n')

# tot zover werden alleen de TRA-waarde op de 10e en de 20e van de maand gevonden
# het volgende deel gaat om de TRA-waarden aan het einde van de maand:
if (tijdreeks[p][5:10]) == '01-31':
    code_meting = code_peilbuis + tijdreeks[p][2:4] + tijdreeks[p][5:7]+'3'
    regel_list = tijdreeks[p].split()
    hele_regel_als_string = str(regel_list)
    import re
    regel = re.split(';','hele_regel_als_string)
    ubod.write(code_meting + '\t' + regel[1] + gewicht_en_groep)
    ubod.write('\n')

if (tijdreeks[p][5:10]) == '02-28':
    code_meting = code_peilbuis + tijdreeks[p][2:4] + tijdreeks[p][5:7]+'3'
    regel_list = tijdreeks[p].split()
    hele_regel_als_string = str(regel_list)
    import re
    regel = re.split(';','hele_regel_als_string)
    ubod.write(code_meting + '\t' + regel[1] + gewicht_en_groep)
    ubod.write('\n')

# hier kunnen nog een of enkele extra secties worden aangemaakt om in schrikkeljaren 02-29 te kiezen

if (tijdreeks[p][5:10]) == '03-31':
    code_meting = code_peilbuis + tijdreeks[p][2:4] + tijdreeks[p][5:7]+'3'

```

```

regel_list = tijdreeks[p].split()
hele_regel_als_string = str(regel_list)
import re
regel = re.split(';',hele_regel_als_string)
ubod.write(code_meting + '\t' + regel[1] + gewicht_en_groep)
ubod.write('\n')

if (tijdreeks[p][5:10]) == '04-30':
    code_meting = code_peilbuis + tijdreeks[p][2:4] + tijdreeks[p][5:7]+'3'
    regel_list = tijdreeks[p].split()
    hele_regel_als_string = str(regel_list)
    import re
    regel = re.split(';',hele_regel_als_string)
    ubod.write(code_meting + '\t' + regel[1] + gewicht_en_groep)
    ubod.write('\n')

if (tijdreeks[p][5:10]) == '05-31':
    code_meting = code_peilbuis + tijdreeks[p][2:4] + tijdreeks[p][5:7]+'3'
    regel_list = tijdreeks[p].split()
    hele_regel_als_string = str(regel_list)
    import re
    regel = re.split(';',hele_regel_als_string)
    ubod.write(code_meting + '\t' + regel[1] + gewicht_en_groep)
    ubod.write('\n')

if (tijdreeks[p][5:10]) == '06-30':
    code_meting = code_peilbuis + tijdreeks[p][2:4] + tijdreeks[p][5:7]+'3'
    regel_list = tijdreeks[p].split()
    hele_regel_als_string = str(regel_list)
    import re
    regel = re.split(';',hele_regel_als_string)
    ubod.write(code_meting + '\t' + regel[1] + gewicht_en_groep)
    ubod.write('\n')

if (tijdreeks[p][5:10]) == '07-31':
    code_meting = code_peilbuis + tijdreeks[p][2:4] + tijdreeks[p][5:7]+'3'
    regel_list = tijdreeks[p].split()
    hele_regel_als_string = str(regel_list)
    import re
    regel = re.split(';',hele_regel_als_string)
    ubod.write(code_meting + '\t' + regel[1] + gewicht_en_groep)
    ubod.write('\n')

if (tijdreeks[p][5:10]) == '08-31':
    code_meting = code_peilbuis + tijdreeks[p][2:4] + tijdreeks[p][5:7]+'3'
    regel_list = tijdreeks[p].split()
    hele_regel_als_string = str(regel_list)
    import re
    regel = re.split(';',hele_regel_als_string)
    ubod.write(code_meting + '\t' + regel[1] + gewicht_en_groep)
    ubod.write('\n')

if (tijdreeks[p][5:10]) == '09-30':
    code_meting = code_peilbuis + tijdreeks[p][2:4] + tijdreeks[p][5:7]+'3'
    regel_list = tijdreeks[p].split()
    hele_regel_als_string = str(regel_list)
    import re
    regel = re.split(';',hele_regel_als_string)
    ubod.write(code_meting + '\t' + regel[1] + gewicht_en_groep)

```

```

ubod.write('\n')

if (tijdreeks[p][5:10]) == '10-31':
    code_meting = code_peilbuis + tijdreeks[p][2:4] + tijdreeks[p][5:7]+'3'
    regel_list = tijdreeks[p].split()
    hele_regel_als_string = str(regel_list)
    import re
    regel = re.split(';','hele_regel_als_string)
    ubod.write(code_meting + '\t' + regel[1] + gewicht_en_groep)
    ubod.write('\n')

if (tijdreeks[p][5:10]) == '11-30':
    code_meting = code_peilbuis + tijdreeks[p][2:4] + tijdreeks[p][5:7]+'3'
    regel_list = tijdreeks[p].split()
    hele_regel_als_string = str(regel_list)
    import re
    regel = re.split(';','hele_regel_als_string)
    ubod.write(code_meting + '\t' + regel[1] + gewicht_en_groep)
    ubod.write('\n')

if (tijdreeks[p][5:10]) == '12-31':
    code_meting = code_peilbuis + tijdreeks[p][2:4] + tijdreeks[p][5:7]+'3'
    regel_list = tijdreeks[p].split()
    hele_regel_als_string = str(regel_list)
    import re
    regel = re.split(';','hele_regel_als_string)
    ubod.write(code_meting + '\t' + regel[1] + gewicht_en_groep)
    ubod.write('\n')

ubod.close()

#stukje code over het splitsen van de regel uit het TRA-bestand
#import re
##re.split('x*', 'axbc')
#sf = re.split(';','1970-01-10;-0.3;-0.29;-0.29;-0.47;-0.15')
#print(sf[1])
#re.split(';','tdrks)
#print(tdrks)

#    if i != 0:
#        if (landgebruik[i]) == '1':
#            #    print (neerslagtabel[dagnummer-1][0])
#            ubppn.write(str(neerslagtabel[dagnummer-1][0]))
#            ubppn.write('\n')
#        if (landgebruik[i]) == '2':
#            #    print (neerslagtabel[dagnummer-1][1])
#            ubppn.write(str(neerslagtabel[dagnummer-1][1]))
#            ubppn.write('\n')
#        if (landgebruik[i]) == '3':
#            #    print (neerslagtabel[dagnummer-1][2])
#            ubppn.write(str(neerslagtabel[dagnummer-1][2]))
#            ubppn.write('\n')

```

10.4.3 Python code for processing transient hydraulic heads of all nodes

```

# inlezen van fth-bestand van alle knopen van een MicroFEM-model
# Frank Smits, Waternet & TU Delft, 18-07-2018

```

```

# definiëren van de paden en de bestandsnamen:
invoer_bestand_FTH = "D:/Jora/Python/scriptje voor fth van alle knopen/RunSA.FTH"

tussen_uitvoer_bestand = "D:/Jora/Python/scriptje voor fth van alle knopen/tussen_uitvoer_vanuit.FTH"

uitvoer_bestand = "D:/Jora/Python/scriptje voor fth van alle knopen/uitvoer_vanuit.FTH"

# tussenuitvoerbestand alvast openen:
tub = open(tussen_uitvoer_bestand, "w")
#eventueel een bovenste regel met kopjes wegschrijven:
#ub.write('knoop'+';'+ 'X'+';'+ 'Y'+';'+ 'laagste'+';'+ 'gemiddelde'+';'+ 'hoogste'+'\n')

# FTH-bestand openen en per regel inlezen:
with open(invoer_bestand_FTH) as invoerb bestand:
    alle_regels_FTH = invoerb bestand.read().splitlines()

# het aantal knopen inlezen en gelijk een stringetje van maken:
tweede_regel = alle_regels_FTH[1].split()
aantal_knopen = int(tweede_regel[1])
#print(aantal_knopen)

# in het .fth-bestand worden maar 250 kolommen per regel weggeschreven
# bij meer dan 250 knopen wordt steeds op een nieuwe regel begonnen
# bij het inlezen van het .fth-bestand moet hier rekening mee worden gehouden:
factor = aantal_knopen / 250
factor_250 = int(factor)
factor_rest = factor - factor_250
#print(factor_250)
#print(factor_rest)

if factor_rest == 0:
    far = factor_250 # 'far' staat voor ' factor aantal regels'
else:
    far = factor_250 + 1
#print(far)

# het aantal tijdstappen bepalen:
aantal_regels = len(alle_regels_FTH) - (3 + 4 * far)
aantal_tijdstappen = int(aantal_regels / far)
#print(aantal_tijdstappen)

# alle knooppuntnummers inlezen, eerst vaststellen van welke tot welke regel:
knooppunten = []
start = 3
finish = start + far
while start < finish:
    regel = alle_regels_FTH[start].split()
    # de eerste kolom bevat loze ruimte: ' _____ "'_', dus die laat ik weg:
    regel_met_knooppunten = regel[1:]
    knooppunten.extend(regel_met_knooppunten)
    start += 1 # a+=1 is a=a+1
#print(knooppunten)

# alle x-coördinaten inlezen, eerst vaststellen van welke tot welke regel:
x_coördinaten = []
start = 3 + 2 * far
finish = start + far
while start < finish:

```

```

regel = alle_regels_FTH[start].split()
# de eerste kolom bevat loze ruimte: ' _____ "'_', dus die laat ik weg:
regel_met_knooppunten = regel[1:]
x_coördinaten.extend(regel_met_knooppunten)
start += 1
#print(x_coördinaten)

# alle y-coördinaten inlezen, eerst vaststellen van welke tot welke regel:
#print('vanaf hier')
y_coördinaten = []
start = 3 + 3 * far
finish = start + far
while start < finish:
    regel = alle_regels_FTH[start].split()
    # de eerste kolom bevat loze ruimte: ' _____ "'_', dus die laat ik weg:
    regel_met_knooppunten = regel[1:]
    y_coördinaten.extend(regel_met_knooppunten)
    start += 1
#print(y_coördinaten)

# de header van het .FTH-bestand is ingelezen, vanaf hier verder met alle stijhoogten:
stijhoogten = []

# bepalen waar er begonnen moet worden aan de weggeschreven stijhoogtes:
regelnummer = 3 + 4 * far

# tellertje om de regels met dezelfde tijdstap achter elkaar te plaatsen:
aantal_far = 0

# de regels met dezelfde tijdstap worden als tussenstap in deze aparte matrix geplaatst:
regel_met_getallen = []

for i in range(len(alle_regels_FTH)):
    if (i >= regelnummer):
        # eerst elke regel opdelen naar de termen tussen de spaties:
        regel = alle_regels_FTH[i].split()
        #print('volgende regel')
        #print(regel)
        for n in range(len(regel)):
            if n > 0:
                getal = float(regel[n])
                regel_met_getallen.append(getal)
        aantal_far += 1
        if aantal_far == far:
            stijhoogten.append(regel_met_getallen)
            regel_met_getallen = []
            aantal_far = 0
#print(aantal_knopen)
#print(aantal_tijdstappen)
#print(stijhoogten[aantal_tijdstappen-1][aantal_knopen-1])

# voor elk knooppunt de grootste stijhoogte bepalen:
kolommetje = []
for kolomnummer in range(aantal_knopen):
    for regelnummer in range(aantal_tijdstappen):
        kolommetje.append(stijhoogten[regelnummer][kolomnummer])
# print(' bij [kolomnummer]')
# print(kolomnummer)

```

```

# print(' hoort >>>>')
# print(kolommetje)
# de ingelezen getallen op volgorde van klein naar groot zetten:
kolommetje.sort()
# print(kolommetje)
laagste_stijghoogte = kolommetje[0]
hoogste_stijghoogte = kolommetje[-1]
# gemiddelde bepalen:
som_voor_gemiddelde = 0
for n in range(aantal_tijdstappen):
    #print(format(kolommetje[n], 'f'))
    som_voor_gemiddelde += kolommetje[n]
gemiddelde = som_voor_gemiddelde / aantal_tijdstappen
# alvast even omzetten naar een stringetje van een beperkt aantal posities:
gemiddelde_als_string = str(gemiddelde)
gemiddelde_als_string = gemiddelde_als_string[0:9]
#print("gemiddelde is: ", gemiddelde)
#print('laagst : ', laagste_stijghoogte)
#print('hoogst : ', hoogste_stijghoogte)

# alle verzamelde informatie in één regel zetten:
weg_te_schrijven_regel = str(knooppunten[kolomnummer])+";"
# was eerst in de blok '-1': weg_te_schrijven_regel = str(knooppunten[kolomnummer-1])+";"
weg_te_schrijven_regel += str(x_coördinaten[kolomnummer])+";"
weg_te_schrijven_regel += str(y_coördinaten[kolomnummer])+";"
weg_te_schrijven_regel += str(laagste_stijghoogte)+";"
weg_te_schrijven_regel += str(gemiddelde_als_string)+";"
weg_te_schrijven_regel += str(hoogste_stijghoogte)+"\n"
# print(weg_te_schrijven_regel)
# de regel wegschrijven naar uitvoerbestand:
tub.write(weg_te_schrijven_regel)

# schoonvegen voor de volgende knoop:
kolommetje = []

# tussenuitvoerbestand sluiten:
tub.close()

# uitvoerbestand openen:
ub = open(uitvoer_bestand, "w")

# tussenuitvoerbestand openen en per regel inlezen:
with open(tussen_uitvoer_bestand) as invoerbestand:
    alle_regels_TUB = invoerbestand.read().splitlines()

for i in range(len(alle_regels_TUB)):
    tekst = str(alle_regels_TUB[i])
    tekst = tekst.replace('.', ',')
    tekst = tekst + '\n'
    ub.write(tekst)

# uitvoerbestand sluiten:
ub.close()

```